POLITECNICO DI TORINO

Master of Science in Civil Engineering

MASTER OF SCIENCE DISSERTATION

MODELLING OF THE SHOTCRETE LINING-ROCK INTERACTION WITH THE HYPERSTATIC REACTION METHOD

Candidate:

Cesar Alejandro Luna Ramos

Supervisor:

Prof. Pierpaolo Oreste

Giovanni Spagnoli, Ph.D.

Academic Year 2017-2018

CONTENTS

INTRODUCTION

The sprayed concrete (or shotcrete) technology, here abbreviated as SC, consists in spraying, by means of a lance, compressed air with a water/cement-additive mixture and accelerators products, immediately after tunnel excavation to provide temporary or permanent stability to the ground opening (Melbye, 1994).

Sprayed concrete is pumped under pressure through a pneumatic hose and projected into place at high velocity (30 to 50 m/s), which is compacted and finally hardens (DIN 18551, 1992; Thomas, 2009; Hemphill, 2013). Two SC methods are known: dry-mix (where the water required for hydration is added at the spraying nozzle) and the wet-mix (the conveyed mixtures already contain the necessary water for hydration) (Melby, 1994).

Aging of SC is influenced by many parameters: cement type, accelerators, retarders, temperature, aggregates, water/cement (w/c) ratio and microsilica content. Among them accelerators play a major role as SC must be designed to reach relatively high strength as well as meeting the long-term performance (Thomas, 2009). Mechanical behavior can be further improved by fibers in terms of compressive and splitting tensile strength, permeability and durability of SC (Melbye, 1994; Wang et al., 2015).

Figure 1. Shotcrete on a tunnel wall during a trial (picture courtesy of Giovanni Spagnoli).

Because of the hydration process within the cement paste, the material properties of the SC gradually change with time, leading to a complex stress–strain history within the tunnel lining during construction, where the loading rate of the SC shell with respect to time plays a major role (Schütz et al., 2011).

Unconfined compressive strength (UCS) is very important for SC. Specifications for compressive strength are 20MPa for temporary SC and 40MPa or higher for permanent SC (Thomas, 2009). Stress-strain relation shows a linear elastic response up to a limit of proportionality followed by a softer response and increasing the confining pressure the behavior becomes ductile (Aydan et al., 1992).

Cracking governs the tensile behavior (Chen, 1982), although, tensile strength is normally ignored in concrete (Thomas, 2009). A stress-strain relation in tension shows an elastic response up to 60% of the maximum stress (Chen, 1982).

The study of the compressive and tensile behavior of the SC linings is performed by means of two-dimensional or even three-dimensional numerical methods. The use of these calculation methods takes time to define the model and to be able to analyze the results in a convenient way. As a matter of fact, a large portion of rock cluster at the tunnel contour in the numerical model is required and it is necessary to proceed correctly to insert the excavation and support phases realized in the tunnel.

Because, SC compared with ordinary concrete has a shorter setting time and high early age mechanical properties (Wang et al., 2015), it is normally used for solving stability problems in tunnels and other underground constructions such as mines, hydropower projects and slope stabilization (e.g. Melby, 1994). SC can be employed for temporary and permanent supports. However, regarding the design and construction of modern tunnels, SC single layer lining is becoming the trend of future development (Franzen et al., 2001). With SC as permanent final lining, long-term performance requirements, such good bonding, high final density, compressive strength and chemical resistance, have to increase (Melby, 1994).

The early-age strength of SC is frequently more important than its ultimate strength. The advance speed of tunnel operations is strongly influenced by the rate of development of early-age strength, since it determines, both in soft ground and weak rock, when excavation face can proceed again. As a matter of fact, re-entry is mainly driven by the tunnel drive progression to ensure the safety of personnel to continue

development (Mohajerani et al., 2015). Re-entry times range from 2 to 4 h, where the Unconfined Compressive Strength (UCS) reaches 1MPa (Clements, 2004; Concrete Institute of Australia, 2010), however, this value is not standardized and it can be also lower, if safety is ensured (see Rispin et al., 2009). Iwaki et al. (2001) empirically determined that an UCS of 0.5–1MPa should be an adequate strength for SC to protect against rock-fall, although the safe re-entry times, based on strength measurements, is still determined on project basis (Mohajerani et al., 2015).

Currently, improvement of early-age strength and stiffness development is achieved by the addition of accelerators, added in liquid form at the nozzle during spraying for the wet-mix SC. Nowadays alkali-free accelerators (AFA) are replacing the traditional accelerators not only because the latter are hazardous products but also because conventional accelerators have the side effect of decreasing the ultimate strength at 28 days in the range between 20 and 50% (Prudencio, 1998), because the products of hydration become unstable, mainly when using water glass, i.e. modified sodium silicate (Thomas, 2009). Besides, AFA enhance the resistance of concrete to internal corrosion caused by the interaction of alkalis with fillers and to extend the life of concrete structures (e.g. Brykov et al., 2013).

Because, coring should not take place until an UCS value of at least 5MPa (Clements, 2004), or between 8–10MPa, as Jolin and Beaupré (2003) suggest, the assessment of strength improvement is normally indirectly performed by means of the J-curves method for minimum strength (DIN EN 14487-1, 2006) by using the needle penetration method up to 1MPa strength (DIN EN 14488-2, 2006) and the stud driving method between 1 and 56MPa strength (DIN EN 14488-2, 2006; ÖVBB, 2006). Conventional compressive strength tests on cored samples are only performed from strength to 5 to 100MPa according to the DIN EN 12504-1 (2009).

After the SC application, with the restart of the tunnel excavation, the lining load phase starts. This loading phase occurs during the curing of the SC when the mechanical characteristics (strength and stiffness) vary over time at a certain rate. Each load step, due to each excavation face advancement, produces different effects on the lining, due to the different stiffness and strength of the SC. The final tensional state and, therefore, the final conditions of the lining are the ultimate result of this complex loading

mechanism due to the excavation face advancement (while the SC cures) and the corresponding variations in its mechanical characteristics (Oreste, 2003).

The Converge Confinement Method (CCM) and the Hyperstatic Reaction Method (HRM) have been used to study in the detail the behavior of the tunnel support under external loads with increasing elastic modulus values of the concrete simulating the curing effect. CCM generally requires a mean stiffness of the SC lining to obtain the support reaction line (Oreste, 2003). In this research, the reaction line of the SC lining is considered as curve, in order to simulate the curing effect of the SC during the loading phase of the support. CCM was useful to evaluate the magnitude of the various loading steps developing over time during the of the excavation face advancement. In the HRM the interaction between ground and support is represented by Winkler type springs. This method permits to determine the displacement of the lining and the developed bending moments and forces in order to design it (Oreste, 2007). In the specific case, at the HRM model different loading steps, obtained with the CCM have been applied, considering each of these the effective stiffness value reached by the SC and hence by the support. Due to the results obtained with the combined analysis of the calculation methods, it was possible to obtain a detailed evaluation of the tensional state of the support, which can consider both the effect of the characteristics of the SC employed (with the evolving curve of strength and stiffness with the time) and the advance rate of the excavation face.

1. THE SPRAYED CONCRETE (SHOTCRETE): CHARACTERISTICS AND MODALITY OF USE

1.1. DEFINITION

Sprayed concrete is a mixture of cement, aggregate and water projected pneumatically from a nozzle into place to produce a dense homogeneous mass consists in spraying, by means of a lance. Sprayed concrete normally incorporates admixtures and may also include additions or fibres or a combination of these (EFNARC, 1996). Sprayed concrete or shotcrete (SC) is pumped under pressure through a pneumatic hose and projected into place at high velocity (30 to 50 m/s), which is compacted and finally hardens. The sprayed concrete provide temporary or permanent stability to the ground opening.

To understand the notion of shotcrete is important to define some important concepts such as (EFNARC, 1996):

- Layer: Is a term used for a discrete thickness of sprayed concrete, built up from a number of passes of the nozzle and allowed to set.
- Rebound losses: Are part of the overall production losses and consist of material which, having been sprayed through the nozzle and struck the surface, does not adhere.
- Nozzle: Is the equipment through which the mix is discharged; it consists of a pipe with a mixing unit into which constituents are injected.
- Binder: Is the total amount of cement and cementitious addition in the sprayed concrete.

1.2. FEATURES & BENEFITS

The shotcrete has often been described not as a material but as a process. Properly applied, is a structurally and durable construction process which exhibits superior hardened properties to high quality conventional concrete, such as high strength, low permeability, good resistance to weathering, resistance to some forms of chemical attack and high durability (US Army Corps of Engineers, 1993). Moreover, the nature of the shotcrete placement process provides additional benefits, such as excellent bond with most substrates and instant or rapid capabilities, particularly on complex forms or shapes (ASA, 2014).

The properties of the shotcrete can be further enhanced through the addition of many different additives or admixtures such as (ASA, 2014):

- Silica Fume: Provides reduced permeability, increased compressive and flexural strength, increased resistance to alkali and chemical attack, improved resistance to water washout, reduced rebound levels, and allows for thicker single pass applications;
- Air-Entraining Admixtures: Improve pumpability and adhesion in wet-process shotcrete and freeze-thaw durability in both wet and dry processes;
- Fibers: Control cracking, increase toughness values, improve impact resistance and energy absorption; and
- Accelerators: Improve placement characteristics in adverse conditions, allow for thicker single pass applications, increase production capabilities, and reduce the occurrence of fallouts on structures subjected to vibration.

The enormous advantages of sprayed concrete as a construction process and the improvement of equipment, materials and application have made it an important tool for various types of work. Sprayed concrete takes care of stability problems in tunnels and other underground constructions. Today sprayed concrete is a key factor for rock support in tunneling, mining operations, hydropower projects and slope stabilization (Melbye T, 1994).

More than 90 % of all sprayed concrete is used for rock support. In comparison with traditional concrete, sprayed concrete is used today to a relatively small extent, but when it is used, it is done so in many different ways. Some examples: Pit curbing, canal lining, sea walls, fire and corrosion protection, spraying of new constructions, plastering and stabilizing of brick walls and others more (Melbye T, 1994).

Sprayed concrete is the building method of the future due to flexibility, rapidity and economy

1.3. SPRAYING METHODS

Today, sprayed concrete is produced in two ways: the dry mix process and the wet mix process. Both methods have their advantages and disadvantages. Depending on the project requirements and the experience of people the best suited method should be chosen.

The situation nowadays is that world-wide 70% of the sprayed concrete is applied by the wet-mix method and 30% by the dry-mix method. In some areas, however, the wet-mix method is already dominating (Scandinavia, Italy: almost 100 %) (Melbye T, 1994).

1.3.1. Dry-mix Method

The cementitious material and aggregate are thoroughly mixed and either bagged in a dry condition, or mixed and delivered directly to the gun. The mixture is normally fed to a pneumatically operated gun which delivers a continuous flow of material through the delivery hose to the nozzle. The interior of the nozzle is fitted with a water ring which uniformly injects water into the mixture as it is being discharged from the nozzle and propelled against the receiving surface (US Army Corps of Engineers, 1993). Material is consolidated on the receiving surface by the high-impact velocity (ASA, 2014).

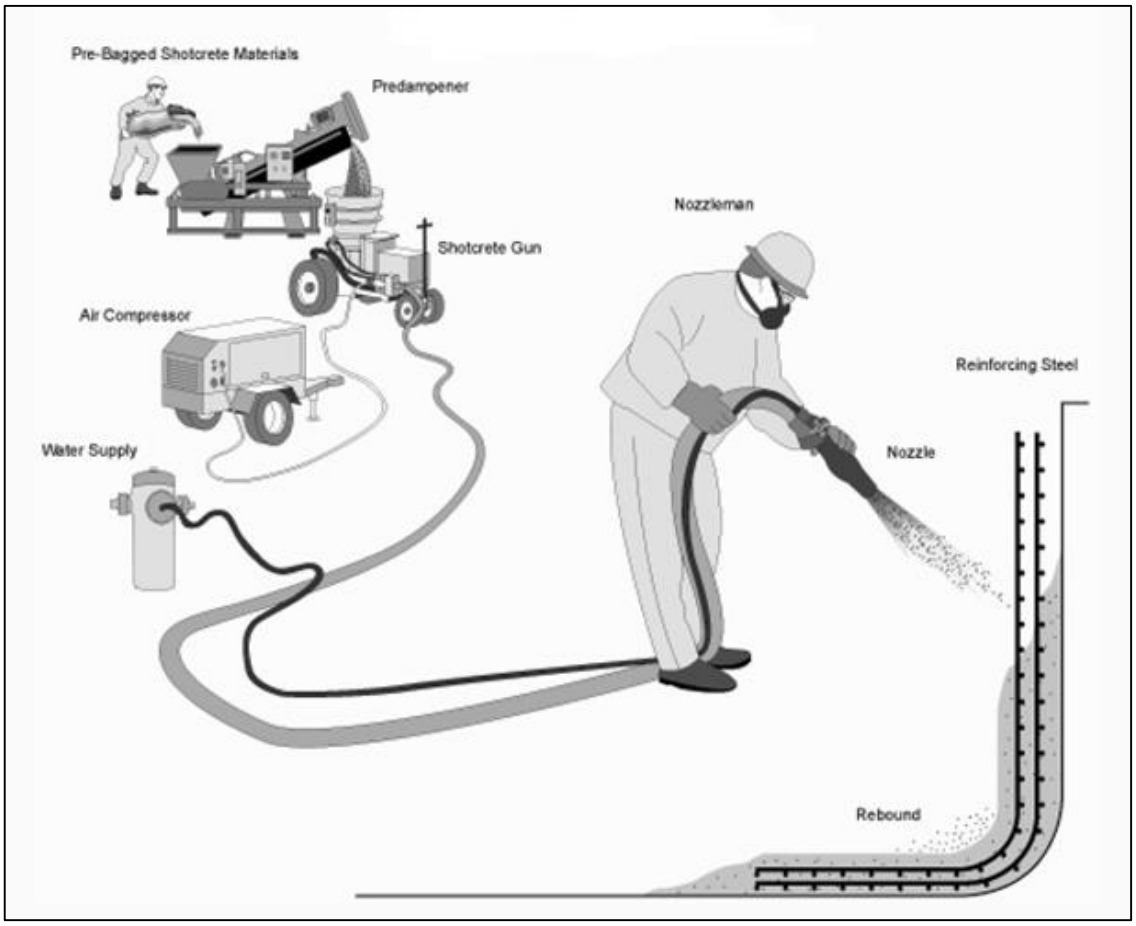

Figure 2. Dry mix process (American Shotcrete Association (ASA), 2014).

1.3.2. Wet-mix Method

The cementitious material, aggregate, water, and admixtures are thoroughly mixed as would be done for conventional concrete. The mixed material is fed to the delivery equipment, such as a concrete pump, which propels the mixture through the delivery hose by positive displacement or by compressed air (US Army Corps of Engineers, 1993). Additional air is added at the nozzle to increase the nozzle discharge velocity and consolidation of the material into the receiving surface (ASA, 2014).

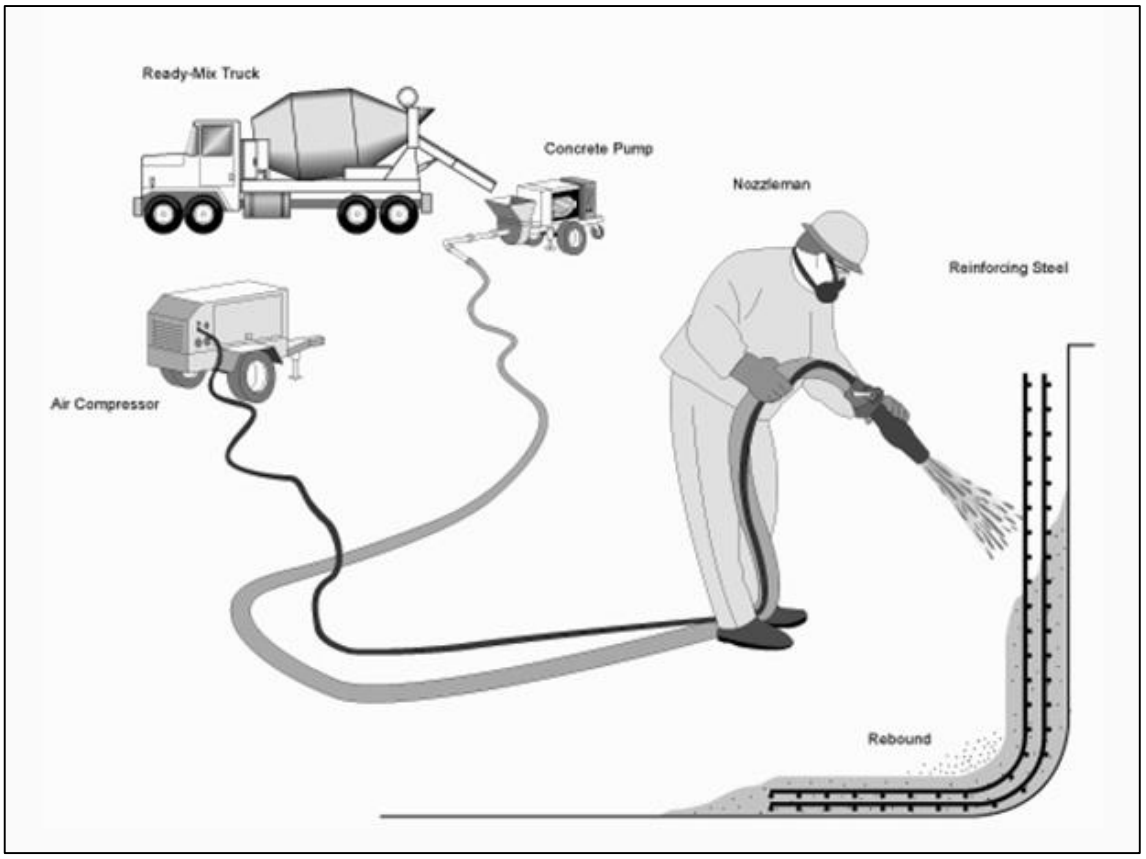

Figure 3. Wet mix process (American Shotcrete Association (ASA), 2014).

The advantages of the wet-mix method compared to the dry-mix method can be summarized as follows (Melbye T, 1994):

- Far less rebound. A loss of 5–10 % is normal with use of correct equipment and trained personnel. These figures also apply to the spraying of fibre reinforced concrete;
- Much larger production and consequently improved total economy;
- Better working environment; dust problem reduced;
- Higher compressive strength and very little variation in results;

- Use of steel fibres and new advanced admixtures;
- Thicker layers because of effective use of the admixing materials;
- Controlled water dosage (constant, defined w/c ratio);
- Improved bonding.

On the other hand, this method also has some disadvantages compared to the dry-mix method, these are the following:

- Limited conveying distance (max. 300 m);
- Only limited interruptions;
- Increased demands on aggregate quality;
- Cleaning costs.

1.4. CONSTITUENT MATERIALS OF SHOTCRETE MIX

The principal elements to compose the shotcrete mix are the following:

- Cement content: For the manufacture of the dry mix, the proportion of the binder is usually between 250 and 450 kg per 1000 litres of aggregate or 320 to 460 kg per m^3 of concrete. In order to judge the actual cement content of the sprayed concrete applied, the rebound must be considered (Melbye T, 1994).
- Water: His quality can have a significant effect on shotcrete performance. Mixing water should be drawn from a source of acceptable quality complying and comprise potable water if possible. If potable water is not available then further testing is required to determine suitability (Concrete Institute of Australia, 2010).

  The water/cement ratio is a decisive factor for the quality of sprayed concrete. The total amount of water used with dry mixes is made up of the mixing water added at the nozzle and the moisture already in the aggregate. In practice, however, the water/cement factor is fairly constant, as there is a limited scope for varying the mixing water quantity: If too little water is added, the result is an immediate excess of dust; if too much water is added, the sprayed concrete does not adhere to the surface but runs down instead. Where work is carried out properly, the water/cement factor varies only slightly and remains below 0.5 (Melbye T, 1994).

- Sand and Aggregates: Forms the bulk of sprayed concrete. A smooth grading curve is essential and rounded aggregates are preferred to angular particles. In a sprayed concrete mix tend to be more fine particles (Thomas A, 2008).
- Natural moisture content: An important aspect of the dry mix is also the natural moisture content. Where the mix is too dry, spraying causes too much dust. If the natural moisture content is too high, this may lead to problems: The sprayed concrete throughput drops drastically, machines and conveying lines become encrusted and get blocked. Ideally, the natural moisture content should lie between 3 and 6% (Melbye T, 1994).
- Admixtures: Various admixtures are available for controlling the properties of sprayed concrete. The most important of these are fast setting admixtures (accelerators). These admixtures reduce the setting time. Sprayed concrete has a quicker setting and higher early strength. This allows subsequent layers of sprayed concrete to be applied sooner and in greater thicknesses.

  On large-scale projects, accelerators definitely help to increase productivity and are an important pre-requisite for many applications. In underground construction works and pit curbing, for instance, the early strength of the sprayed concrete is decisive and an essential requirement (Melbye T, 1994).
- Additives: Unlike chemical admixtures, the action of additives is mainly physical. These substances, lead to an important improvement in the quality of the sprayed concrete, apparent in the increased compressive strength and density (Melbye T, 1994).
- Fibres: For sprayed concrete, steel and synthetic fibres can be used. Their chief virtue lies in the fact that they lead to an improved fracture energy and/or shrinkage behaviour of the sprayed concrete (Melbye T, 1994).

1.5. PROPERTIES OF SHOTCRETE

As is the case with conventional concrete, shotcrete properties vary dramatically depending on water-cement ratio, aggregate quality, size, and type, admixtures used, type of cement used, and construction practices. The proper use of admixtures, fibers, silica fume, and polymers can improve certain properties. Depending on the needs of the particular application, properties of the shotcrete materials and mixtures should be tested prior to final application (US Army Corps of Engineers, 1993).

- Strength: In terms of compressive and flexural strength, shotcrete can produce strength generally equivalent to conventional concrete. Typical compressive strength is cited in the literature at a value of 10,000 psi. The ratio between compressive and flexural strength appears to be the same as for conventional concrete. Early strength of shotcrete can be very high, reaching 1,000 psi in 5 hours and 3,000 psi in 24 hours (US Army Corps of Engineers, 1993).
- Modulus of Elasticity: Is a measure of the mechanical rigidity of shotcrete. The Modulus of Elasticity generally falls between 25-30 GPa at an age of 1 year. Accelerated shotcrete is generally less stiff than non-accelerated shotcrete. The Modulus of Elasticity is affected by the type of coarse aggregate used in a mix, but is difficult to control and therefore is rarely specified in shotcrete applications (Concrete Institute of Australia, 2010).
- Toughness. The addition of fibers to shotcrete can result in a product displaying significant load carrying capability after the occurrence of the first crack. The relationship of post-crack load capacity to load capacity at first crack is defined as toughness. The type, size, shape, and amount of fiber determines the extent of this performance (US Army Corps of Engineers, 1993).
- Shrinkage: Drying shrinkage is most influenced by the water content of the mixture. Typical values of unrestrained shrinkage range from 600 to 1,000 millionths. Shrinkage is reduced in coarse-aggregate shotcrete and increased in shotcrete without coarse aggregate or shotcrete subject to high rebound.
- Resistance to freezing and thawing: Wet-mix shotcrete frost resistance is ensured by entraining a proper air-void system. Typically, an air content of 8 to 12 percent in the mixture results in in-place shotcrete having a proper air-void system. Although many dry-mix applications have performed well when subjected to mild freezing and thawing, dry-mix shotcrete is more subject to problems from freezing and thawing than wet-mix shotcrete. This is due to the difficulty in entraining air and creating an adequate air-void system in dry-mix shotcrete (US Army Corps of Engineers, 1993).
- Density: The ratio mass/unit volume of good quality weight shotcrete is typically between 2200 and 2400 kg/m^3. Variations will occur as a result of changes in mix design, selection of source rocks such as basalt, dolerite, or similar high-density rocks to produce aggregates, and changes in compaction. The relative

density of in-place shotcrete compared to the cast shotcrete as supplied provides an indication of application quality and should be greater than 98% (Concrete Institute of Australia, 2010).

- Creep: Is the time-dependent deformation of a material under load. The creep strain suffered by a material is commonly expressed as a multiple of the short-term strain suffered as a result of elastic deformation. This multiplier is termed the 'creep coefficient'. The creep of shotcrete in flexure is not necessarily related to the creep of the same material in compression, especially after cracking has occurred. For a well-designed shotcrete mix with a low water-cementitious ratio, a magnitude of creep strain similar to those exhibited by high–quality cast concrete can be expected. When the water content is high the creep strain suffered under a given level of stress will be higher (Concrete Institute of Australia, 2010).

1.6. SPRAYED CONCRETE IN TUNNELING

The sprayed concrete is ideal to effectively stabilize earth and rock excavations accompanied by a variety of reinforcement and anchoring systems. Using shotcrete for soil stabilization in excavation has greater advantages than traditional techniques.

The sprayed concrete provides early ground support after blasting or excavation; early strength development that offers flexibility to allow ground stabilization and stress relief. In addition, it has the ability to adjust to the natural irregular profile of the soil without formwork and provides long-term stability because it can be used as a final or permanent coating, which makes it ideal for use in mining and tunneling (ASA, 2014).

The main reasons why the shotcrete technique for the tunnel design is adopted are the following (Thomas A, 2008):

- Sprayed concrete is a structural material that can be used as a permanent lining;
- The material behavior of shotcrete (which is initially soft and creeps under load but can withstand large strains at an early age) is compatible with the goal of a lining which permits ground deformation (and therefore stress redistribution in the ground);
- The material behavior (specifically the increase in stiffness and strength with age) is also compatible with the need to control this deformation so that strain softening in the ground does not lead to failure;

- Sprayed concrete lining can be formed as and when required and in whatever shape is required. Hence the geometry of the tunnel and timing of placement of the lining can be tailored to suit a wide range of ground conditions. Sprayed concrete can also be combined with other forms of support such as rock bolts and steel arches.

The use of Sprayed Concrete Lining (SCL) is an established method of soft ground tunneling using sprayed concrete to support the excavation both temporarily and permanently. Compared with other tunneling methods, such as using a Tunnel Boring Machine (TBM), the biggest advantage of the SCL technique is that it allows tunnels and junctions to be built at varying cross sections and sizes with relative ease. Besides, the SCL technique has low mobilization costs, making it suitable for short lengths of tunnel construction (Su, J. et al, 2013).

The SCL designed as temporary structures consisting of a layer of temporary sprayed primary lining, a layer of sheet waterproofing membrane and another layer of permanent cast secondary lining, dominated the market; mainly because of concerns over safety, water tightness and durability. The reason why the SCL was only treated as a temporary structure was due to two aspects: limitations of sprayed concrete technology and design method (Su, J. et al, 2013).

Several advances have made the use of SCL as a permanent structure possible: The shift in producing SCL from the dry-mix process to a wet-mix process substantially improved the quality control and productivity (Austin & Robins 1995). The adoption of alkali-free accelerators enabled rapid setting, improved early and final strengths, reduced environmental impact and enhanced safety for tunnel workers (Kusterle 1997). The use of fibre reinforcement instead of mesh reinforcement shortened construction programme and saved overall cost (Thomas 2008). The shift from hand spraying to robotic spraying speeded up progress and produced less material waste (Franzén 1992). The use of real-time surveying with total stations instead of lattice girders to ensure the correct profile of the tunnel excavation and control the lining thickness has accelerated construction and also removed a key durability concern.

The improvement in the quality of sprayed concrete has enabled the mature sprayed concrete to be treated as normal cast in-situ concrete, with the same long-term strength development, low permeability and durability performance (Annett et al. 1997).

Permanent sprayed concrete has been widely accepted in the world and in soft ground applications.

For soft ground SCL tunneling exists an option called Double Shell SCL, which consists of a layer of permanent sprayed concrete primary lining, a layer of spray applied waterproofing membrane and a layer of sprayed or cast secondary lining, with no adhesive and shear bond assumed at the sprayed concrete-membrane interfaces. Steel fibres are used as the main reinforcement, and no steel bars and meshes are used except at the tunnel junctions. Lattice girders are eliminated and the tunnel profile is controlled by the total station. This design option has been adopted on several important projects, such as Crossrail and A3 Hindhead in UK (Su, J. et al, 2013).

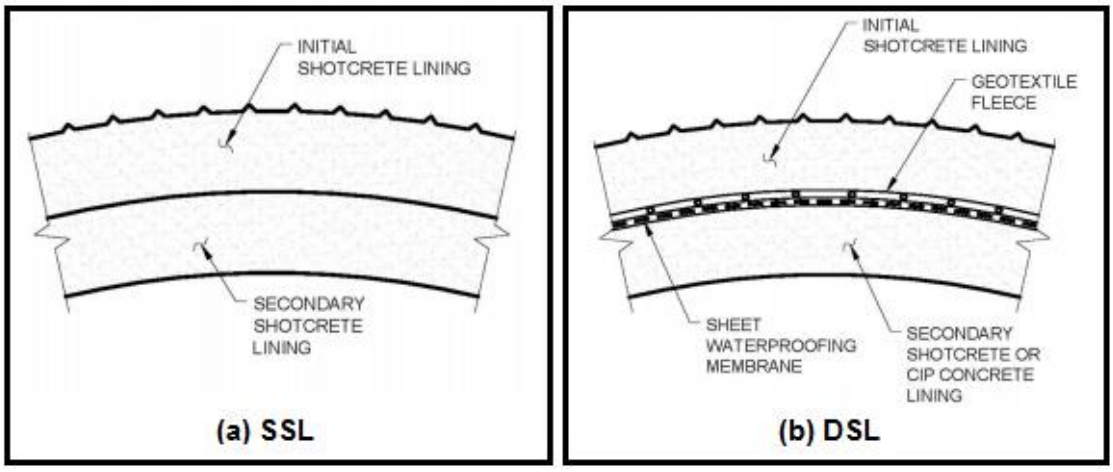

Figure 4. Two-pass lining system: (a) Single Shell Lining, used generally for temporary lining. (b) Double Shell Lining, commonly used in permanent structures (Sun Y. et al, 2013).

1.7. SHORT LITERATURE REVIEW ON SC MODELLING

Since the mechanical properties of SC are highly influenced by the hydration reaction and rate of the hydration reaction, non-linear elastoplastic behavior under compression and brittle behavior in tension, SC is normally modelled by using several numerical codes. Numerical analyses are helpful because different conditions can be considered (e.g. Son and Cording, 2007; Li and Wang, 2008; Mason and Stacey, 2008).

The most common model is a linear elastic method with a constant stiffness because of its simplicity (Thomas, 2009). Elastic models predict axial forces and bending moments in linings which are very high if compared with field data (e.g. Pöttler, 1990; Rokhar

and Zachow, 1997). According to Feenstra and de Borst (1993) this is normal as SC behaves in a linear elastic way only up to 30% of its UCS and the stiffness (e.g. elastic modulus, Poisson's ratio), varies considerably during the early age of the SC (Thomas, 2009). Stiffness can be artificially increased with age; however, as there are few experimental data for the stiffness at the design stage (Thomas, 2009), elastic modulus can be estimated by the UCS using the equation of Chang and Stille (1993):

$$E = 3.86 \cdot UCS^{0.60.} \quad \text{(with } E \text{ is in GPa and } UCS \text{ in MPa)} \qquad (1)$$

Berwanger (1986), Pöttler (1990), Cosciotti et al. (2001) found that increasing the stiffness of lining with age increase the stresses in it.

Another approach to model primary tunnel linings is assuming a linear elastic material behavior. One of the first attempts to include the early age material response in a tunnel lining design was the so called Hypothetical Modulus of Elasticity (HME) approach, which consists of reducing the Young's modulus of the SC by introducing factors which account for the increase in stiffness with time, creep and shrinkage, 3D tunnel advance and pre-relaxation ahead of the tunnel face (Pöttler, 1990). However, appropriate reduction factors are lacking in the literature and therefore the estimated HME values are purely based on back analysis and experience and therefore this approach results in too high internal forces (Schütz et al., 2011; Saurer et al., 2014).

Because failure in compression for SC is governed by cracking under uniaxial compression and crushing under multi-axial stress (Chen, 1982; Neville, 1995), the size of the micro-cracks increases. This in turn decreases the effective area resisting to the applied load and the stress rises faster than the load stress (Neville, 1995; Thomas, 2009), leading to strain hardening and the stress-strain curve for concrete in compression is non-linear at stresses above 30% of its UCS (Aydan et al., 1992). The non-linearity can be implemented in numerical modelling either as strain-hardening plasticity or non-linear elasticity. Cauchy, Hyperelastic and Hypoelastic models try to replicate the non-linear stress-strain behavior of concrete (e.g. Kotsovos and Newman, 1978; Chen, 1982; Moussa, 1993), however, Thomas (2009) points out that non-linear elastic models are valid only up to 85% of the ultimate strength.

Elastic perfectly plastic constitutive models require an explicit stress-strain relationship within the elastic region, a failure criterion and a flow-rule, which governs the plastic strains for compressive region (Thomas, 2009). Linear elasticity is assumed up to 30 to

40% of the UCS. Conventional yield criteria used in concrete are Mohr-Coulomb and Drucker-Prager. Associate flow rules assume that the plastic potential coincides with the yield function. Regarding the yield in tension the Rankin criterion is normally employed, therefore brittle fracture occurs when the maximum principal stress reaches a value equal to the tensile strength (Chen, 1982). In many normal loads failure in tensions (cracks) may occur while UCS is well below the failure level (Chen, 1982). Among plastic models, Meschke (1996), Schütz et al. (2011) and Schädlich and Schweiger (2014), to name a few, developed sophisticated constitutive model for SC based on viscoplasticity, elasto-plasticity and elastoplastic strain hardening/softening plasticity.

In this document a new numerical model based on the finite elements using the method of hyperstatic reactions (e.g. Duddeck and Erdmann, 1985; Leca and Clough, 1992) is presented to model the interaction SC lining-ground during excavation phases. The model is particularly suitable for the dimensioning of support structures (Oreste 2007; Do et al., 2014a, 2014b; Hassani and Basirat, 2016). The model is able to analyze the behavior of circular linings, considering the interaction between the lining and the rock. The lining is simulated across trapezoidal elements describing half of the entire profile around the tunnel and the interaction is taken into account through normal and tangential springs present on the nodes of the model, with the ideal elastic-plastic behavior.

2. EVOLUTION OF THE SHOTCRETE MECHANICAL CHARACTERISTICS OVER THE TIME

The primary material property specified for plain shotcrete is the compressive strength, this is the resistance provided by a material to an axially applied crushing force. The unconfined compressive strength (UCS) of hardened shotcrete is one of many indicators of the quality of the concrete. The UCS should be used as an indicator of the compressive strength of a mix once hardened, and it can be used as an indirect measure of other mechanical properties of a mix (Concrete Institute of Australia, 2010).

It is important to distinguish between the compressive strength of shotcrete as supplied compared to its performance in compression in-place. The strength of a mix as supplied can be affected by many variables during the placing process such as temperature, addition of set accelerators, poor spraying and compaction, and inadequate curing. Specifications for Unconfined compressive strength (UCS) are 20MPa for temporary SC and 40MPa or higher for permanent SC (Thomas, 2009).

The compressive strength of shotcrete as sprayed should never be determined by spraying shotcrete into cylinder molds because of excessive collection of rebound within the molds. The compressive strength of shotcrete as-supplied is best measured using cast cylinders that incorporate concrete sampled directly as supplied (Concrete Institute of Australia, 2010).

2.1. EARLY-AGE STRENGTH

Shotcrete for ground support is often required to reach a minimum strength at an early age often within the first few hours after spraying. Early-age strength is the strength of the shotcrete required at a time earlier than the conventional 28 days specified for normal concrete supply (Concrete Institute of Australia, 2010).

It is important to define the timespan over which the strength of shotcrete can be classed as early age. Shotcrete of ages under 24 hours is generally considered fresh shotcrete. Early-age shotcrete is then described as shotcrete that is 1–3 days old after application. Yet, testing shotcrete during these early periods is only necessary until it is deemed safe to reenter, or the strength of the shotcrete is at a level that would permit construction to continue underneath or in nearby locations (Mohajerani A et al, 2015).

The early-age strength of SC is frequently more important than its ultimate strength. The advance speed of tunnel operations is strongly influenced by the rate of development of early-age strength, since it determines, both in soft ground and weak rock, when excavation face can proceed again. As a matter of fact, re-entry is mainly driven by the tunnel drive progression to ensure the safety of personnel to continue development (Mohajerani et al., 2015). Re-entry times range from 2 to 4h, where the Unconfined Compressive Strength (UCS) reaches 1MPa (Clements, 2004; Concrete Institute of Australia, 2010). However, it is important to note that different places have different standards for a safe reentry strength (Mohajerani A et al, 2015).

This strength development determines when heading can continue to advance. The early strength development determines the progress with tunneling (Höfler J, 2004). The aim of testing shotcrete early-age strength is to determine safe reentry times for tunneling and mining drive progression. Therefore, rather than just determining a strength value that is deemed adequate, it is important to understand what types of failure early-age linings are subjected to in order to better understand and develop testing techniques (Mohajerani A et al, 2015).

Through experimental work, Bernard (2008) determined that there are two main types of failure mode for early-age shotcrete. These are shear punching failure and flexural delaminating failure. The majority of shotcrete failures are the result of individual loose rocks and small blocks of fractured zones punching through the lining and that it is seldom the case that shotcrete linings fail in total collapse. Empirically it has been determined that a UCS of 0.5–1.0 MPa is deemed an adequate strength for shotcrete to protect against rock-fall (Iwaki et al, 2001).

The inability to obtain direct UCS values for shotcrete strength presents the issue that the testing methods currently being used in the industry make use of a correlation factor to convert their measured data to UCS values. Based on the available literature, exist various successful testing methods like: Beam End Testing, soil penetrometer, meyco needle penetrometer, pneumatic pin penetration and shear wave velocity (Mohajerani A et al, 2015).

2.2. FINAL STRENGTH

Alongside the early strength required specifically for sprayed concrete, there are mechanical requirements for the hardened sprayed concrete, just as there are for

conventional concrete, generally after 28 days. The compressive strength is measured on cores taken from the structure or from sprayed panels (Höfler J, 2004).

The properties of the sprayed concrete are tested on samples taken directly from the structure or from panels sprayed parallel to the application under conditions of maximum similarity and then taken for sampling without destroying the structure. Sprayed panels with defined dimensions are also used for the plate test to determine the tensile strengths and the ductility of the reinforced sprayed concrete (Höfler J, 2004).

2.3. EVOLUTION WITH TIME OF THE COMPRESSIVE STRENGTH

Due to the long process of setting of the cement and the growth of the crystals, the mechanical strength of the concrete increases during the course of time, however the maximum intensity of its growth occurs in the initial period of its setting (Sánchez J, 2015).

Because of the hydration process within the cement paste, the material properties of the SC gradually change with time, leading to a complex stress–strain history within the tunnel lining during construction, where the loading rate of the SC shell with respect to time plays a major role (Schütz et al., 2011).

The rate of hardening changes for different types of shotcrete. Some typical values of the uniaxial compressive strength of shotcrete in time are illustrated in Table 1 (Oreste, 2003).

Table 1. Typical values of uniaxial compressive strength (MPa) for three types of shotcrete (Hoek and Brown, 1980).

Type of shotcrete	Hardening time			
	1–3 h	3–8 h	1 day	28 days
Shotcrete without accelerants	0	0.2	5.2	41.4
Shotcrete with accelerants (3%)	0.69	5.2	10.3	34.5
Shotcrete with regulated hardening	8.27	10.3	13.8	34.5

The standards offer expressions to predict the evolution of mechanical properties over time. Sánchez J. (2015) indicates the following expression to obtain the average resistance of concrete to compression from the value of the average resistance to compression at the age of 28 days:

$$f_{cm}(t) = \beta_{cc}(t) \cdot f_{cm} \quad (2)$$

Where:

f_{cm}: Average compressive strength obtained by 28-day trial.

$\beta_{cc}(t)$: Coefficient that depends on the age of the concrete.

$$\beta_{cc}(t) = \exp(0{,}5 \cdot (1 - 28/t) \cdot s) \quad (3)$$

s: Coefficient that depends on the speed of hardening of the cement.

t: Concrete age in days.

3. THE HYPERSTATIC REACTION METHOD (HRM) FOR SOTHCRETE LINING DESIGN

3.1. DEFINITION OF HRM

The Hyperstatic Reaction Method (HRM) aims to study the behavior of a shotcrete lining under the loads applied by the rock mass and considering the interaction between the lining and the rock mass (Oreste, 2007, Do et al., 2014a). The HRM can model half of a tunnel section by beam elements connected by nodes: these elements can develop bending moments, axial forces and shear forces. The interaction between ground and support is represented by "Winkler" type springs in the normal (perpendicular to the lining) and tangential direction (parallel to the lining) for each node of the model.

HRM simulates only the lining and not the rock portion at the tunnel outline. This calculation method does not consider the excavation and support phases that occur in the tunnel, and the rock stress acting on the lining has to be considered. In general, two different types of load on the linings are required: vertical and horizontal. The identification of the stress acting on the lining is not easy and it is still characterized by an uncertainty. This is turn is linked to the uncertainties and variability present on other fundamental parameters of the interaction between the lining and the rock: the lithostatic tension state and the geomechanical quality of the intact rock. In order to have a summary evaluation of loads acting on the SC lining, the characteristic curve method can be considered (e.g. Oreste, 2003; 2009; 2015; Spagnoli et al., 2017).

It is possible to perform numerous calculations with the HRM in a few seconds, investigating the uncertainty effect of some input parameters on the calculation results. It is therefore possible to perform parametric analyzes to allow evaluating the calculation results by varying the uncertain parameters at a certain interval.

The developed model allowed performing an extensive parametric analysis considering the typical variability during rock tunnel excavation. This study is useful to a preliminary design of the SC linings required for a subsequent more complicated numerical analysis.

The model is also able to develop more complex analyzes, which allow to give to the elements representing the SC lining, more sophisticated features. As a matter of fact, it is possible to consider:

- An elastic modulus which evolves over time due to the concrete curing during loading of the linings during the advance of the excavation face;
- The mechanical characteristics which evolve over time according to a law of creep;
- The mechanical properties of the concrete with a possible hardening behavior law, in the presence of any reinforcing elements such as fibers.

In addition, studies are also possible to assess the behavior of the SC lining under dynamic conditions in the presence of earthquakes. Such studies are hardly performed by the usual numerical calculation methods due to the long calculation time.

To use the HRM, it is necessary to distinguish the active loads and the passive loads. The active loads that are applied directly to the support structure by the rock mass, these are the initial loads as ground and water pressure. The passive loads are bound with the equilibrium of the structure and the reaction of the rock mass to the displacement of the support structure. The support–rock interaction influences the stress state in the structure and this interaction depends on the mechanical characteristics of the rock mass. This method allows determining the bending moments, shear forces and axial forces inside each element of the lining in order to design it properly. (Oreste, 2007).

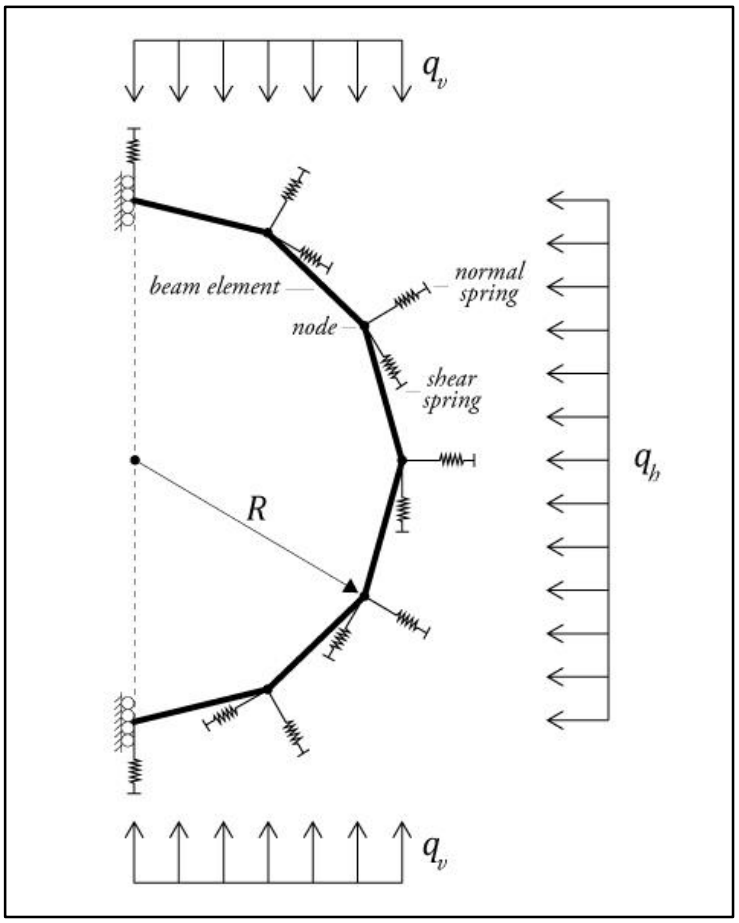

Figure 5. Sketch of the half tunnel section for the HRM in 2D. The SC lining is represented by the one-dimensional straight elements, which has an axial and flexural rigidity. At each node of the model two springs are connected which permit to consider in the model the normal and shear interaction with the rock. The external stress applied from the rock are vertical (q_v) and horizontal (q_h) stresses.

3.2. ASSEMBLING THE GLOBAL STIFFNESS MATRIX

In the HRM, the support structure is subdivided into a finite number of linear sub-dominions, called elements (for which it is possible to describe the stress–strain law in a simple way), which are connected for nodes. The mono-dimensional elements that are able to develop bending moments, axial forces and shear forces (Oreste, 2007).

The parameters characterize the generic beam element are: the inertia modulus J_Z and area A of the transversal section of the lining, the elastic modulus E of the constituent material and the length l (distance between the terminal connecting nodes). A unitary length in the direction of the tunnel axis is generally considered (Oreste, 2007).

The unknown parameters of the problem are the nodal displacement of the lining. From these displacements, it is then possible to obtain the stresses state inside each element and therefore the bending moments, shear forces and axial forces along the whole SC lining.

In order to obtain the unknown nodal displacements, the global stiffness matrix considering the connections to the surrounding rock mass must be evaluated.

The global stiffness matrix is obtained by assembling the local stiffness matrices [6x6] of each single element. The local stiffness matrix $[k_x]_i$ of the *i* element is obtained by setting the work produced by the inner forces of the finite element equal to that produced by the external nodal forces, which are evaluated according to a local reference system (Do, N.A. et al., 2014). One therefore obtains:

$$[k_x]_i \cdot \{s\}_i = \{f\}_i \tag{4}$$

Where the stiffness matrix $[k_x]_i$ of the element *i* in the local reference system is calculated in the follow way:

$$[k_x]_i = \begin{bmatrix} \frac{EA}{l} & 0 & 0 & -\frac{EA}{l} & 0 & 0 \\ 0 & \frac{12EJ_z}{l^3} & \frac{6EJ_z}{l^2} & 0 & -\frac{12EJ_z}{l^3} & \frac{6EJ_z}{l^2} \\ 0 & \frac{6EJ_z}{l^2} & \frac{4EJ_z}{l} & 0 & -\frac{6EJ_z}{l^2} & \frac{4EJ_z}{l} \\ -\frac{EA}{l} & 0 & 0 & \frac{EA}{l} & 0 & 0 \\ 0 & -\frac{12EJ_z}{l^3} & -\frac{6EJ_z}{l^2} & 0 & \frac{12EJ_z}{l^3} & -\frac{6EJ_z}{l^2} \\ 0 & \frac{6EJ_z}{l^2} & \frac{4EJ_z}{l} & 0 & -\frac{6EJ_z}{l^2} & \frac{4EJ_z}{l} \end{bmatrix} \tag{5}$$

$\{s\}_i$ is the vector of displacements in the nodes of element *i*, evaluated according to the local reference system.

$$\{s\}_i = [d_i \quad x_i \quad \varphi_i \quad d_{i+1} \quad x_{i+1} \quad \varphi_{i+1}] \tag{6}$$

d, x: Axial and transversal displacement in the local reference system

φ: Rotation of the element in correspondence to the nodes

$\{f\}_i$ is the vector of the external nodal forces and the nodal forces applied by the neighboring elements, which are evaluated according to the local reference system.

$$\{f\}_i = [fd_i \quad fx_i \quad m_{zi} \quad fd_{i+1} \quad fx_{i+1} \quad m_{z_{i+1}}] \tag{7}$$

$fd,\ fx$: Axial and transversal nodal forces evaluated in the local reference system

m: Bending moment in correspondence to the nodes of the element

Re-written in explicit form, becomes:

$$\begin{bmatrix} \frac{EA}{l} & 0 & 0 & -\frac{EA}{l} & 0 & 0 \\ 0 & \frac{12EJ_z}{l^3} & \frac{6EJ_z}{l^2} & 0 & -\frac{12EJ_z}{l^3} & \frac{6EJ_z}{l^2} \\ 0 & \frac{6EJ_z}{l^2} & \frac{4EJ_z}{l} & 0 & -\frac{6EJ_z}{l^2} & \frac{4EJ_z}{l} \\ -\frac{EA}{l} & 0 & 0 & \frac{EA}{l} & 0 & 0 \\ 0 & -\frac{12EJ_z}{l^3} & -\frac{6EJ_z}{l^2} & 0 & \frac{12EJ_z}{l^3} & -\frac{6EJ_z}{l^2} \\ 0 & \frac{6EJ_z}{l^2} & \frac{4EJ_z}{l} & 0 & -\frac{6EJ_z}{l^2} & \frac{4EJ_z}{l} \end{bmatrix} \cdot \begin{Bmatrix} d_i \\ x_i \\ \phi_i \\ d_{i+1} \\ x_{i+1} \\ \phi_{i+1} \end{Bmatrix} = \begin{Bmatrix} fd_i \\ fx_i \\ m_i \\ fd_{i+1} \\ fx_{i+1} \\ m_{i+1} \end{Bmatrix} \tag{8}$$

In this point it is necessary to move the equations of the each element from the local reference system to the global reference system. To do that, the displacement vector and the forces vector have to be multiplied by a rotation matrix $[\lambda]_i$.

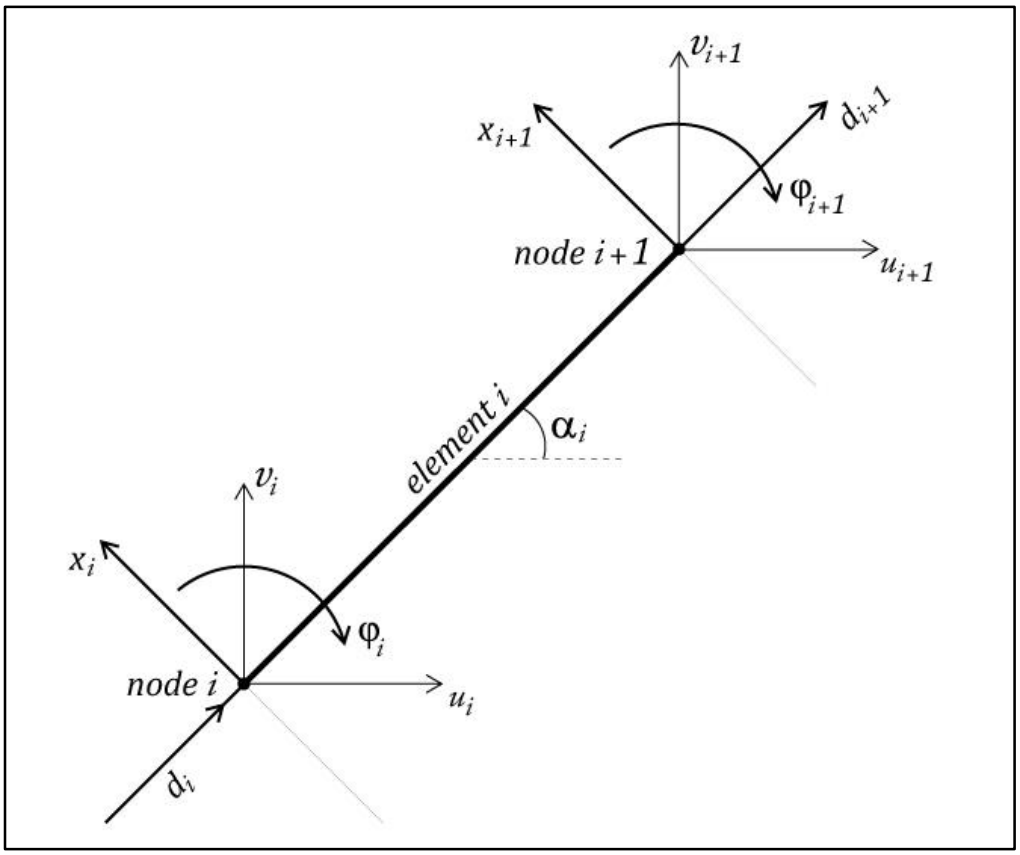

Figure 6. Scheme of the behaviour of a beam-type finite element, with reference to the local and global Cartesian coordinates.

In the global Cartesian reference system, the nodal displacements $\{s\}_i$ are connected to $\{S\}_i$ through the following matrix expression:

$$\{s\}_i = [\lambda]_i \cdot \{S\}_i \qquad (9)$$

$$[\lambda]_i = \begin{bmatrix} \cos\alpha_i & \sin\alpha_i & 0 & 0 & 0 & 0 \\ -\sin\alpha_i & \cos\alpha_i & 0 & 0 & 0 & 0 \\ 0 & 0 & 1 & 0 & 0 & 0 \\ 0 & 0 & 0 & \cos\alpha_i & \sin\alpha_i & 0 \\ 0 & 0 & 0 & -\sin\alpha_i & \cos\alpha_i & 0 \\ 0 & 0 & 0 & 0 & 0 & 1 \end{bmatrix} \qquad (10)$$

$$\begin{Bmatrix} d_i \\ x_i \\ \phi_i \\ d_{i+1} \\ x_{i+1} \\ \phi_{i+1} \end{Bmatrix}_x = \begin{bmatrix} \cos\alpha_i & \sin\alpha_i & 0 & 0 & 0 & 0 \\ -\sin\alpha_i & \cos\alpha_i & 0 & 0 & 0 & 0 \\ 0 & 0 & 1 & 0 & 0 & 0 \\ 0 & 0 & 0 & \cos\alpha_i & \sin\alpha_i & 0 \\ 0 & 0 & 0 & -\sin\alpha_i & \cos\alpha_i & 0 \\ 0 & 0 & 0 & 0 & 0 & 1 \end{bmatrix} \begin{Bmatrix} u_i \\ v_i \\ \phi_i \\ u_{i+1} \\ v_{i+1} \\ \phi \end{Bmatrix}_X \quad (11)$$

Where $\{S\}_i$ is the vector of the nodal displacements of element i; u_i and v_i are the displacements along axes X and Y in the global Cartesian reference system; φ is the rotation of the element, $[\lambda]_i$ is the rotation matrix or matrix of direction cosines of the element and α_i is the angle that forms the local Cartesian reference system of element with respect to the global Cartesian reference system.

In the same way, in the global Cartesian reference system, the nodal forces are given by the following matrix expressions:

$$\{f\}_i = [\lambda]_i \cdot \{F\}_i \quad (12)$$

$$\begin{Bmatrix} fd_i \\ fx_i \\ m_{zi} \\ fd_{i+1} \\ fx_{i+1} \\ m_{zi+1} \end{Bmatrix}_x = \begin{bmatrix} \cos\alpha_i & \sin\alpha_i & 0 & 0 & 0 & 0 \\ -\sin\alpha_i & \cos\alpha_i & 0 & 0 & 0 & 0 \\ 0 & 0 & 1 & 0 & 0 & 0 \\ 0 & 0 & 0 & \cos\alpha_i & \sin\alpha_i & 0 \\ 0 & 0 & 0 & -\sin\alpha_i & \cos\alpha_i & 0 \\ 0 & 0 & 0 & 0 & 0 & 1 \end{bmatrix} \begin{Bmatrix} Fx_i \\ Fy_i \\ M_i \\ Fx_{i+1} \\ Fy_{i+1} \\ M_{i+1} \end{Bmatrix}_X \quad (13)$$

Where $\{F\}_i$ is the vector of external nodal forces according to the global Cartesian reference system, Fx and Fy are the axial and transversal nodal forces and M is the bending moment in correspondence to the nodes of the element.

Making the necessary substitutions, it becomes possible to write in the global Cartesian reference system the following equation (Oreste, 2007).

$$[k_x]_i \cdot \{s\}_i = \{f\}_i \quad (14)$$

$$[k_x]_i \cdot [\lambda]_i \cdot \{S\}_i = [\lambda]_i \cdot \{F\}_i \quad (15)$$

$$([\lambda]_i^T \cdot [k_x]_i \cdot [\lambda]_i) \cdot \{S\}_i = \{F\}_i \quad (16)$$

$$[k_X]_i \cdot \{S\}_i = \{F\}_i \quad (17)$$

Where $[k_X]_i$ is the local stiffness matrix of the element i in the global Cartesian reference system:

$$[k_X]_i = ([\lambda]_i^T \cdot [k]_{xi} \cdot [\lambda]_i)_i \quad (18)$$

$$[k_X]_i = \begin{bmatrix} \frac{EA}{I}c^2+\frac{12EJ_z}{I^3}s^2 & \frac{EA}{I}c^2-\frac{12EJ_z}{I^3}s^2 & -\frac{6EJ_z}{I^2}s & -\frac{EA}{I}c^2-\frac{12EJ_z}{I^3}s^2 & -\frac{EA}{I}c^2+\frac{12EJ_z}{I^3}s^2 & -\frac{6EJ_z}{I^2}s \\ \frac{EA}{I}cs-\frac{12EJ_z}{I^3}cs & \frac{EA}{I}s^2+\frac{12EJ_z}{I^3}c^2 & \frac{6EJ_z}{I^2}c & -\frac{EA}{I}cs+\frac{12EJ_z}{I^3}cs & -\frac{EA}{I}s^2-\frac{12EJ_z}{I^3}c^2 & \frac{6EJ_z}{I^2}c \\ -\frac{6EJ_z}{I^2}s & \frac{6EJ_z}{I^2}c & \frac{4EJ_z}{I} & \frac{6EJ_z}{I^2}s & -\frac{6EJ_z}{I^2}c & \frac{2EJ_z}{I} \\ -\frac{EA}{I}c^2-\frac{12EJ_z}{I^3}s^2 & -\frac{EA}{I}cs+\frac{12EJ_z}{I^3}cs & \frac{6EJ_z}{I^2}s & \frac{EA}{I}c^2+\frac{12EJ_z}{I^3}s^2 & \frac{EA}{I}cs-\frac{12EJ_z}{I^3}cs & \frac{6EJ_z}{I^2}s \\ -\frac{EA}{I}cs+\frac{12EJ_z}{I^3}cs & -\frac{EA}{I}s^2-\frac{12EJ_z}{I^3}c^2 & -\frac{6EJ_z}{I^2}c & \frac{EA}{I}cs-\frac{12EJ_z}{I^3}cs & \frac{EA}{I}s^2+\frac{12EJ_z}{I^3}c^2 & -\frac{6EJ_z}{I^2}c \\ -\frac{6EJ_z}{I^2}s & \frac{6EJ_z}{I^2}c & \frac{2EJ_z}{I} & \frac{6EJ_z}{I^2}s & -\frac{6EJ_z}{I^2}c & \frac{4EJ_z}{I} \end{bmatrix} \quad (19)$$

Where: $c = cos(\alpha_i)$ and $s = sin(\alpha_i)$

The matrix $[k_X]_i$ is the local stiffness matrix in the global Cartesian reference system and it allows building the global stiffness matrix $[K]$. This matrix is obtained adding the local stiffness matrix along the diagonal of the global matrix using the criteria illustrated in Huebner et al (2001).

$$\begin{bmatrix} k_{1,a} & k_{1,b} & 0 & 0 & 0 & \cdots & 0 \\ k_{1,c} & k_{1,d}+k_{2,a} & k_{2,b} & 0 & 0 & \cdots & 0 \\ 0 & k_{2,c} & k_{2,d}+k_{3,a} & k_{3,b} & 0 & \cdots & 0 \\ 0 & 0 & k_{3,c} & k_{3,d}+k_{4,a} & \ddots & \cdots & 0 \\ 0 & 0 & 0 & \ddots & \ddots & \ddots & 0 \\ \vdots & \vdots & \vdots & \vdots & \ddots & \ddots & k_{i,b} \\ 0 & 0 & 0 & 0 & 0 & k_{i,c} & k_{i,d} \end{bmatrix} \cdot \begin{Bmatrix} S_1 \\ S_2 \\ S_3 \\ S_4 \\ \vdots \\ \vdots \\ S_{i+1} \end{Bmatrix} = \begin{Bmatrix} F_1 \\ F_2 \\ F_3 \\ F_4 \\ \vdots \\ \vdots \\ F_{i+1} \end{Bmatrix} \quad (20)$$

At the end of this stage, the matrix of the global stiffness $[K]$, is obtained. It should be noted that because the full cross-section of the tunnel lining is considered (Oreste, 2007).

Each components of local stiffness matrix contains information about 2 nodes, that why we add components to create the global stiffness. The global stiffness matrix is $(3i + 3)$ x $(3i + 3)$ size where i is the total number of elements. The vector of displacements $\{S\}$ and the vector of nodal forces $\{F\}$ both of them are constituted by $(3i + 3)$ elements (Oreste, 2007).

$[k_{i,a}], [k_{i,b}], [k_{i,c}], [k_{i,d}]$ are the sub-matrices of $[k_X]_i$,each of them of 3 x 3 dimension:

$$[k]_i = \begin{bmatrix} k_{i,a} & k_{i,b} \\ k_{i,c} & k_{i,d} \end{bmatrix} \quad (21)$$

$S_1, S_2, S_3, \ldots, S_{i+1}$ are the sub-vectors composed of the three displacements in each node:

$$\{S_i\} = \begin{Bmatrix} u_i \\ v_i \\ \varphi_i \end{Bmatrix} \quad (22)$$

$F_1, F_2, F_3, \ldots, F_{i+1}$ are the sub-vectors composed of the three external forces applied to each node:

$$\{F_i\} = \begin{Bmatrix} Fx_i \\ Fy_i \\ M_i \end{Bmatrix} \quad (23)$$

The unknown of the final equation is the displacement; therefore the matrix system has to be solved to found it.

The developed numerical model divides half of the tunnel section in 36 elements, the enumeration of elements starts from the lowest. The length of each element is constant and depends of the radius of the tunnel R.

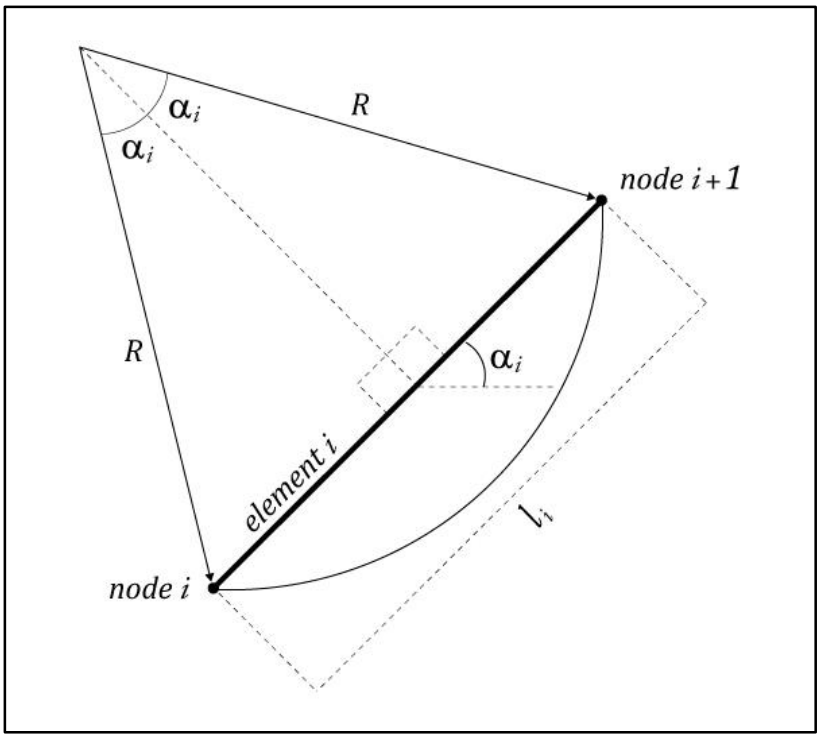

Figure 7. Scheme and calculation of beam element length.

The first element has an angle of inclination $\alpha_i = 2.5°$, for the rest of elements the rotation increases in 5°. For this case the length l is defined as:

$$l = 2 \cdot R \cdot cos(87.5°) \quad (24)$$

The code starts by calculating the local stiffness matrix of the first element, and then it writes the local stiffness matrix in the global reference system. This step is repeated for the 36 elements. The global stiffness matrix is created adding the local stiffness matrix along the diagonal of the matrix. Its dimension is (111×111). As each node is bound to 2 elements, except for the first node, the components of the stiffness matrix of the first element related to the second node is added to the component of the stiffness matrix of the second element related to the second node, and so on.

3.3. INTERACTION OF THE ROCK MASS WITH THE TUNNEL SUPPORT

The HRM assumes the hypothetical existence of normal and shear springs all around the support for simulate the interaction with the rock mass. For this Winkler's approach is used, where reactive forces of the foundation are assumed to be proportional to the deflection of the beam at every point. These develop forces that linearly depend on the relative displacements between the structure and the rock mass (Hassani et al., 2016).

Some of the elements of the stiffness matrix $[K]$ are modified along the diagonal to consider the presence of this interaction springs (Oreste, 2007).

The normal springs are located in the radial direction of the tunnel, i.e. in the perpendicular direction to the axis formed by the middle angle α_{medi} between two neighboring elements.

$$\alpha_{medi} = \frac{\alpha_i + \alpha_{i+1}}{2} \quad (25)$$

Where α_i and α_{i+1} are the angles of inclination of the element respect to the global reference system.

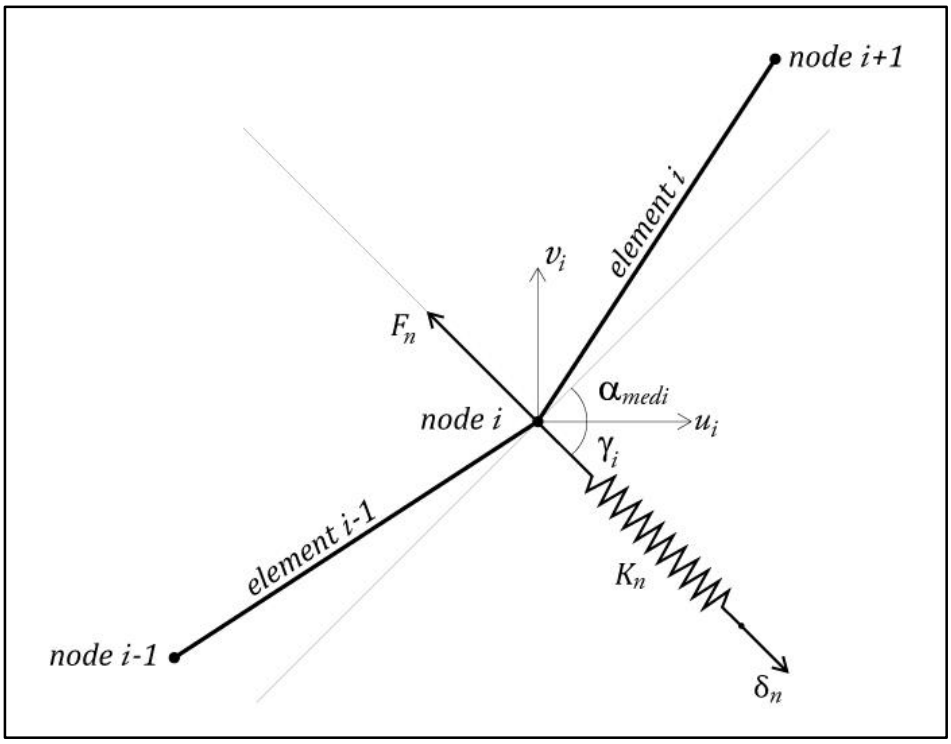

Figure 8. Details of the rock–support interaction through Winkler normal springs connected to the support nodes.

The radial spring induces a normal force Fn_i in the direction of the spring axis to each node. This Fn_i is an elastic force directly proportional to the normal stiffness of the interaction spring K_n and the nodal normal displacement δn_i between the structure and the rock mass.

$$Fn_i = K_n \cdot \delta n_i \quad (26)$$

Where δn_i is in terms of the horizontal and vertical displacements of the node in the global reference system u_i, v_i and the angle γ_i:

$$\delta n_i = u_i \cdot cos(\gamma_i) - v_i \cdot sin(\gamma_i) \quad (27)$$

$$\gamma_i = \frac{\pi}{2} - \alpha_{medi} \quad (28)$$

Using the components of this normal force Fn_i is possible to know the contribution of these normal springs to the global stiffness matrix $[K]$ as follows:

$$Fx_i = -Fn_i \cdot cos(\gamma_i) \quad (29)$$

$$Fx_i = -K_n \cdot [u_i \cdot cos(\gamma_i) - v_i \cdot sin(\gamma_i)] \cdot cos(\gamma_i) \quad (30)$$

$$Fx_i = -u_i \cdot K_n \cdot cos^2(\gamma_i) + v_i \cdot K_n \cdot sin(\gamma_i) \cdot cos(\gamma_i) \quad (31)$$

$$Fy_i = Fn_i \cdot sin(\gamma_i) \quad (32)$$

$$Fy_i = K_n \cdot [u_i \cdot cos(\gamma_i) - v_i \cdot sin(\gamma_i)] \cdot sin(\gamma_i) \quad (33)$$

$$Fy_i = u_i \cdot K_n \cdot sin(\gamma_i) \cdot cos(\gamma_i) - v_i \cdot K_n \cdot sin^2(\gamma_i) \quad (34)$$

As a result we obtain the matrix $[K_{N.S}]_i$, which contains the contribution to the global stiffness matrix $[K]$ due to the interaction of the support with the normal spring at node *i*, it must be adhered to the diagonal of the global stiffness matrix $[K]$ for each node.

$$[K_{N.S}]_i = \begin{bmatrix} K_n \cdot cos^2(\gamma_i) & -K_n \cdot sin(\gamma_i) \cdot cos(\gamma_i) & 0 \\ -K_n \cdot sin(\gamma_i) \cdot cos(\gamma_i) & K_n \cdot sin^2(\gamma_i) & 0 \\ 0 & 0 & 0 \end{bmatrix} \quad (35)$$

The shear springs are located in the tangential direction of the tunnel, i.e in the parallel direction to the axis formed by the middle angle α_{medi} between two neighboring elements.

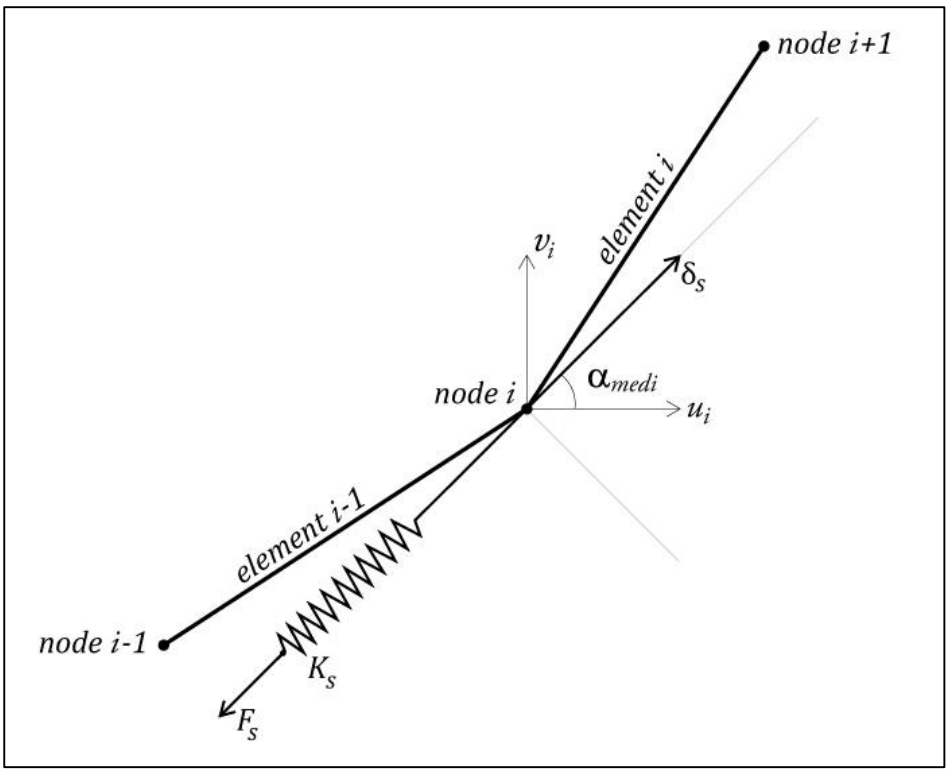

Figure 9. Details of the rock–support interaction through Winkler shear springs connected to the support nodes.

The tangential spring induces a shear force Fs_i in the direction of the spring axis. This force is an elastic force directly proportional to the shear stiffness K_s of the interaction spring connected to node and the nodal tangential displacement δs_i between the structure and the rock mass.

$$Fs_i = K_s \cdot \delta s_i \quad (36)$$

Where δs_i is in terms of the horizontal and vertical displacements of the node in the global reference system u_i, v_i and the angle α_{medi}:

$$\delta s_i = u_i \cdot cos(\alpha_{medi}) + v_i \cdot sin(\alpha_{medi}) \quad (37)$$

In the same way as in normal springs, using the components of this shear force Fs_i is possible to know the contribution of these shear springs to the global stiffness matrix $[K]$ as follows:

$$Fx_i = -Fs_i \cdot cos(\alpha_{medi}) \quad (38)$$

$$Fx_i = -K_s \cdot [u_i \cdot cos(\alpha_{medi}) + v_i \cdot sin(\alpha_{medi})] \cdot cos(\alpha_{medi}) \quad (39)$$

$$Fx_i = -u_i \cdot K_s \cdot cos^2(\alpha_{medi}) - v_i \cdot K_s \cdot sin(\alpha_{medi}) \cdot cos(\alpha_{medi}) \quad (40)$$

$$Fy_i = -Fs_i \cdot sin(\alpha_{medi}) \quad (41)$$

$$Fy_i = -K_s \cdot [u_i \cdot cos(\alpha_{medi}) + v_i \cdot sin(\alpha_{medi})] \cdot sin(\alpha_{medi}) \quad (42)$$

$$Fy_i = -u_i \cdot K_s \cdot sin(\alpha_{medi}) \cdot cos(\alpha_{medi}) - v_i \cdot K_s \cdot sin^2(\alpha_{medi}) \quad (43)$$

$$[K_{S.S}]_i = \begin{bmatrix} K_s \cdot cos^2(\alpha_{medi}) & K_s \cdot sin(\alpha_{medi}) \cdot cos(\alpha_{medi}) & 0 \\ K_s \cdot sin(\alpha_{medi}) \cdot cos(\alpha_{medi}) & K_s \cdot sin^2(\alpha_{medi}) & 0 \\ 0 & 0 & 0 \end{bmatrix} \quad (44)$$

Where $[K_{S.S}]_i$ is the matrix of contribution to the global stiffness matrix $[K]$ due to the interaction of the support with the tangential spring at node *i*.

The global stiffness matrix $[K]$ is complete with the spring's contribution. The constraints of the structure are placed by simply eliminating, from the stiffness matrix, the rows and columns that refer to the nodal displacement that is prevented by the constraint. The dimension of $[K]$ therefore reduces in function of the number of degrees of freedom that have been eliminated by the constraints (Oreste, 2007).

In the code the boundary condition allows reducing the global stiffness matrix because there are not rotation and horizontal displacement in the first node and the 37th node due to the symmetry of the tunnel. The dimension of the global stiffness matrix becomes (107×107).

3.4. BEHAVIOUR OF THE INTERACTION SOIL-STRUCTURE

The lining-rock mass interaction can be described through a pressure–displacement relation $(p - \delta)$ with an elastic-perfectly plastic behavior, where p_{lim} is the maximum reaction pressure that the rock mass can offer and δ_{lim} is the maximum displacement of the elastic zone before starting the irreversible displacement zone, i.e. when the mass rock arrives at fault. .

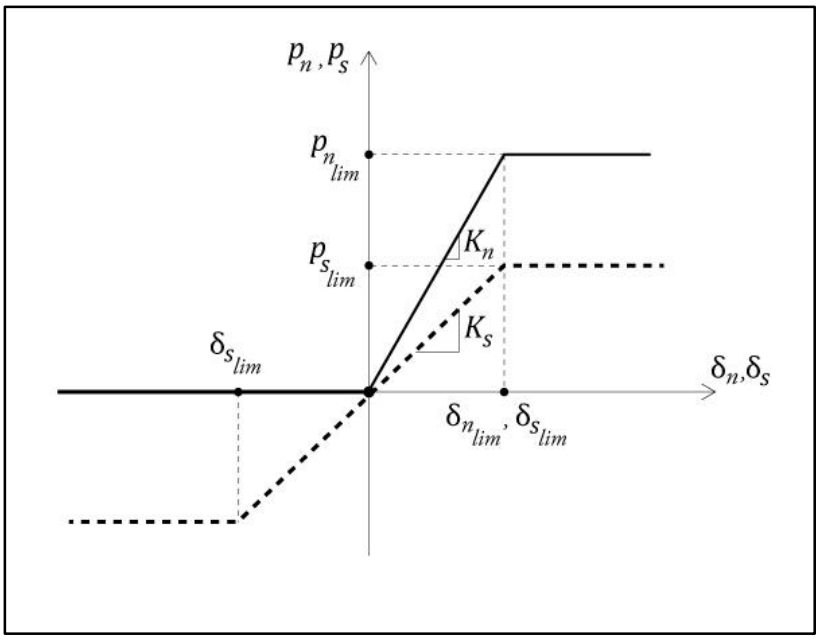

Figure 10. Behavior of the elastic-perfectly plastic lining-rock mass interaction between the reaction pressure of the rock mass p and the displacement of the lining δ, at each node, in the normal (n) and tangential (s) direction.

The value of the maximum normal reaction pressure $p_{n_{lim}}$ can be estimated starting from the cohesion values c_{rm} and the angle of friction φ_{rm} of the rock mass, under the hypothesis of zero confining pressure (Oreste, 2007).

$$p_{n_{lim}} = \frac{2 \cdot c_{rm} \cdot cos(\varphi_{rm})}{1 - sin(\varphi_{rm})} \quad (45)$$

The value of $p_{s_{lim}}$ is calculated using the strength criterion of Mohr-Coulomb in the following way:

$$p_{s_{lim}} = \left[Fn - Fx_i \cdot sin(\alpha_{medi}) + Fy_i \cdot cos(\alpha_{medi})\right] \cdot \frac{tan(\varphi_{rm})}{[l \cdot \cos(\alpha_i - \alpha_{medi})]} + c_{rm} \quad (46)$$

Where Fn is the normal force due to the interaction of the support with the rock mass, Fx_i and Fy_i are the external loads applied at node in the direction X and Y in the global reference system, l is the element length, c_{rm} is the cohesion and φ_{rm} is the friction angle of the rock mass. As only compressive loads are possible in the normal direction, in which the tunnel support moves towards the rock mass (Do, N.A. et al., 2014), the value of Fn can change:

$$p_{s_{lim}} = If\ \delta n_i < 0\ , Fn = 0 \quad (47)$$

$$If\ \delta n_i > \delta n_{lim}\ , Fn = Fn_{lim} = p_{n_{lim}} \cdot l \cdot cos(\alpha_i - \alpha_{med_i}) \quad (48)$$

The initial stiffness of the normal and shear springs has to be determined (K_n and K_s respectively). The initial normal stiffness of the springs K_n are usually evaluated from the rock mass data using very simple relationships as those derived from Winkler theory. For example, Oreste (2007) suggests:

$$K_n = \frac{2 \cdot E_{rm}}{R} \quad (49)$$

The initial shear stiffness of the springs K_s are usually evaluated in terms of the normal stiffness Kn through a coefficient smaller than 1. In this case:

$$K_s = 0.5 \cdot K_n \quad (50)$$

Where E_{rm} is the elastic modulus of the rock mass and R is the radius of the tunnel.

The normal springs disappear in zones where the support structure moves towards the tunnel: this is generally the case of the roof, but when the horizontal active loads are greater than the vertical ones, it occurs at the sidewalls. Therefore, only compressive loads are possible in the normal direction, where the tunnel support moves towards the rock mass: normal springs only work in compression (Hassani et al., 2016).

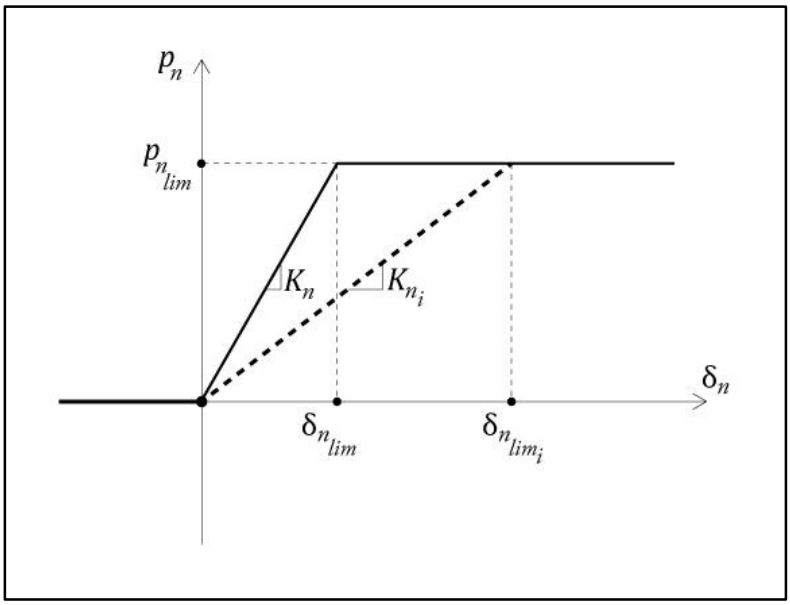

Figure 11. Change of normal spring stiffness K_n when the limit stress condition are reached.

The shear springs instead allow one to take both the positive and negative stresses in the tangential direction into account (Do, N.A. et al., 2014).

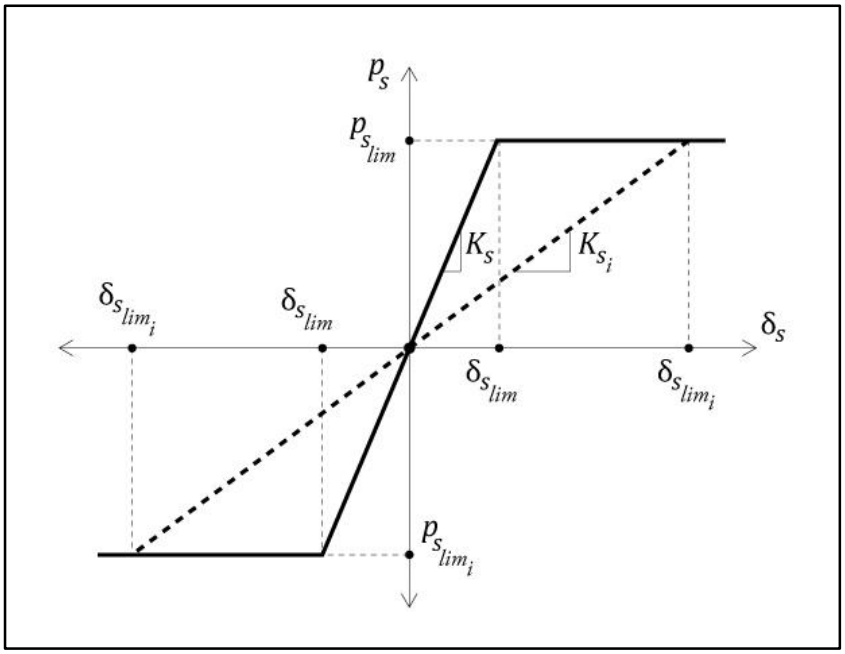

Figure 12. Change of normal spring stiffness K_s when the limit stress condition are reached.

Besides, when the displacement at each node is greater than the limit displacement ($\delta_{n_{lim}} = \frac{p_{n_{lim}}}{Kn}$ or $\delta_{s_{lim}} = \frac{p_{s_{lim}}}{Ks}$), the plastic condition has been reached and the normal and tangential stiffness of the springs become lower than their initial values: the determination of the stiffness is evaluated during the numerical calculation as the ratio between $p_{lim}$and the reached nodal displacement (in the normal or tangential direction).

3.5. LOADS APPLIED TO THE SC LINING

Loads considered in the design of the lining are categorized according to their frequency of magnitude, continuity and variation. Vertical and horizontal earth pressure, water pressure, dead weight of the lining, effects of surcharge and other factors are fundamental ones, which continuously act on the lining without large variation and should be always considered in the design of lining (Hassani et al., 2016).

The evaluation of the external active loads acting on the lining results to be difficult. Generally, the convergence-confinement method can be used. However, some authors obtained empirical correlations to estimate the active external vertical load q_v (e.g. Barton et al., 1974; Unal, 1983; Bieniawski, 1989; Singh et al., 1992; Goel et al., 1995;

Barton, 2002). The horizontal loads q_h (Fig. 5) are usually considered to be a percentage of the vertical ones (Oreste, 2007). The horizontal and vertical external forces applied at each node are calculated on the base of the external active loads:

$$Fy_i = q_v \cdot \left(\frac{l \cdot \cos(\alpha_i) + l \cdot \cos(\alpha_{i-1})}{2} \right) \quad (51)$$

$$Fx_i = -q_h \cdot \left(\frac{l \cdot \sin(\alpha_i) + l \cdot \sin(\alpha_{i-1})}{2} \right) \quad (52)$$

For the first and last node the external forces are:

$$Fy_i = q_v \cdot \left(\frac{l \cdot \cos(\alpha_i)}{2} \right) \quad (53)$$

$$Fx_i = -q_h \cdot \left(\frac{l \cdot \sin(\alpha_i)}{2} \right) \quad (54)$$

3.6. CALCULATION OF DISPLACEMENTS AND INTERNAL FORCES IN THE BEAM ELEMENT

Once the vector of external forces applied to the nodes $\{F\}$ and the global stiffness matrix of the tunnel support $[K]$ are built, it is possible to obtain the vector of the displacements in the nodes $\{S\}$ evaluated according to the global Cartesian reference by the expression:

$$\{S\} = [K]^{-1} \cdot \{F\} \quad (55)$$

Having the vector of displacement in the global reference system $\{S\}_i$, the vector of displacements in the local reference system $\{s\}_i$ is found for each element.

$$\{s\}_i = [\lambda]_i \cdot \{S\}_i \quad (56)$$

Later, the code calculates the total vector force in the local reference system in each element using this equation:

$$[k_x]_i \cdot [\lambda]_i \cdot \{S\}_i = \{f\}_i \quad (57)$$

The internal vector $\{f_{int}\}_i$ is obtained subtracting the total vector force $\{f\}_i$ to the external vector force. $\{f_{ext}\}_i$:

$$\{f\}_i = \{f_{ext}\}_i + \{f_{int}\}_i \quad (58)$$

$$\{f_{int}\} = \{f\}_i - \{f_{ext}\}_i = [k_x]_i \cdot \{s\}_i - \{f_{ext}\}_i \quad (59)$$

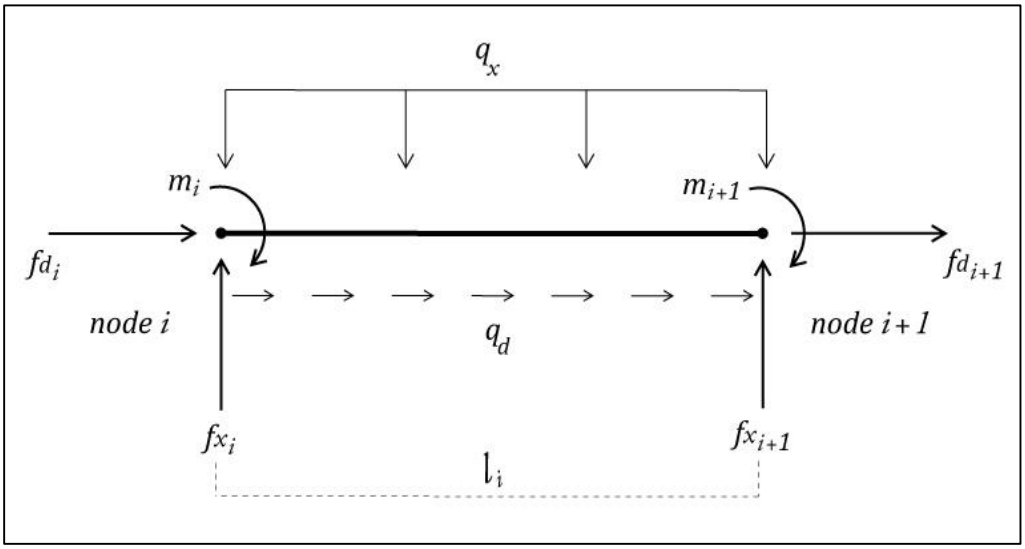

Figure 13. Details of distributed forces q_d and q_x in the beam element.

The equivalent nodal external forces fd_i, fx_i can be obtained in the case of distributed loads q_x and q_d in the beam element (Gugliota, 2002) as follows, the nodal moments m_i for this case zero:

$$\{f_{ext}\}_i = \begin{Bmatrix} fd_i \\ fx_i \\ m_i \\ fd_{i+1} \\ fx_{i+1} \\ m_{i+1} \end{Bmatrix} = \begin{Bmatrix} q_d \cdot \frac{l}{2} \\ q_x \cdot \frac{l}{2} \\ 0 \\ q_d \cdot \frac{l}{2} \\ q_x \cdot \frac{l}{2} \\ 0 \end{Bmatrix} \quad (60)$$

Finally, from the internal force vector it is possible to obtain the value of the axial force, shear force and bending moment at each node and also along the whole lining perimeter.

The developed code divides the external active loads in 25 steps, with a load increases of 4% for each step. The determination of the stiffness of the springs at each node is evaluated on the basis of the nodal displacements reached in the previous step.

3.7. NUMERICAL EXAMPLE OF HRM

The numerical model was used to study the behavior of SC linings in circular tunnel, for the typical situations which may occur during real lining installations. 1944 analyses were developed, by modifying the input parameters of the calculation within the range of variability.

Three different tunnel radius values have been considered: 2.0, 4.5 and 7.0m, in order to analyze the SC lining behavior in small, medium and large tunnels.

Three different rock properties have been also considered taking into account the Rock Mass Rating (RMR) (Bieniawski, 1989): a rock with low (RMR=40), medium (RMR=60) and high quality (RMR=80). In Table 2 the geomechanical parameters used for the different rocks are shown.

Table 2. Geomechanical parameters assumed for the different rocks considered in the numerical simulation.

Parameter	RMR=40	RMR=60	RMR=80
Cohesion of rock mass c (MPa)	1.5	2.0	3.75
Friction angle of rock mass φ (°)	33	37	42
Elastic modulus of rock mass E (MPa)	2117.0	3490.3	5754.6
Stiffness of the normal spring at the nodes K_n (MN/m^3)	1845.09	3042.03	5015.47

Besides, three different stress ratios acting on the linings have been investigated:

$k = \frac{q_h}{q_v} = 1$, $\frac{q_h}{q_v} = 0.5$ and $\frac{q_h}{q_v} = 0$.

As for the lining characteristics, the thicknesses of 0.1, 0.2 and 0.3m, which are the typical SC lining thickness values (Melbye, 1994) and three values of the average elastic modulus of the SC were arbitrary considered: 6000, 9000 and 12000MPa. These mean values represent the behavior of the SC linings during the loading phase when it exhibits an evolution of stiffness and resistance parameters due to physical-chemical phenomena during the curing stage.

The study took into account four different values of vertical loads applied to the linings, so that various possible depths of the tunnel could be analyzed: q_v = 0.5, 1.0, 1.5 and 2.0MPa.

All possible combinations of the above data have been analyzed. In addition, two different cases were studied in relation to the shear interaction between the linings and the rocky wall of the tunnel:

- Stiffness of the tangential springs at nodes equal to half the stiffness of the normal springs $K_s = 0.5 \cdot K_n$ (which is typical employed in the calculations);
- Stiffness of tangential springs at nodes equal to zero K_s=0.

The two alternatives shown above permit to verify the influence of the shear interaction between the lining with the rock at the tunnel contour. This is normally neglected in the conventional calculation tools analyzing the behavior of the support structures in tunnels.

From the developed study, it was possible to detect the maximum and minimum values of bending moment, axial force and shear stress along the SC linings. These stress values are fundamental for the lining design therefore are a useful aid to the design phase of the tunnel supporting structure. The results obtained by the case I, i.e. $K_s = 0.5 \cdot K_n$, are reported in Table 3.

Table 3. Values of the maximum positive moment (M+), maximum negative moment (M-) in kNm/m, max positive shear stress (T+), max negative shear stress (T-), maximum axial force (N+) in kN/m, by changing applied stress q_v, for different k values, for different RMR and for changing SC lining thickness and mean elastic modulus for the case I.

RMR 40 Tunnel radius 2m SC elastic modulus 6000MPa																
q_v	k	**SC thickness 0.1m**					**SC thickness 0.2m**					**SC thickness 0.3m**				
		M+	M-	T+	T-	N+	M+	M-	T+	T-	N+	M+	M-	T+	T-	N+
0.5	0	1.20	-2.17	0.08	-43.55	997.56	8.50	-8.01	0.06	-42.45	972.26	21.30	-17.14	2.11	-40.16	919.89
1	0	2.39	-4.33	0.15	-87.11	1995.11	16.99	-16.02	0.12	-84.90	1944.51	42.59	-34.28	4.21	-80.33	1839.77
1.5	0	3.58	-6.51	0.23	-130.67	2992.73	25.49	-24.03	0.18	-127.35	2916.77	63.89	-51.42	6.32	-120.49	2759.66
2	0	4.77	-9.09	0.26	-174.36	3993.42	33.96	-32.19	0.24	-169.83	3889.86	85.18	-68.56	8.42	-160.65	3679.55
0.5	0.5	0.61	-0.61	-0.87	-43.52	996.89	3.14	-3.14	-0.85	-43.30	991.83	8.49	-8.49	-0.76	-42.84	981.17
1	0.5	1.22	-1.22	-1.74	-87.05	1993.77	6.28	-6.28	-1.71	-86.61	1983.66	16.98	-16.98	-1.51	-85.68	1962.34
1.5	0.5	1.82	-1.82	-2.62	-130.57	2990.66	9.43	-9.43	-2.56	-129.91	2975.49	25.47	-25.47	-2.27	-128.52	2943.50
2	0.5	2.43	-2.43	-3.49	-174.10	3987.54	12.57	-12.57	-3.42	-173.22	3967.33	33.96	-33.96	-3.03	-171.35	3924.67
0.5	1	0.00	0.00	-1.74	-43.62	999.05	0.00	0.00	-1.74	-43.62	999.05	0.00	0.00	-1.74	-43.62	999.05
1	1	0.00	0.00	-3.49	-87.24	1998.10	0.00	0.00	-3.49	-87.24	1998.10	0.00	0.00	-3.49	-87.24	1998.10
1.5	1	0.00	0.00	-5.23	-130.86	2997.14	0.00	0.00	-5.23	-130.86	2997.14	0.00	0.00	-5.23	-130.86	2997.14
2	1	0.00	0.00	-6.98	-174.48	3996.19	0.00	0.00	-6.98	-174.48	3996.19	0.00	0.00	-6.98	-174.48	3996.19
RMR 60 Tunnel radius 2m SC elastic modulus 6000MPa																
		SC thickness 0.1m					**SC thickness 0.2m**					**SC thickness 0.3m**				

q_v	k	M+	M-	T+	T-	N+	M+	M-	T+	T-	N+	M+	M-	T+	T-	N+
0.5	0	0.93	-1.34	0.07	-43.45	995.25	4.21	-5.15	1.92	-43.25	990.67	10.91	-10.27	5.65	-42.51	973.58
1	0	1.86	-2.67	0.14	-86.91	1990.51	8.42	-10.30	3.84	-86.51	1981.34	21.82	-20.54	11.30	-85.01	1947.16
1.5	0	2.79	-4.01	0.21	-130.36	2985.76	12.63	-15.45	5.76	-129.76	2972.01	32.73	-30.82	16.95	-127.52	2920.74
2	0	3.72	-5.33	0.27	-173.81	3980.93	16.83	-20.60	7.67	-173.02	3962.74	43.63	-41.09	22.60	-170.03	3894.32
0.5	0.5	0.47	-0.47	-0.87	-43.54	997.16	2.06	-2.06	-0.87	-43.40	993.99	4.98	-4.98	-0.83	-43.14	988.17
1	0.5	0.94	-0.94	-1.74	-87.07	1994.32	4.11	-4.11	-1.73	-86.80	1987.99	9.96	-9.96	-1.66	-86.29	1976.34
1.5	0.5	1.41	-1.41	-2.62	-130.61	2991.48	6.17	-6.17	-2.60	-130.20	2981.98	14.94	-14.94	-2.49	-129.43	2964.51
2	0.5	1.88	-1.88	-3.49	-174.15	3988.65	8.23	-8.23	-3.46	-173.60	3975.98	19.91	-19.91	-3.32	-172.58	3952.68
0.5	1	0.00	0.00	-1.74	-43.62	999.05	0.00	0.00	-1.74	-43.62	999.05	0.00	0.00	-1.74	-43.62	999.05
1	1	0.00	0.00	-3.49	-87.24	1998.10	0.00	0.00	-3.49	-87.24	1998.10	0.00	0.00	-3.49	-87.24	1998.10
1.5	1	0.00	0.00	-5.23	-130.86	2997.14	0.00	0.00	-5.23	-130.86	2997.14	0.00	0.00	-5.23	-130.86	2997.14
2	1	0.00	0.00	-6.98	-174.48	3996.19	0.00	0.00	-6.98	-174.48	3996.19	0.00	0.00	-6.98	-174.48	3996.19

RMR 80 Tunnel radius 2m SC elastic modulus 6000MPa

q_v	k	SC thickness 0.1m					SC thickness 0.2m					SC thickness 0.3m				
		M+	M-	T+	T-	N+	M+	M-	T+	T-	N+	M+	M-	T+	T-	N+
0.5	0	0.87	-1.00	6.70	-43.46	995.40	3.54	-3.69	11.45	-43.24	990.39	8.17	-7.62	13.58	-42.84	981.13
1	0	1.73	-1.99	13.41	-86.92	1990.80	7.08	-7.37	22.90	-86.48	1980.78	16.34	-15.24	27.15	-85.67	1962.26
1.5	0	2.60	-2.99	20.11	-130.38	2986.20	10.61	-11.06	34.34	-129.72	2971.16	24.51	-22.86	40.73	-128.51	2943.39
2	0	3.46	-3.98	26.81	-173.84	3981.60	14.15	-14.75	45.79	-172.97	3961.55	32.68	-30.48	54.30	-171.35	3924.51
0.5	0.5	0.43	-0.43	-0.87	-43.54	997.23	1.77	-1.77	-0.87	-43.42	994.57	4.04	-4.04	-0.85	-43.23	990.04
1	0.5	0.87	-0.87	-1.75	-87.08	1994.47	3.54	-3.54	-1.74	-86.85	1989.13	8.08	-8.08	-1.69	-86.45	1980.09
1.5	0.5	1.30	-1.30	-2.62	-130.62	2991.70	5.31	-5.31	-2.60	-130.27	2983.70	12.11	-12.11	-2.54	-129.68	2970.13
2	0.5	1.73	-1.73	-3.49	-174.16	3988.94	7.08	-7.08	-3.47	-173.69	3978.27	16.15	-16.15	-3.38	-172.91	3960.18
0.5	1	0.00	0.00	-1.74	-43.62	999.05	0.00	0.00	-1.74	-43.62	999.05	0.00	0.00	-1.74	-43.62	999.05
1	1	0.00	0.00	-3.49	-87.24	1998.10	0.00	0.00	-3.49	-87.24	1998.10	0.00	0.00	-3.49	-87.24	1998.10
1.5	1	0.00	0.00	-5.23	-130.86	2997.14	0.00	0.00	-5.23	-130.86	2997.14	0.00	0.00	-5.23	-130.86	2997.14
2	1	0.00	0.00	-6.98	-174.48	3996.19	0.00	0.00	-6.98	-174.48	3996.19	0.00	0.00	-6.98	-174.48	3996.19

RMR 40 Tunnel radius 2m SC elastic modulus 9000MPa

q_v	k	SC thickness 0.1m					SC thickness 0.2m					SC thickness 0.3m				
		M+	M-	T+	T-	N+	M+	M-	T+	T-	N+	M+	M-	T+	T-	N+
0.5	0	1.58	-2.53	0.03	-43.56	997.73	11.32	-9.53	0.17	-41.65	953.99	26.15	-19.78	7.67	-41.09	891.23
1	0	3.17	-5.07	0.05	-87.12	1995.46	22.63	-19.06	0.33	-83.30	1907.97	52.30	-39.56	15.34	-82.18	1782.46
1.5	0	4.75	-7.60	0.08	-130.69	2993.19	33.95	-28.59	0.50	-124.96	2861.96	78.45	-59.34	23.01	-123.26	2673.69
2	0	6.27	-10.45	0.09	-174.36	3993.40	45.26	-38.12	0.67	-166.61	3815.96	104.54	-78.97	30.52	-164.56	3565.21
0.5	0.5	0.70	-0.70	-0.87	-43.52	996.70	3.88	-3.88	-0.85	-43.24	990.37	11.41	-8.87	-0.69	-42.44	971.94
1	0.5	1.41	-1.41	-1.74	-87.03	1993.39	7.75	-7.75	-1.69	-86.48	1980.73	22.83	-17.74	-1.39	-84.87	1943.88
1.5	0.5	2.11	-2.11	-2.61	-130.55	2990.09	11.63	-11.63	-2.54	-129.72	2971.10	34.24	-26.61	-2.08	-127.31	2915.82
2	0.5	2.81	-2.81	-3.49	-174.07	3986.79	15.51	-15.51	-3.39	-172.96	3961.46	45.66	-35.48	-2.78	-169.74	3887.76
0.5	1	0.00	0.00	-1.74	-43.62	999.05	0.00	0.00	-1.74	-43.62	999.05	0.00	0.00	-1.74	-43.62	999.05
1	1	0.00	0.00	-3.49	-87.24	1998.10	0.00	0.00	-3.49	-87.24	1998.10	0.00	0.00	-3.49	-87.24	1998.10
1.5	1	0.00	0.00	-5.23	-130.86	2997.14	0.00	0.00	-5.23	-130.86	2997.14	0.00	0.00	-5.23	-130.86	2997.14
2	1	0.00	0.00	-6.98	-174.48	3996.19	0.00	0.00	-6.98	-174.48	3996.19	0.00	0.00	-6.98	-174.48	3996.19

RMR 60 Tunnel radius 2m SC elastic modulus 9000MPa

q_v	k	SC thickness 0.1m					SC thickness 0.2m					SC thickness 0.3m				
		M+	M-	T+	T-	N+	M+	M-	T+	T-	N+	M+	M-	T+	T-	N+

0.5	0	0.96	-1.56	0.28	-43.46	995.40	4.86	-5.65	0.92	-43.20	989.46	13.05	-12.05	3.63	-42.12	964.68
1	0	1.93	-3.12	0.56	-86.92	1990.81	9.73	-11.30	1.83	-86.40	1978.93	26.10	-24.10	7.27	-84.24	1929.36
1.5	0	2.89	-4.69	0.84	-130.38	2986.21	14.59	-16.95	2.75	-129.60	2968.39	39.14	-36.14	10.90	-126.36	2894.04
2	0	3.85	-6.25	1.11	-173.84	3981.58	19.46	-22.61	3.66	-172.80	3957.87	52.19	-48.19	14.53	-168.48	3858.72
0.5	0.5	0.49	-0.49	-0.87	-43.53	997.11	2.26	-2.26	-0.86	-43.38	993.60	5.63	-5.63	-0.82	-43.09	986.88
1	0.5	0.99	-0.99	-1.74	-87.07	1994.22	4.51	-4.51	-1.73	-86.76	1987.20	11.25	-11.25	-1.64	-86.18	1973.75
1.5	0.5	1.48	-1.48	-2.62	-130.60	2991.33	6.77	-6.77	-2.59	-130.14	2980.80	16.88	-16.88	-2.45	-129.26	2960.63
2	0.5	1.98	-1.98	-3.49	-174.14	3988.44	9.02	-9.02	-3.46	-173.53	3974.40	22.51	-22.51	-3.27	-172.35	3947.51
0.5	1	0.00	0.00	-1.74	-43.62	999.05	0.00	0.00	-1.74	-43.62	999.05	0.00	0.00	-1.74	-43.62	999.05
1	1	0.00	0.00	-3.49	-87.24	1998.10	0.00	0.00	-3.49	-87.24	1998.10	0.00	0.00	-3.49	-87.24	1998.10
1.5	1	0.00	0.00	-5.23	-130.86	2997.14	0.00	0.00	-5.23	-130.86	2997.14	0.00	0.00	-5.23	-130.86	2997.14
2	1	0.00	0.00	-6.98	-174.48	3996.19	0.00	0.00	-6.98	-174.48	3996.19	0.00	0.00	-6.98	-174.48	3996.19

RMR 80 Tunnel radius 2m SC elastic modulus 9000MPa

q_v	k	SC thickness 0.1m					SC thickness 0.2m					SC thickness 0.3m				
		M+	M-	T+	T-	N+	M+	M-	T+	T-	N+	M+	M-	T+	T-	N+
0.5	0	0.88	-1.11	3.63	-43.46	995.35	3.65	-4.00	7.40	-43.24	990.45	8.64	-8.26	11.01	-42.80	980.30
1	0	1.76	-2.23	7.27	-86.92	1990.70	7.30	-7.99	14.80	-86.49	1980.90	17.27	-16.52	22.02	-85.60	1960.60
1.5	0	2.64	-3.34	10.90	-130.37	2986.05	10.95	-11.99	22.19	-129.73	2971.34	25.91	-24.78	33.03	-128.40	2940.90
2	0	3.52	-4.45	14.53	-173.83	3981.40	14.60	-15.98	29.59	-172.98	3961.79	34.55	-33.04	44.04	-171.20	3921.20
0.5	0.5	0.44	-0.44	-0.87	-43.54	997.22	1.83	-1.83	-0.87	-43.42	994.46	4.22	-4.22	-0.84	-43.21	989.68
1	0.5	0.88	-0.88	-1.75	-87.08	1994.44	3.65	-3.65	-1.74	-86.84	1988.91	8.44	-8.44	-1.68	-86.42	1979.36
1.5	0.5	1.32	-1.32	-2.62	-130.62	2991.66	5.48	-5.48	-2.60	-130.26	2983.37	12.66	-12.66	-2.53	-129.63	2969.04
2	0.5	1.76	-1.76	-3.49	-174.16	3988.88	7.30	-7.30	-3.47	-173.68	3977.83	16.88	-16.88	-3.37	-172.84	3958.72
0.5	1	0.00	0.00	-1.74	-43.62	999.05	0.00	0.00	-1.74	-43.62	999.05	0.00	0.00	-1.74	-43.62	999.05
1	1	0.00	0.00	-3.49	-87.24	1998.10	0.00	0.00	-3.49	-87.24	1998.10	0.00	0.00	-3.49	-87.24	1998.10
1.5	1	0.00	0.00	-5.23	-130.86	2997.14	0.00	0.00	-5.23	-130.86	2997.14	0.00	0.00	-5.23	-130.86	2997.14
2	1	0.00	0.00	-6.98	-174.48	3996.19	0.00	0.00	-6.98	-174.48	3996.19	0.00	0.00	-6.98	-174.48	3996.19

RMR 40 Tunnel radius 2m SC elastic modulus 12000MPa

q_v	k	SC thickness 0.1m					SC thickness 0.2m					SC thickness 0.3m				
		M+	M-	T+	T-	N+	M+	M-	T+	T-	N+	M+	M-	T+	T-	N+
0.5	0	2.10	-2.85	0.00	-43.48	995.78	13.75	-11.41	0.26	-40.94	937.61	30.04	-22.11	12.71	-43.65	869.37
1	0	4.20	-5.70	0.00	-86.95	1991.56	27.50	-22.82	0.53	-81.87	1875.23	60.08	-44.23	25.43	-87.30	1738.74
1.5	0	6.30	-8.56	0.01	-130.43	2987.35	41.25	-34.23	0.79	-122.81	2812.84	90.12	-66.34	38.14	-130.95	2608.10
2	0	8.34	-11.50	0.01	-173.96	3984.38	55.00	-45.63	1.13	-163.75	3750.46	119.98	-88.00	50.33	-174.65	3478.63
0.5	0.5	0.80	-0.80	-0.87	-43.51	996.51	4.87	-3.98	-0.84	-43.13	987.73	14.48	-10.76	-0.63	-41.88	959.25
1	0.5	1.59	-1.59	-1.74	-87.02	1993.02	9.75	-7.95	-1.67	-86.25	1975.45	28.96	-21.52	-1.26	-83.76	1918.49
1.5	0.5	2.39	-2.39	-2.61	-130.53	2989.53	14.62	-11.93	-2.51	-129.38	2963.18	43.44	-32.27	-1.89	-125.64	2877.74
2	0.5	3.19	-3.19	-3.49	-174.03	3986.03	19.49	-15.90	-3.34	-172.50	3950.91	57.92	-43.03	-2.52	-167.53	3836.99
0.5	1	0.00	0.00	-1.74	-43.62	999.05	0.00	0.00	-1.74	-43.62	999.05	0.00	0.00	-1.74	-43.62	999.05
1	1	0.00	0.00	-3.49	-87.24	1998.10	0.00	0.00	-3.49	-87.24	1998.10	0.00	0.00	-3.49	-87.24	1998.10
1.5	1	0.00	0.00	-5.23	-130.86	2997.14	0.00	0.00	-5.23	-130.86	2997.14	0.00	0.00	-5.23	-130.86	2997.14
2	1	0.00	0.00	-6.98	-174.48	3996.19	0.00	0.00	-6.98	-174.48	3996.19	0.00	0.00	-6.98	-174.48	3996.19

RMR 60 Tunnel radius 2m SC elastic modulus 12000MPa

q_v	k	SC thickness 0.1m					SC thickness 0.2m					SC thickness 0.3m				
		M+	M-	T+	T-	N+	M+	M-	T+	T-	N+	M+	M-	T+	T-	N+
0.5	0	1.00	-1.63	0.16	-43.48	995.84	5.62	-6.07	0.38	-43.09	986.94	15.12	-13.17	2.88	-41.66	954.18
1	0	2.00	-3.25	0.31	-86.96	1991.68	11.24	-12.14	0.75	-86.18	1973.89	30.23	-26.33	5.75	-83.32	1908.35

1.5	0	2.99	-4.88	0.47	-130.44	2987.52	16.86	-18.21	1.13	-129.27	2960.83	45.35	-39.50	8.63	-124.98	2862.53
2	0	3.99	-6.52	0.62	-173.92	3983.36	22.47	-24.28	1.50	-172.36	3947.78	60.47	-52.66	11.50	-166.64	3816.71
0.5	0.5	0.52	-0.52	-0.87	-43.53	997.06	2.45	-2.45	-0.86	-43.36	993.20	6.27	-6.27	-0.81	-43.03	985.59
1	0.5	1.04	-1.04	-1.74	-87.07	1994.12	4.91	-4.91	-1.72	-86.73	1986.41	12.54	-12.54	-1.61	-86.06	1971.18
1.5	0.5	1.56	-1.56	-2.62	-130.60	2991.18	7.36	-7.36	-2.59	-130.09	2979.61	18.81	-18.81	-2.42	-129.10	2956.78
2	0.5	2.08	-2.08	-3.49	-174.13	3988.24	9.82	-9.82	-3.45	-173.46	3972.81	25.08	-25.08	-3.23	-172.13	3942.37
0.5	1	0.00	0.00	-1.74	-43.62	999.05	0.00	0.00	-1.74	-43.62	999.05	0.00	0.00	-1.74	-43.62	999.05
1	1	0.00	0.00	-3.49	-87.24	1998.10	0.00	0.00	-3.49	-87.24	1998.10	0.00	0.00	-3.49	-87.24	1998.10
1.5	1	0.00	0.00	-5.23	-130.86	2997.14	0.00	0.00	-5.23	-130.86	2997.14	0.00	0.00	-5.23	-130.86	2997.14
2	1	0.00	0.00	-6.98	-174.48	3996.19	0.00	0.00	-6.98	-174.48	3996.19	0.00	0.00	-6.98	-174.48	3996.19

RMR 80 Tunnel radius 2m SC elastic modulus 12000MPa

q_v	k	SC thickness 0.1m					SC thickness 0.2m					SC thickness 0.3m				
		M+	M-	T+	T-	N+	M+	M-	T+	T-	N+	M+	M-	T+	T-	N+
0.5	0	0.89	-1.34	0.35	-43.46	995.29	3.77	-4.40	5.39	-43.25	990.56	9.14	-8.74	9.61	-42.75	979.18
1	0	1.79	-2.69	0.70	-86.91	1990.58	7.53	-8.81	10.77	-86.50	1981.13	18.27	-17.48	19.22	-85.50	1958.36
1.5	0	2.68	-4.03	1.04	-130.37	2985.87	11.30	-13.21	16.16	-129.75	2971.69	27.41	-26.22	28.83	-128.26	2937.54
2	0	3.58	-5.37	1.39	-173.82	3981.16	15.06	-17.61	21.54	-173.00	3962.26	36.55	-34.95	38.44	-171.01	3916.72
0.5	0.5	0.45	-0.45	-0.87	-43.54	997.21	1.88	-1.88	-0.87	-43.41	994.35	4.40	-4.40	-0.84	-43.19	989.32
1	0.5	0.89	-0.89	-1.74	-87.08	1994.41	3.76	-3.76	-1.73	-86.83	1988.69	8.81	-8.81	-1.68	-86.39	1978.63
1.5	0.5	1.34	-1.34	-2.62	-130.62	2991.62	5.64	-5.64	-2.60	-130.24	2983.04	13.21	-13.21	-2.52	-129.58	2967.95
2	0.5	1.79	-1.79	-3.49	-174.16	3988.82	7.53	-7.53	-3.47	-173.66	3977.38	17.61	-17.61	-3.36	-172.78	3957.27
0.5	1	0.00	0.00	-1.74	-43.62	999.05	0.00	0.00	-1.74	-43.62	999.05	0.00	0.00	-1.74	-43.62	999.05
1	1	0.00	0.00	-3.49	-87.24	1998.10	0.00	0.00	-3.49	-87.24	1998.10	0.00	0.00	-3.49	-87.24	1998.10
1.5	1	0.00	0.00	-5.23	-130.86	2997.14	0.00	0.00	-5.23	-130.86	2997.14	0.00	0.00	-5.23	-130.86	2997.14
2	1	0.00	0.00	-6.98	-174.48	3996.19	0.00	0.00	-6.98	-174.48	3996.19	0.00	0.00	-6.98	-174.48	3996.19

RMR 40 Tunnel radius 4.5m SC elastic modulus 6000MPa

q_v	k	SC thickness 0.1m					SC thickness 0.2m					SC thickness 0.3m				
		M+	M-	T+	T-	N+	M+	M-	T+	T-	N+	M+	M-	T+	T-	N+
0.5	0	1.02	-2.18	-0.01	-97.90	2242.34	4.43	-8.40	0.09	-97.97	2243.98	13.90	-18.56	0.52	-97.72	2238.06
1	0	2.04	-4.36	-0.01	-195.81	4484.68	8.87	-16.80	0.18	-195.95	4487.96	27.80	-37.13	1.05	-195.43	4476.13
1.5	0	3.07	-6.50	-0.02	-293.69	6726.70	13.27	-25.27	0.26	-293.93	6732.09	41.70	-55.69	1.57	-293.15	6714.19
2	0	4.10	-9.43	-0.02	-391.44	8965.52	17.92	-35.81	0.26	-392.14	8981.48	54.80	-75.08	2.08	-391.15	8958.78
0.5	0.5	0.50	-0.50	-1.97	-98.03	2245.27	2.35	-2.35	-1.96	-97.96	2243.64	6.02	-6.02	-1.96	-97.82	2240.38
1	0.5	1.01	-1.01	-3.93	-196.06	4490.55	4.70	-4.70	-3.93	-195.92	4487.27	12.04	-12.04	-3.91	-195.63	4480.77
1.5	0.5	1.51	-1.51	-5.90	-294.09	6735.82	7.05	-7.05	-5.89	-293.88	6730.91	18.06	-18.06	-5.87	-293.45	6721.15
2	0.5	2.02	-2.02	-7.86	-392.12	8981.09	9.40	-9.40	-7.85	-391.84	8974.55	24.08	-24.08	-7.83	-391.27	8961.54
0.5	1	0.00	0.00	-3.93	-98.14	2247.86	0.00	0.00	-3.93	-98.14	2247.86	0.00	0.00	-3.93	-98.14	2247.86
1	1	0.00	0.00	-7.85	-196.29	4495.72	0.00	0.00	-7.85	-196.29	4495.72	0.00	0.00	-7.85	-196.29	4495.72
1.5	1	0.00	0.00	-11.78	-294.43	6743.58	0.00	0.00	-11.78	-294.43	6743.58	0.00	0.00	-11.78	-294.43	6743.58
2	1	0.00	0.00	-15.70	-392.57	8991.43	0.00	0.00	-15.70	-392.57	8991.43	0.00	0.00	-15.70	-392.57	8991.43

RMR 60 Tunnel radius 4.5m SC elastic modulus 6000MPa

q_v	k	SC thickness 0.1m					SC thickness 0.2m					SC thickness 0.3m				
		M+	M-	T+	T-	N+	M+	M-	T+	T-	N+	M+	M-	T+	T-	N+
0.5	0	0.88	-1.75	1.28	-97.92	2242.81	3.70	-5.16	0.00	-97.80	2240.10	8.57	-12.00	1.06	-97.68	2237.26
1	0	1.77	-3.49	2.55	-195.85	4485.63	7.40	-10.31	0.00	-195.61	4480.20	17.14	-24.00	2.12	-195.36	4474.53
1.5	0	2.65	-5.24	3.83	-293.77	6728.44	11.09	-15.47	-0.01	-293.41	6720.31	25.71	-36.00	3.19	-293.04	6711.79
2	0	3.54	-6.96	5.09	-391.69	8971.26	14.79	-20.58	-0.01	-391.21	8960.19	34.23	-48.05	4.15	-390.73	8949.07

0.5	0.5	0.44	-0.44	-1.97	-98.03	2245.33	1.86	-1.86	-1.96	-97.98	2244.07	4.37	-4.37	-1.96	-97.88	2241.85
1	0.5	0.89	-0.89	-3.93	-196.07	4490.66	3.71	-3.71	-3.93	-195.96	4488.15	8.73	-8.73	-3.92	-195.76	4483.70
1.5	0.5	1.33	-1.33	-5.90	-294.10	6735.98	5.57	-5.57	-5.89	-293.94	6732.22	13.10	-13.10	-5.88	-293.64	6725.55
2	0.5	1.77	-1.77	-7.86	-392.13	8981.31	7.43	-7.43	-7.85	-391.91	8976.30	17.46	-17.46	-7.84	-391.53	8967.40
0.5	1	0.00	0.00	-3.93	-98.14	2247.86	0.00	0.00	-3.93	-98.14	2247.86	0.00	0.00	-3.93	-98.14	2247.86
1	1	0.00	0.00	-7.85	-196.29	4495.72	0.00	0.00	-7.85	-196.29	4495.72	0.00	0.00	-7.85	-196.29	4495.72
1.5	1	0.00	0.00	-11.78	-294.43	6743.58	0.00	0.00	-11.78	-294.43	6743.58	0.00	0.00	-11.78	-294.43	6743.58
2	1	0.00	0.00	-15.70	-392.57	8991.43	0.00	0.00	-15.70	-392.57	8991.43	0.00	0.00	-15.70	-392.57	8991.43

RMR 80 Tunnel radius 4.5m SC elastic modulus 6000MPa

q_v	k	SC thickness 0.1m					SC thickness 0.2m					SC thickness 0.3m				
		M+	M-	T+	T-	N+	M+	M-	T+	T-	N+	M+	M-	T+	T-	N+
0.5	0	0.85	-1.20	4.24	-97.92	2242.83	3.46	-4.07	12.81	-97.82	2240.49	7.84	-8.40	21.16	-97.65	2236.65
1	0	1.71	-2.40	8.48	-195.85	4485.65	6.91	-8.14	25.63	-195.64	4480.99	15.69	-16.80	42.31	-195.31	4473.29
1.5	0	2.56	-3.61	12.72	-293.77	6728.48	10.37	-12.20	38.44	-293.47	6721.48	23.53	-25.20	63.47	-292.96	6709.94
2	0	3.41	-4.81	16.96	-391.70	8971.30	13.82	-16.27	51.25	-391.29	8961.97	31.38	-33.60	84.63	-390.62	8946.58
0.5	0.5	0.43	-0.43	-1.97	-98.03	2245.34	1.73	-1.73	-1.96	-97.98	2244.19	3.93	-3.93	-1.96	-97.90	2242.24
1	0.5	0.85	-0.85	-3.93	-196.07	4490.68	3.45	-3.45	-3.93	-195.97	4488.38	7.86	-7.86	-3.92	-195.80	4484.47
1.5	0.5	1.28	-1.28	-5.90	-294.10	6736.03	5.18	-5.18	-5.89	-293.95	6732.57	11.79	-11.79	-5.88	-293.69	6726.71
2	0.5	1.71	-1.71	-7.86	-392.14	8981.37	6.91	-6.91	-7.86	-391.93	8976.76	15.72	-15.72	-7.84	-391.59	8968.95
0.5	1	0.00	0.00	-3.93	-98.14	2247.86	0.00	0.00	-3.93	-98.14	2247.86	0.00	0.00	-3.93	-98.14	2247.86
1	1	0.00	0.00	-7.85	-196.29	4495.72	0.00	0.00	-7.85	-196.29	4495.72	0.00	0.00	-7.85	-196.29	4495.72
1.5	1	0.00	0.00	-11.78	-294.43	6743.58	0.00	0.00	-11.78	-294.43	6743.58	0.00	0.00	-11.78	-294.43	6743.58
2	1	0.00	0.00	-15.70	-392.57	8991.43	0.00	0.00	-15.70	-392.57	8991.43	0.00	0.00	-15.70	-392.57	8991.43

RMR 40 Tunnel radius 4.5m SC elastic modulus 9000MPa

q_v	k	SC thickness 0.1m					SC thickness 0.2m					SC thickness 0.3m				
		M+	M-	T+	T-	N+	M+	M-	T+	T-	N+	M+	M-	T+	T-	N+
0.5	0	1.08	-2.69	-0.01	-97.89	2242.06	5.74	-9.97	0.00	-98.09	2246.56	19.67	-22.68	0.44	-97.19	2226.06
1	0	2.15	-5.38	-0.01	-195.78	4484.13	11.47	-19.94	0.00	-196.17	4493.12	39.34	-45.35	0.89	-194.38	4452.12
1.5	0	3.23	-8.06	-0.02	-293.66	6725.88	17.21	-29.91	0.00	-294.26	6739.70	59.01	-68.03	1.33	-291.58	6678.19
2	0	4.39	-11.20	-0.02	-391.41	8964.78	23.14	-41.71	0.00	-392.60	8992.06	78.44	-91.21	1.77	-388.88	8906.73
0.5	0.5	0.55	-0.55	-1.97	-98.03	2245.24	2.69	-2.69	-1.96	-97.95	2243.34	7.15	-7.15	-1.96	-97.77	2239.39
1	0.5	1.09	-1.09	-3.93	-196.06	4490.47	5.37	-5.37	-3.92	-195.89	4486.68	14.29	-14.29	-3.91	-195.55	4478.77
1.5	0.5	1.64	-1.64	-5.90	-294.09	6735.71	8.06	-8.06	-5.89	-293.84	6730.02	21.44	-21.44	-5.87	-293.32	6718.16
2	0.5	2.19	-2.19	-7.86	-392.12	8980.94	10.75	-10.75	-7.85	-391.79	8973.35	28.58	-28.58	-7.82	-391.09	8957.54
0.5	1	0.00	0.00	-3.93	-98.14	2247.86	0.00	0.00	-3.93	-98.14	2247.86	0.00	0.00	-3.93	-98.14	2247.86
1	1	0.00	0.00	-7.85	-196.29	4495.72	0.00	0.00	-7.85	-196.29	4495.72	0.00	0.00	-7.85	-196.29	4495.72
1.5	1	0.00	0.00	-11.78	-294.43	6743.58	0.00	0.00	-11.78	-294.43	6743.58	0.00	0.00	-11.78	-294.43	6743.58
2	1	0.00	0.00	-15.70	-392.57	8991.43	0.00	0.00	-15.70	-392.57	8991.43	0.00	0.00	-15.70	-392.57	8991.43

RMR 60 Tunnel radius 4.5m SC elastic modulus 9000MPa

q_v	k	SC thickness 0.1m					SC thickness 0.2m					SC thickness 0.3m				
		M+	M-	T+	T-	N+	M+	M-	T+	T-	N+	M+	M-	T+	T-	N+
0.5	0	0.91	-1.57	0.61	-97.92	2242.80	3.83	-6.49	0.63	-97.80	2240.02	9.15	-13.14	0.09	-97.74	2238.68
1	0	1.82	-3.13	1.23	-195.85	4485.60	7.66	-12.99	1.26	-195.60	4480.03	18.30	-26.29	0.18	-195.49	4477.37
1.5	0	2.73	-4.70	1.84	-293.77	6728.39	11.50	-19.48	1.89	-293.40	6720.05	27.45	-39.43	0.27	-293.23	6716.05
2	0	3.64	-6.24	2.44	-391.69	8971.16	15.31	-25.95	2.51	-391.20	8959.87	36.57	-52.57	0.37	-390.98	8954.84
0.5	0.5	0.45	-0.45	-1.97	-98.03	2245.32	1.95	-1.95	-1.96	-97.97	2243.99	4.67	-4.67	-1.96	-97.87	2241.58
1	0.5	0.91	-0.91	-3.93	-196.07	4490.64	3.89	-3.89	-3.93	-195.95	4487.99	9.33	-9.33	-3.92	-195.74	4483.17

1.5	0.5	1.36	-1.36	-5.90	-294.10	6735.95	5.84	-5.84	-5.89	-293.92	6731.98	14.00	-14.00	-5.88	-293.61	6724.75
2	0.5	1.82	-1.82	-7.86	-392.13	8981.27	7.79	-7.79	-7.85	-391.90	8975.98	18.67	-18.67	-7.84	-391.48	8966.33
0.5	1	0.00	0.00	-3.93	-98.14	2247.86	0.00	0.00	-3.93	-98.14	2247.86	0.00	0.00	-3.93	-98.14	2247.86
1	1	0.00	0.00	-7.85	-196.29	4495.72	0.00	0.00	-7.85	-196.29	4495.72	0.00	0.00	-7.85	-196.29	4495.72
1.5	1	0.00	0.00	-11.78	-294.43	6743.58	0.00	0.00	-11.78	-294.43	6743.58	0.00	0.00	-11.78	-294.43	6743.58
2	1	0.00	0.00	-15.70	-392.57	8991.43	0.00	0.00	-15.70	-392.57	8991.43	0.00	0.00	-15.70	-392.57	8991.43

RMR 80 Tunnel radius 4.5m SC elastic modulus 9000MPa

q_v	k	SC thickness 0.1m					SC thickness 0.2m					SC thickness 0.3m				
		M+	M-	T+	T-	N+	M+	M-	T+	T-	N+	M+	M-	T+	T-	N+
0.5	0	0.86	-1.13	3.43	-97.92	2242.82	3.51	-4.12	8.95	-97.82	2240.41	7.99	-9.97	9.50	-97.65	2236.52
1	0	1.72	-2.25	6.87	-195.85	4485.64	7.01	-8.25	17.90	-195.64	4480.83	15.99	-19.95	18.99	-195.30	4473.05
1.5	0	2.58	-3.38	10.30	-293.77	6728.46	10.52	-12.37	26.85	-293.46	6721.24	23.98	-29.92	28.49	-292.95	6709.57
2	0	3.44	-4.50	13.74	-391.69	8971.29	14.02	-16.49	35.80	-391.27	8961.65	31.98	-39.89	37.99	-390.59	8946.09
0.5	0.5	0.43	-0.43	-1.97	-98.03	2245.34	1.75	-1.75	-1.96	-97.98	2244.17	4.01	-4.01	-1.96	-97.89	2242.16
1	0.5	0.86	-0.86	-3.93	-196.07	4490.68	3.50	-3.50	-3.93	-195.96	4488.33	8.03	-8.03	-3.92	-195.79	4484.32
1.5	0.5	1.29	-1.29	-5.90	-294.10	6736.02	5.26	-5.26	-5.89	-293.95	6732.50	12.04	-12.04	-5.88	-293.68	6726.49
2	0.5	1.72	-1.72	-7.86	-392.13	8981.36	7.01	-7.01	-7.86	-391.93	8976.67	16.06	-16.06	-7.84	-391.58	8968.65
0.5	1	0.00	0.00	-3.93	-98.14	2247.86	0.00	0.00	-3.93	-98.14	2247.86	0.00	0.00	-3.93	-98.14	2247.86
1	1	0.00	0.00	-7.85	-196.29	4495.72	0.00	0.00	-7.85	-196.29	4495.72	0.00	0.00	-7.85	-196.29	4495.72
1.5	1	0.00	0.00	-11.78	-294.43	6743.58	0.00	0.00	-11.78	-294.43	6743.58	0.00	0.00	-11.78	-294.43	6743.58
2	1	0.00	0.00	-15.70	-392.57	8991.43	0.00	0.00	-15.70	-392.57	8991.43	0.00	0.00	-15.70	-392.57	8991.43

RMR 40 Tunnel radius 4.5m SC elastic modulus 12000MPa

q_v	k	SC thickness 0.1m					SC thickness 0.2m					SC thickness 0.3m				
		M+	M-	T+	T-	N+	M+	M-	T+	T-	N+	M+	M-	T+	T-	N+
0.5	0	1.09	-3.40	-0.01	-97.90	2242.29	7.22	-11.86	0.00	-98.06	2245.93	25.77	-26.17	0.39	-96.41	2208.21
1	0	2.19	-6.80	-0.01	-195.80	4484.58	14.43	-23.71	0.00	-196.12	4491.86	51.54	-52.35	0.78	-192.83	4416.42
1.5	0	3.27	-10.29	-0.02	-293.69	6726.66	21.65	-35.57	0.01	-294.18	6737.78	77.31	-78.52	1.17	-289.24	6624.63
2	0	5.85	-15.14	-0.02	-391.50	8966.90	28.68	-48.03	0.01	-392.40	8987.47	103.04	-104.90	1.56	-385.67	8833.39
0.5	0.5	0.59	-0.59	-1.97	-98.03	2245.20	3.02	-3.02	-1.96	-97.93	2243.04	8.27	-8.27	-1.95	-97.73	2238.39
1	0.5	1.18	-1.18	-3.93	-196.05	4490.40	6.05	-6.05	-3.92	-195.87	4486.08	16.54	-16.54	-3.91	-195.46	4476.78
1.5	0.5	1.77	-1.77	-5.90	-294.08	6735.59	9.07	-9.07	-5.89	-293.80	6729.12	24.81	-24.81	-5.86	-293.19	6715.17
2	0.5	2.36	-2.36	-7.86	-392.11	8980.79	12.09	-12.09	-7.85	-391.73	8972.16	33.08	-33.08	-7.82	-390.92	8953.56
0.5	1	0.00	0.00	-3.93	-98.14	2247.86	0.00	0.00	-3.93	-98.14	2247.86	0.00	0.00	-3.93	-98.14	2247.86
1	1	0.00	0.00	-7.85	-196.29	4495.72	0.00	0.00	-7.85	-196.29	4495.72	0.00	0.00	-7.85	-196.29	4495.72
1.5	1	0.00	0.00	-11.78	-294.43	6743.58	0.00	0.00	-11.78	-294.43	6743.58	0.00	0.00	-11.78	-294.43	6743.58
2	1	0.00	0.00	-15.70	-392.57	8991.43	0.00	0.00	-15.70	-392.57	8991.43	0.00	0.00	-15.70	-392.57	8991.43

RMR 60 Tunnel radius 4.5m SC elastic modulus 12000MPa

q_v	k	SC thickness 0.1m					SC thickness 0.2m					SC thickness 0.3m				
		M+	M-	T+	T-	N+	M+	M-	T+	T-	N+	M+	M-	T+	T-	N+
0.5	0	0.93	-1.67	0.13	-97.92	2242.75	3.94	-6.42	0.37	-97.83	2240.61	9.86	-15.18	0.51	-97.80	2240.03
1	0	1.87	-3.33	0.26	-195.84	4485.50	7.87	-12.84	0.74	-195.65	4481.21	19.72	-30.37	1.03	-195.60	4480.06
1.5	0	2.80	-5.00	0.39	-293.76	6728.25	11.81	-19.26	1.12	-293.48	6721.82	29.57	-45.55	1.54	-293.41	6720.10
2	0	3.74	-6.63	0.50	-391.68	8970.92	15.72	-25.66	1.48	-391.30	8962.33	39.41	-60.77	2.06	-391.21	8960.22
0.5	0.5	0.47	-0.47	-1.97	-98.03	2245.31	2.04	-2.04	-1.96	-97.97	2243.91	4.97	-4.97	-1.96	-97.86	2241.32
1	0.5	0.93	-0.93	-3.93	-196.06	4490.62	4.07	-4.07	-3.93	-195.94	4487.83	9.94	-9.94	-3.92	-195.72	4482.63
1.5	0.5	1.40	-1.40	-5.90	-294.10	6735.92	6.11	-6.11	-5.89	-293.91	6731.74	14.91	-14.91	-5.88	-293.57	6723.95
2	0.5	1.86	-1.86	-7.86	-392.13	8981.23	8.15	-8.15	-7.85	-391.89	8975.66	19.88	-19.88	-7.84	-391.43	8965.26

0.5	1	0.00	0.00	-3.93	-98.14	2247.86	0.00	0.00	-3.93	-98.14	2247.86	0.00	0.00	-3.93	-98.14	2247.86
1	1	0.00	0.00	-7.85	-196.29	4495.72	0.00	0.00	-7.85	-196.29	4495.72	0.00	0.00	-7.85	-196.29	4495.72
1.5	1	0.00	0.00	-11.78	-294.43	6743.58	0.00	0.00	-11.78	-294.43	6743.58	0.00	0.00	-11.78	-294.43	6743.58
2	1	0.00	0.00	-15.70	-392.57	8991.43	0.00	0.00	-15.70	-392.57	8991.43	0.00	0.00	-15.70	-392.57	8991.43

RMR 80 Tunnel radius 4.5m SC elastic modulus 12000MPa

q_v	k	SC thickness 0.1m					SC thickness 0.2m					SC thickness 0.3m				
		M+	M-	T+	T-	N+	M+	M-	T+	T-	N+	M+	M-	T+	T-	N+
0.5	0	0.87	-1.16	2.66	-97.92	2242.82	3.56	-5.47	1.09	-97.81	2240.31	8.14	-10.89	3.39	-97.65	2236.49
1	0	1.73	-2.32	5.31	-195.85	4485.64	7.12	-10.94	2.18	-195.63	4480.61	16.27	-21.79	6.77	-195.29	4472.98
1.5	0	2.60	-3.48	7.97	-293.77	6728.45	10.68	-16.41	3.27	-293.44	6720.92	24.41	-32.68	10.16	-292.94	6709.47
2	0	3.46	-4.64	10.62	-391.69	8971.27	14.23	-21.88	4.35	-391.26	8961.23	32.54	-43.58	13.54	-390.59	8945.96
0.5	0.5	0.43	-0.43	-1.97	-98.03	2245.34	1.78	-1.78	-1.96	-97.98	2244.14	4.10	-4.10	-1.96	-97.89	2242.09
1	0.5	0.87	-0.87	-3.93	-196.07	4490.67	3.56	-3.56	-3.93	-195.96	4488.29	8.20	-8.20	-3.92	-195.78	4484.18
1.5	0.5	1.30	-1.30	-5.90	-294.10	6736.01	5.33	-5.33	-5.89	-293.94	6732.43	12.29	-12.29	-5.88	-293.67	6726.26
2	0.5	1.73	-1.73	-7.86	-392.13	8981.35	7.11	-7.11	-7.86	-391.93	8976.58	16.39	-16.39	-7.84	-391.57	8968.35
0.5	1	0.00	0.00	-3.93	-98.14	2247.86	0.00	0.00	-3.93	-98.14	2247.86	0.00	0.00	-3.93	-98.14	2247.86
1	1	0.00	0.00	-7.85	-196.29	4495.72	0.00	0.00	-7.85	-196.29	4495.72	0.00	0.00	-7.85	-196.29	4495.72
1.5	1	0.00	0.00	-11.78	-294.43	6743.58	0.00	0.00	-11.78	-294.43	6743.58	0.00	0.00	-11.78	-294.43	6743.58
2	1	0.00	0.00	-15.70	-392.57	8991.43	0.00	0.00	-15.70	-392.57	8991.43	0.00	0.00	-15.70	-392.57	8991.43

For intermediate stress values between those considered in the analysis, interpolation can be used, which is based on the cubic law when four values are available (such as the case for q_v). Alternatively, a parabolic law can be employed when three values of each parameters such as k, RMR, SC linining thickness and elastic modulus and tunnel radius are available. The use of the interpolation can also permit to obtain an estimation of the loads for values outside those considered in the parametric analysis.

If, for instance, the bending moments and axial forces for a SC lining with thickness 0.15cm, elastic modulus of 8000MPa, k =0.5, RMR=60, tunnel radius of 4.5m and stress of 0.75MPa are required, then it is possible to proceed as following:

1. First of all, it is possible to identify the values, by proceeding with the parabolic interpolation for the lining thickness values.

Table 4. Bending moments and axial forces for SC elastic modulus equal to 6000, 9000 and 12000MPa for RMR=60 and thickness 0.15m.

q_v	k	M+	M-	N+
0.5	0.5	1,01	-1,01	2244,79
1	0.5	2,03	-2,03	4489,62
1.5	0.5	3,04	-3,04	6734,43
2	0.5	4,05	-4,05	8979,26
q_v	k	M+	M-	N+
0.5	0.5	1,05	-1,05	2244,82
1	0.5	2,09	-2,09	4489,59
1.5	0.5	3,14	-3,14	6734,37
2	0.5	4,19	-4,19	8979,17
q_v	k	M+	M-	N+
0.5	0.5	1,09	-1,09	2244,74
1	0.5	2,16	-2,16	4489,53
1.5	0.5	3,24	-3,24	6734,29
2	0.5	4,33	-4,33	8979,08

2. Afterwards, it is possible to proceed with the parabolic interpolation regarding the values of the mean elastic modulus of the SC.

Table 5. Bending moments and axial forces for SC elastic modulus equal to 8000MPa for RMR=60 and thickness 0.15m.

q_v	k	M+	M-	N+
0.5	0.5	1,04	-1,04	2244,57
1	0.5	2,03	-2,03	4489,71
1.5	0.5	3,11	-3,24	6734,52
2	0.5	4,14	-4,14	8979,20

3. Finally, it is possible to proceed with the cubic interpolation regarding the vertical stress q_v.

Table 6. Bending moments and axial forces for SC elastic modulus for 8000MPa for RMR=60 and thickness 0.15m.

q_v	k	M+	M-	N+
0,75	0.5	1,51	-1,51	3367,19

When the stress values, regarding the specific case are known, it is possible, through the simple buckling method of the rectangular section, to determine the maximum compression load acting on SC lining. In the above-mentioned example, the maximum

compression load is 22.85MPa. By comparing the maximum load acting on the SC lining with the concrete strength it is possible to see whether the thickness of the hypothesized lining is suitable to guarantee the tunnel stability without wasting any material, therefore by saving costs.

Just as an example the diagrams showing maximum and minimum bending moments (positive and negative), maximum and minimum shear stress and maximum axial forces for the case RMR=60, tunnel radius=4.5 and k =0 are shown. The diagrams allow to obtain the load parameters for changing vertical load q_v, applied at the SC lining for different elastic modulus E, and lining thickness values.

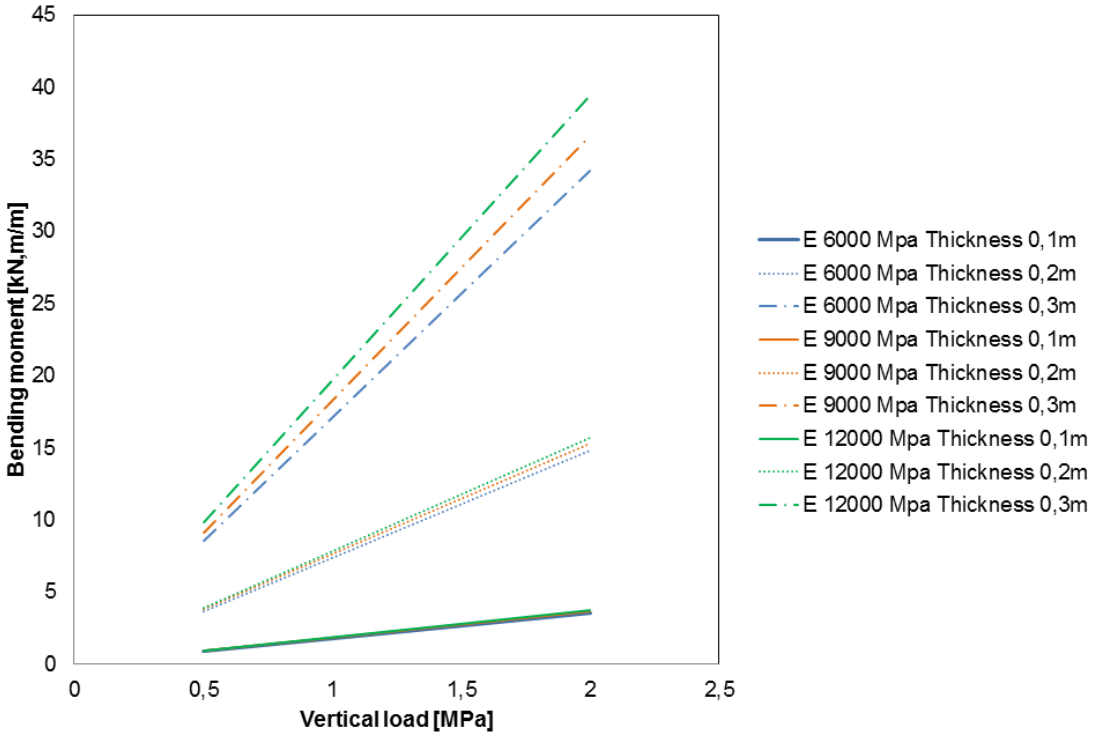

Figure 14. Path of the maximum positive bending moment in the SC lining by varying the applied q_v for different mean elastic modulus of the concrete and lining thickness for RMR=60, R=4.5 and k =0.

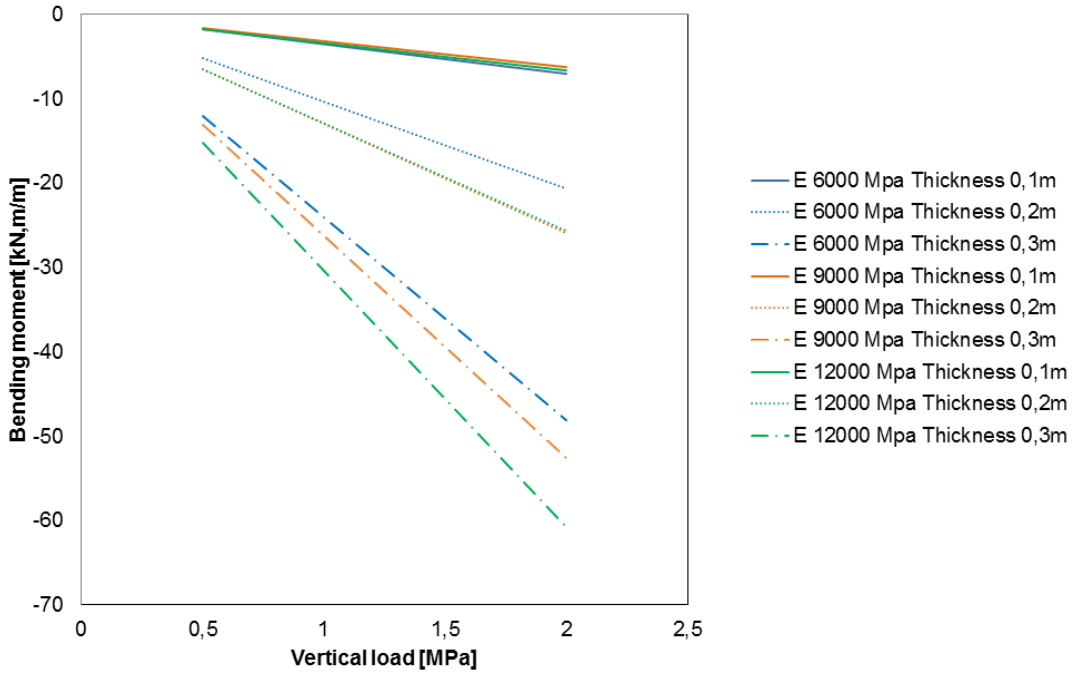

Figure 15. Path of the maximum negative bending moment in the SC lining by varying the applied q_v for different mean elastic modulus of the concrete and lining thickness for RMR=60, R=4.5 and k =0.

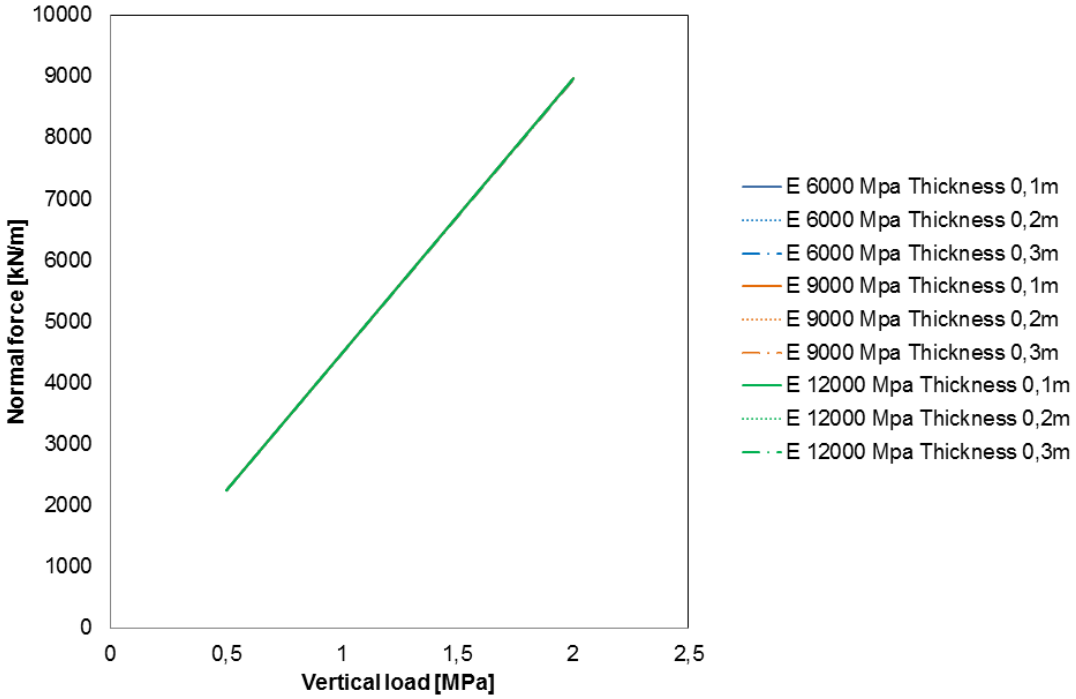

Figure 16. Path of the maximum axial force in the SC lining by varying the applied q_v for different mean elastic modulus of the concrete and lining thickness for RMR=60, R=4.5 and k =0.

From Figures 14 to 15 it is possible to notice how the lining thickness has a strong influence on the bending moment value which develops inside. The mean elastic modulus value has also a certain effect, above all for large SC lining thickness values. The maximum axial force is not practically influenced by the lining elastic modulus and thickness (Figure 16). Both maximum bending moments and maximum axial forces increase in a linear way with the load value, q_v.

Tunnel radius, k values, and RMR of the rock mass have also a great influence on the maximum bending moment and axial forces.

By comparing the analysis considering $K_s = 0.5 \cdot K_n$ with $K_s = 0$, it is possible to note how the absence of shear interaction between the lining and the rock mass ($K_s = 0$) cause bending moment values in the lining higher with respect to the case where $K_s = 0.5 \cdot K_n$. Besides, with $K_s = 0$ also the maximum axial forces in the lining increase, but only slightly with respect to the $K_s = 0.5 \cdot K_n$ case.

4. THE CCM-HRM COMBINED ANALYSIS FOR THE ASSESSMENT OF THE TENSIONAL STATE IN THE SHOTCRETE LINING

The numerical procedure developed to obtain a detailed analysis of the tensional and deformational state of a SC lining tunnel requires analysis combined with CCM and HRM. The necessary calculation parameters are as follows: mechanical parameters of the rock, tunnel radius, lithostatic tension state of the tunnel at the corresponding depth, lining thickness, evolving curve of the strength and stiffness of the SC with the time, the advancement speed of the excavation face and the frequency and duration of the excavation operation stand still, to allow the support installation and other operations on the site.

The CCM is based on the analysis of the stress and strain state that develops in the rock around a tunnel. The simplicity of the method is due to the important hypotheses on which it is based (e.g. Oreste, 2009; 2014; Spagnoli et al., 2017):

- Circular and deep tunnels (boundary conditions of the problem to infinity);
- Lithostatic stresses of a hydrostatic type and constant in the surrounding medium of the tunnel (the variation of the stresses with depth due to the weight of the rock is neglected);
- Continuous, homogeneous and isotropic rock mass;
- Bi-dimensional problem and plane stress field.

CCM consists of the definition of the convergence-confinement curve (CCC), that is the relationship between the internal pressure and the radial displacement $(p - |u|)$ on the boundary of the tunnel represented by a circular void (Oreste, 2009), see Figure 17.

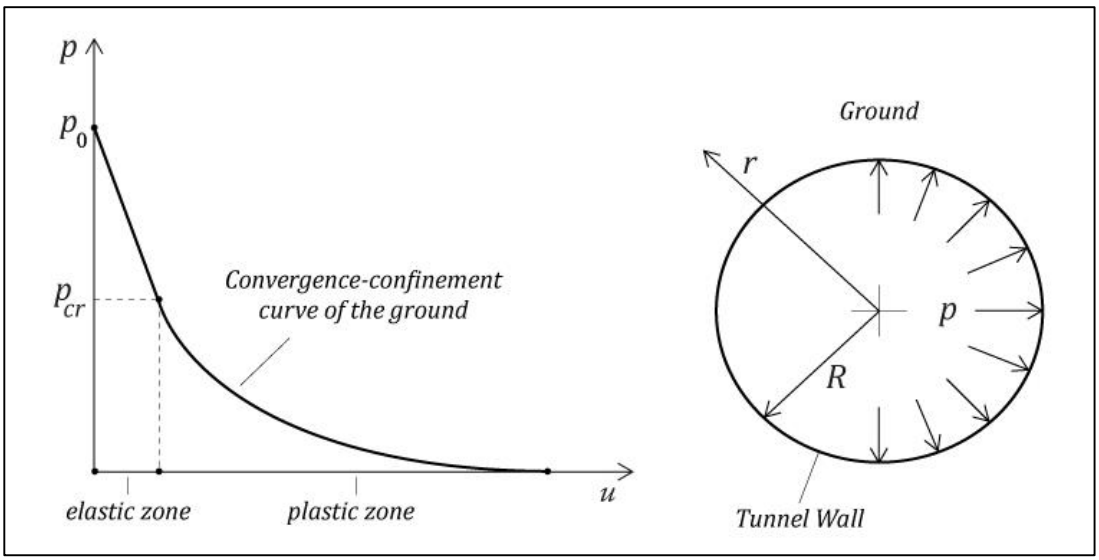

Figure 17. Convergence-confinement method: Geometry of the problem and example of a convergence-confinement curve. Key: p: Internal tunnel pressure, R: Tunnel radius, r: Radial coordinate, u: Radial displacement of the tunnel, p_0: Lithostatic stress, p_{cr}: Critical pressure (modified by Oreste, 2009).

4.1. MOHR COULOMB EQUATIONS FOR THE CONVERGENCE CONFINEMENT CURVE OF THE ROCK MASS

For an internal pressure equal to p_0 (lithostatic stress) there is no change in the initial stress and strain state around the hole and therefore the radial displacement of the wall is zero. With a diminishing of the internal pressure p the radial displacement of the wall begins to appear: Initially this increases linearly.

At a certain point, for pressures lower than p_{cr}, the trend can result to be of a curvilinear type. In the simplest case of rock behavior of an elastic type, the convergence-confinement curve is represented by a linear segment.

In the more general case of rock with elastic-plastic behavior, the elastic limit of the rock is reached when, for a certain internal pressure p and with the decreasing of r, the stress state reaches the limit conditions defined by the strength criterion. Such a value of r is called the plastic radius R_{pl}. The radial pressure on the plastic radius is called the critical pressure p_{cr}, which is only a function of the peak strength parameters of the rock mass and is therefore independent of R_{pl} (Oreste, 2009). For the Mohr-Coulomb strength criterion:

$$p_{cr} = p_0 \cdot (1 - sin\,\varphi_p) - c_p \cdot cos\,\varphi_p \quad (61)$$

Where, c_p and φ_p are the peak cohesion and friction angle.

If p_{cr} results to be negative or equal to zero, the convergence-confinement curve continues to appear as a linear segment, that is, though the material has an elastic-plastic behaviour, the elastic limit is not reached in any point and the material remains in the elastic field throughout. Instead if p_{cr} is positive, a zone of thickness $(R_{pl} - R)$ under plastic behaviour appears for $p < p_{cr}$ around the void. The plastic radius therefore identifies the limit of the area under plastic behavior. The material continues to remain in elastic conditions for any distance greater than R_{pl}.

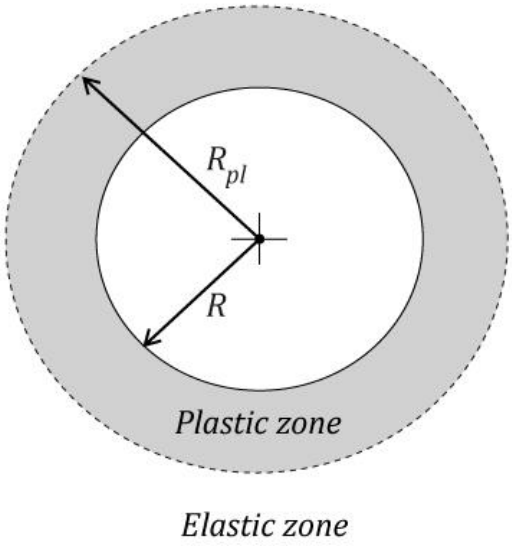

Figure 18. The elastic and plastic zones around the tunnel.

The expression of the plastic radius for the Mohr-Coulomb strength criterion is the following:

$$R_{pl} = R \cdot \left[\frac{\left(p_0 + \frac{c_r}{tg\varphi_r}\right) - \left(p_0 + \frac{c_p}{tg\,\varphi_p}\right) \cdot sin\,\varphi_p}{p + \frac{c_r}{tg\,\varphi_r}} \right]^{\frac{1}{N\varphi - 1}} \quad (62)$$

Where:

$$N_\varphi = \frac{1 + sin(\varphi_r)}{1 - sin(\varphi_r)} \quad (63)$$

It can be noticed how, for $p = p_{cr}$, the plastic radius coincides with the radius of the void and the plastic zone has therefore nil thickness. For lower internal pressures, R_{pl} begins to increase and the plastic zone increases in thickness.

For values of r greater than the plastic radius, the rock maintains an elastic behavior, as described in the following equation:

$$u = \frac{1+v}{E_{rm}} \cdot (p_0 - p\,) \cdot R \tag{64}$$

The detailed analysis of the strain behavior in the plastic zone also allows one to obtain the expression of the radial displacement of the tunnel wall for $p < p_{cr}$. With the hypothesis of the Mohr-Coulomb strength criterion and considering the expression of the plastic potential of the same type as the strength criterion, it is possible to obtain a rigorous solution in closed form of the radial displacement u of the tunnel wall for $p < p_{cr}$, that is, for $R_{pl} > R$ (Oreste, 2009):

$$u = \frac{1+v}{E_{rm}} \cdot [A + B - C] \tag{65}$$

Where:

$$A = \frac{R_{pl}^{N_\psi+1}}{R^{\,N_\psi}} \cdot \left(p_0 + \frac{c_p}{tg\ \varphi_p}\right) \cdot \sin\varphi_p \tag{66}$$

$$B = (1 - 2\cdot v) \cdot \left(p_0 + \frac{c_r}{tg\varphi_r}\right) \cdot \left(\frac{R_{pl}^{N_\psi+1}}{R^{\,N_\psi}} - R\right) \tag{67}$$

$$A = \frac{R_{pl}^{N_\psi+1}}{R^{\,N_\psi}} \cdot \left(p_0 + \frac{c_p}{tg\ \varphi_p}\right) \cdot \sin\varphi_p \tag{68}$$

$$C = \left(\frac{1 + N_\varphi \cdot N_\psi - v\cdot\left(N_\psi+1\right)\cdot\left(N_\varphi+1\right)}{\left(N_\varphi + N_\psi\right)\cdot R^{N_\varphi+1}}\right) \cdot \left(p + \frac{c_r}{tg\ \varphi_r}\right) \cdot \left(\frac{R_{pl}^{(N_\varphi+N_\psi)}}{R^{\,N_\psi}} - R^{\,N_\varphi}\right) \tag{69}$$

$$N_\psi = \frac{1+sin(\psi)}{1-sin(\psi)} \tag{70}$$

Where ψ is the dilatancy.

The most important adopted simplification consists in considering the total deformations in the plastic field (and not the elastic component which is governed by elastic parameters) separately from the plastic component (which is governed by the plastic potential).

4.2. DEFINITION OF THE FRICTIONAL PRESSURE AND ADVANCEMENT OF THE TUNNEL

The convergence-confinement curve that was described previously does not take any possible support structure in the tunnel into consideration, but only considers a generic internal pressure which, varying, provokes a different tunnel response both in terms of convergence and in terms of extension of the plastic zone. In order to analyse the interaction between the tunnel and the support structures in more detail, it is necessary to represent the support structures through their own reaction line and to introduce the concept of fictitious internal pressure.

The fictitious internal pressure is a quantity that is introduced in order to allow one to face a three-dimensional problem (due to the presence of the excavation face) with a simplified bi-dimensional scheme as in fact the convergence-confinement method is. After having identified a precise section to study along the tunnel axis, the following different situations are taken into consideration (Oreste, 2009):

- When the excavation face is still very far from the studied section, the internal pressure acting on the perimeter of the future tunnel is equal to p_0: The stress perturbation produced by the excavation works at the studied section can be considered negligible (Figure 19.A).
- As the excavation face comes closer to the studied section, a certain stress release is produced ahead of the face which involves a reduction of the internal pressure and the appearance of radial displacements on the perimeter of the future tunnel even before it is excavated (Figure 19.B).
- When the face passes the studied section, the contribution offered by the face to the static of the tunnel can be taken into consideration through the fictitious internal pressure concept which diminishes, until it disappears, in function of the distance from the tunnel face (Figure 19.D-E).

With the concept of the fictitious internal pressure, it is therefore possible to consider the convergence-confinement curve as a graphic representation of the strain situation that is produced along the tunnel axis.

Each point of the curve represents the situation in a particular section with reference to the position of the excavation face.

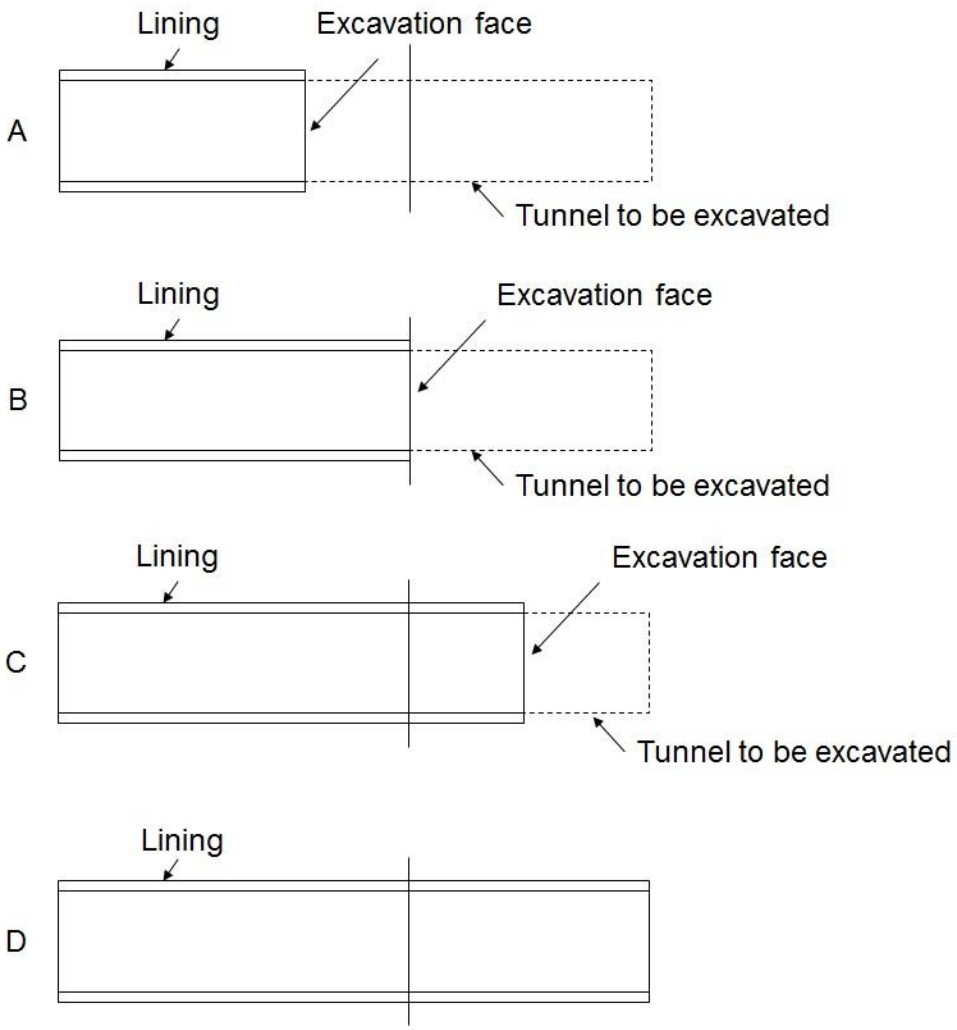

Figure 19. Location of the excavation face with respect to the considered studied section (modified after Oreste, 2009).

SC lining is placed close to the excavation face, when the static contribution offered by the face still exists. Its characteristics, the increase of its mechanical parameters in time in the hardening period, make the understanding of its behaviour, and therefore its correct design, difficult. As the SC hardens, the gradual loading of the lining takes place, while the excavation face gradually advances. These transient conditions not only represent critical situations for the stability of the support structure during the construction of the tunnel, but also influence the final equilibrium of the lining (in the long term, far from the excavation face) (Oreste, 2003).

4.3. DEFINITION AND FORMULATION FOR THE REACTION LINE OF THE SHOTCRETE LINING

Along with the CCC it is possible to drawn on the same graph also the reaction line of the SC lining (RLSL) as can be seen in Figure 20. This reaction line starts from a point on the abscissa (where pressure in zero) but the displacement u^* is different than zero. The line increases when the pressure p (the radial load on the lining, corresponding to the radial pressure applied by the lining on the tunnel wall) with increasing displacement u (the radial displacement of the tunnel wall). At the lining installation (initial point of the reaction line), the pressure applied at the extrados is zero, but a displacement of the tunnel wall, u^*, already occurred (Oreste, 2003).

The reduction of the pressure p on the ground reaction curve before installation of the lining ($p < p^*$) is due to the stress release that occurs in the core of the rock ahead of the excavation face. The SC lining is installed in B (see Figure 20) close to the excavation face: the rock ahead of the face produces a stabilizing effect on the tunnel which can be considered through a fictitious internal pressure p_{fict} that acts on the tunnel boundary, and which progressively decreases with the advancement of the face. Apart from the fictitious internal pressure, the pressure due to the SC lining p_{lin} also acts on the boundary of the already excavated tunnel. This pressure increases as the face advances and the lining is loaded when the tunnel tends to close (that is, with an increase in u).

Initially, in B (see Figure 20), the pressure p of the ground reaction curve is entirely supplied by the fictitious pressure produced by the face, while in D (see Figure 20), at the final equilibrium point (far from the excavation face), pressure p is caused by the action of the lining (Oreste, 2003).

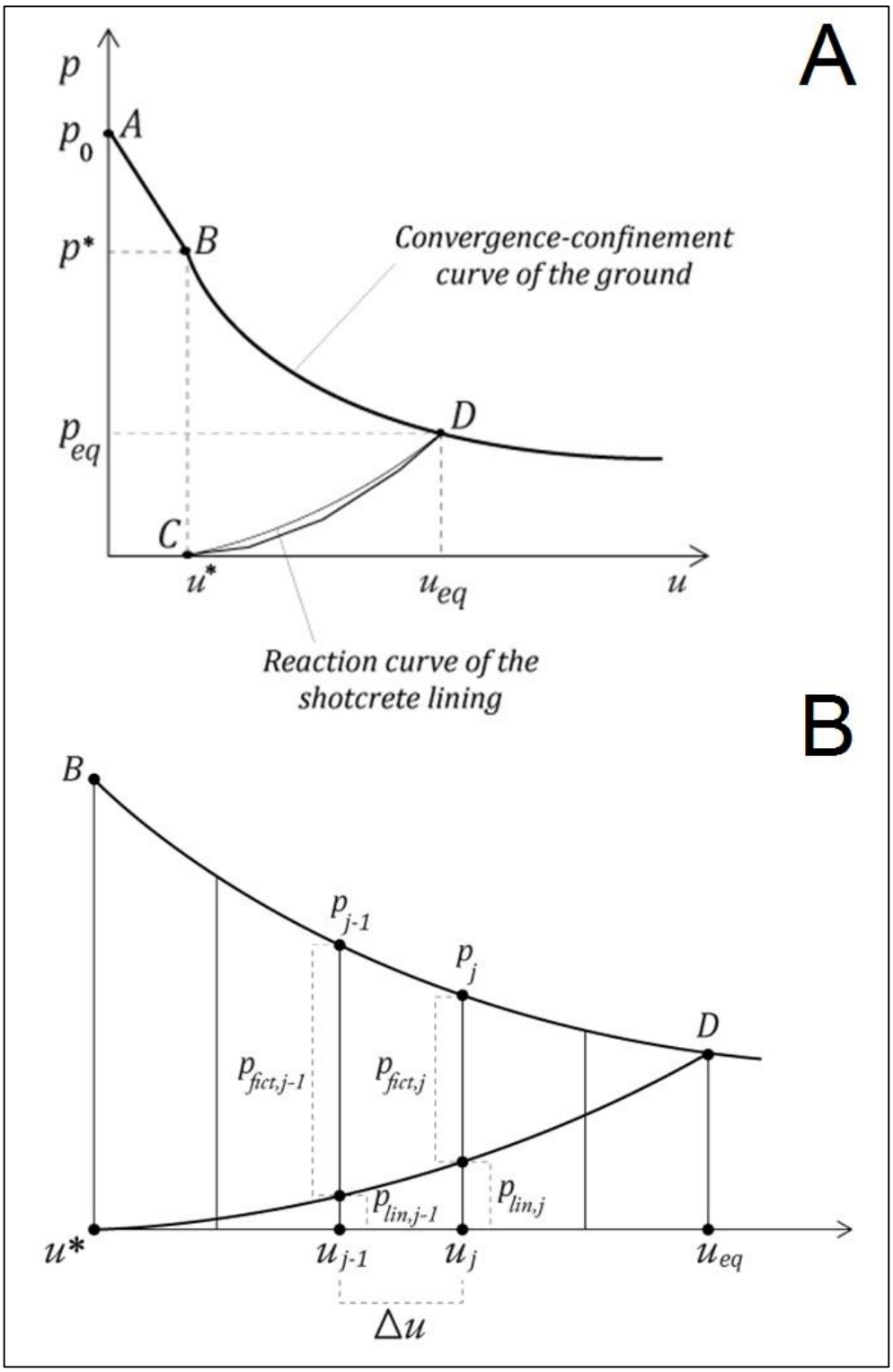

Figure 20. Ground reaction curve and reaction curve of the shotcrete lining (A); Numerical integration of the reaction curve of the shotcrete lining and a calculation step (B).

The reaction line is concave because the stiffness of the SC increases over the time, therefore with increasing load on the lining and with increasing radial displacement of the tunnel wall (Oreste, 2003). The pressure difference at a certain displacement level u between the CCC and RLSL is called fictitious pressure (p_{fict}) and it is the static contribute of the excavation face on the investigated vertical section of the tunnel. The fictitious pressure can be evaluated as a function of the (positive) distance x between the investigated section and the excavation face, with the well-known equation of Panet and Guenot, 1982:

$$p_{fict} = a \cdot p_0 \cdot \frac{b}{x + b} \quad (71)$$

Where:

$$a = 0.72 \quad (72)$$

$$b = 0.845 \cdot R \quad (73)$$

If a cross section of the SC lining is considered, the distance x of this section from the face depends on the mean advancement velocity va of the excavation face and on dead time t_0 that is foreseen for the lining installation and hardening (Figure 21).

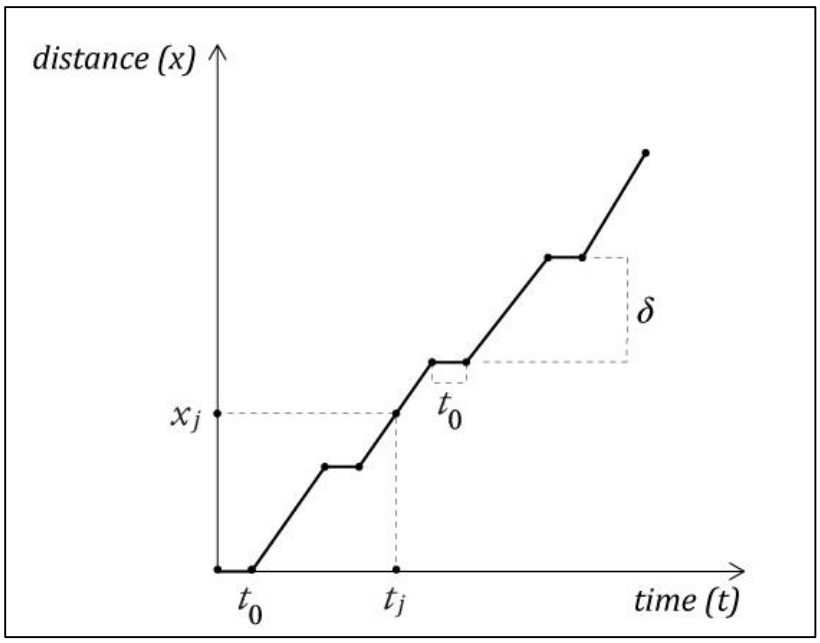

Figure 21. Graph of the excavation face advancement x, following the installation of the shotcrete lining. t_0 is the dead time due to the installation of the lining and waiting for it to harden; δ is the advancement step.

A calculation procedure is presented which is able to provide the reaction curve of a lining with increasing stiffness, by taking into account the variability due to time of the SC stiffness and strength, as well as the face advancement rate (Oreste, 2003).

Starting from the initial point of the reaction line ($p = 0; u = u^*$) and knowing the initial elastic modulus of the SC after the re-entry, it is possible to obtain the initial slope of the reaction line, k (Oreste, 2009) based on the support geometry (external radius and thickness), the elastic modulus and the Poisson ratio of the SC. Proceeding with a numerical approach, an initial segment of the RLSL for a small increase Δu of u is drawn. At the end of this first segment, p_{fict} can be evaluated as the difference between CCC and RLSL and from the fictitious pressure the distance x reached by the excavation face, using Equation 71.

As excavation advance is known, and hence the relation linking x to the time, t, at each distance x reached by the excavation face with respect to the investigated section, a time value t corresponding subsequent to the SC lining installation can be given. At first load step Δp (evaluated as the difference in the initial linear part of RLSL) the reached time at the end of the first trait, can be associated and therefore also the mean elastic modulus of the SC in the period corresponding to the initial linear part of RLSL. The method continues in the same way for successive small linear traits, until the intersection between the CCC and the RLSL is obtained. The intersection point between the two curves represents the final stage of the loading process when the excavation face is advanced at a distance where static effects on the vertical section of the tunnel are negligible (Figure 20).

The procedure for the calculation step j is the following:

- Evaluation of the pressure p reached by the RLSL in the final point of the previous trait $p_{lin,j-1}$ and by difference between CCC and RLSL in such a point; evaluation of the fictitious pressure $p_{fict,j-1=}\, p_{j-1} - p_{lin,j-1}$, p_{j-1} is the pressure read on CCC in correspondence of the displacement u_{j-1};
- If the $p_{fict,j-1}$ is known, the corresponding distance x_{j-1} of the excavation face is calculated using Equation 71;

- Knowing the advance excavation rate, the duration and frequency of still stands of the excavation phase, i.e. the relation $x = f(t)$, it is possible to determine the time t_{j-1} subsequent to the installation of the SC in the studied section;
- If the evolving trend of the elastic modulus of the SC over the time is known, it is possible to determine the elastic modulus E_{j-1} and therefore the stiffness of the SC k_{j-1} over the time t_{j-1} through the following equation:

$$k_{j-1} = \frac{R^2 - (R - s_{shot})^2}{(1 + v_{shot}) \cdot [(1 - 2 \cdot v_{shot}) \cdot R^2 + (R - s_{shot})^2]} \cdot \frac{1}{R} \cdot E_{shot,t_{j-1}} \quad (74)$$

Where:

$E_{shot,t_{j-1}}$ is the SC elastic modulus at the previous calculation step;

v_{shot} is Poisson ratio of the SC;

R is the tunnel radius;

s_{shot} is the lining thickness.

- The knowledge of the stiffness k_{j-1} allow to draw the new straight line of the RLSL for the step j for a predetermined amplitude of the radial displacement u equal to Δu; at the end of such a train we obtain: $p_{lin,j-1=}\, p_{linj-1} - k_{j-1} \cdot \Delta u$;
- The difference $p_{lin,j-}\, p_{linj-1}$ is the first loading step $\Delta p_{lin,j}$ of the step j, linked to the mean elastic modulus of the SC $E_{med,j}$ in the step j.

$$E_{med,j} = 0.5 \cdot (E_{j-1} + E_j) \quad (75)$$

Therefore, in the detailed study of the tensional state in the SC lining, the knowledge of the evolving trend of the SC, $E = f(t)$, is important. Generally, the variation of the UCS over the time, $\sigma_c = f(t)$, is evaluated. Then, the relation between the elastic modulus and UCS is considered constant. This is given by the equation of Chang (1993):

$$\sigma_{c,t} = \left(\frac{E_{lin,t}}{3.86}\right)^{1/0.6} \quad (76)$$

Where:

$E_{lin,t}$ is the SC elastic modulus at the time t;

$\sigma_{c,t}$ is the UCS for the SC at the time t.

A method to represent the variation of the elastic modulus over the time is given by Pottler (1990):

$$E_{lin,t} = E_{lin,0} \cdot (1 - e^{-\alpha \cdot t}) \quad (77)$$

Where:

$E_{lin,0}$ is the value of the asymptotic elastic modulus of the shotcrete, for $t = \infty$;

α is a time constant (t^{-1}).

From the practical point of view, UCS of SC is measured over the time subsequent to the lining installation and from this value, a series of elastic modulus values for different timings is obtained.

Then the negative exponential curve, which best approximates the obtained points, i.e. the pairs of values of the elastic modulus and associated time, is obtained. This curve will have particular values of the asymptotic elastic modulus $E_{lin,0}$, and of the coefficient α in Equation 77.

The proposed calculation method permits one to obtain:

- The effective reaction curve of the SC lining;
- Changes in the normal and shear nodal displacements, internal shear and normal forces, rotations and bending moments along the tunnel perimeter taking into account the evolution in time of the SC elastic modulus simulating the time of maturation of the support and the distance from the excavation face. In this way, it is possible to assess the influence of transient state on the final conditions of the SC lining.

5. EXAMPLE OF APPLICATION AND COMMENTS ON THE FINAL RESULTS

The calculation procedure proposed in this research has been applied to some examples, in order to verify which can be the effect on the stress state in the SC lining, by varying the characteristics of the concrete (in particular the curing rate and final elastic module) and the advance speed of the excavation face.

Different geometries of the tunnel were considered, along with various rock types. In general, six main examples are presented, each of which has four cases. The cases considered include the following assumptions, in accordance with the underlying hypotheses of the calculation methods which were used in the procedure presented.

- A bi-dimensional stress state considering circular and deep tunnels;
- A hydrostatic-type lithostatic stresses in the surrounding ground (the variation of the tensions with the depth due to the weight of the rock is neglected)
- A continuous, homogeneous and isotropic rock mass.

The first example (example 1) refers to a tunnel of 2 m radius excavated in a rock of poor quality. Geomechanical parameters are shown in Table 7. The lithostatic stress p_0 is 7 MPa and the fictitious internal pressure p_{fict} at the face is $0.72 \cdot p_0$, where the shotcrete lining is installed. SC lining has a thickness of 20 cm. The horizontal stress in the lithostatic field is ½ of the vertical one (K_0 =0.

Table 7. Geomechanical parameters for the rock mass for example 1.

Rock Mass Parameters	
Elastic modulus [MPa]	3160
Poisson ratio	0.30
Peak Cohesion [MPa]	0.15
Residual Cohesion [MPa]	0.12
Peak Angle of Friction [°]	20
Residual Angle of Friction [°]	16
Dilatancy [°]	16

Since the calculation code uses HRM, the values of the stiffness of the interaction springs of the support with the ground are obtained by the following expressions:

$$b = 2 \cdot R \cdot cos(2{,}5°) \cdot sin(2{,}5°) \quad (78)$$

$$K_n = 2 \cdot \frac{E_{rm}}{R} \cdot b \quad (79)$$

$$Fn_{lim} = \frac{2 \cdot c_p \cdot cos\,(\varphi_p)}{1 - sin(\varphi_p)} \cdot b \quad (80)$$

$$K_s = \frac{K_n}{2} \quad (81)$$

Two different types of SC were assumed with a final and asymptotic value of the elastic modulus ($E_{SC,0}$) of 6000 and 12000MPa, both with a Poisson ratio 0.15. The time constant α has a value of 0.05 h-1.

The other parameter to be varied is the daily rate of tunnel advance (arbitrary assumed as 2 m/day and 10m/day), with support installation time t_0 and the advancement step δ equal to 1h and 1.2m respectively. The diagrams for advancing the tunnel face for the two speeds mentioned above are shown below.

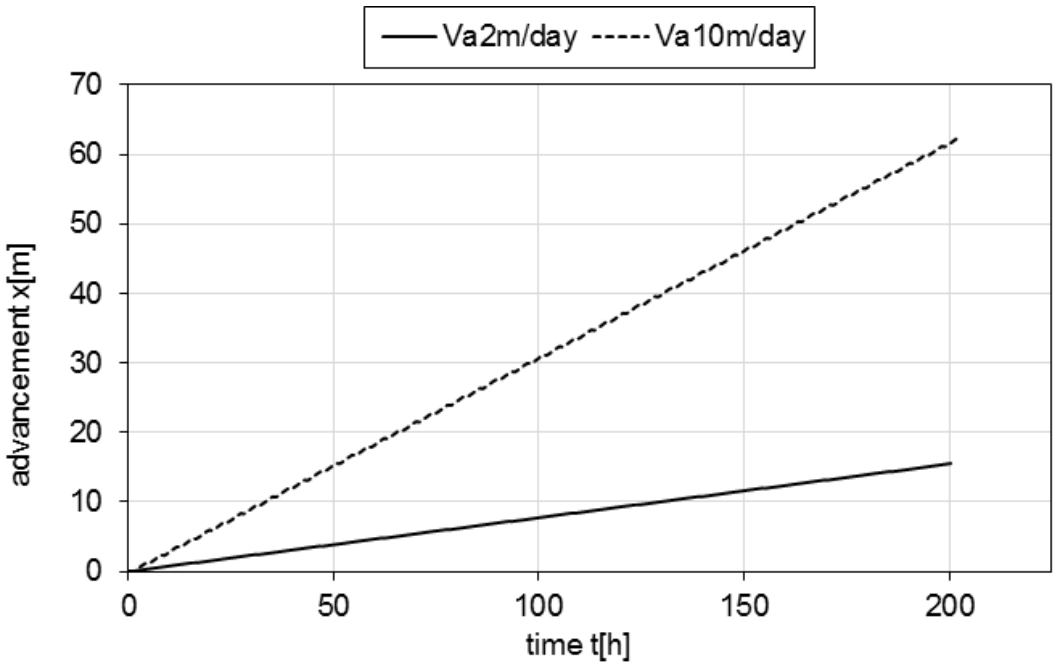

Figure 22. Graph of the tunnel excavation with face advancements rate equal to 2 and 10m/day.

The diagrams relating the time to the modulus of elasticity and UCS are shown below.

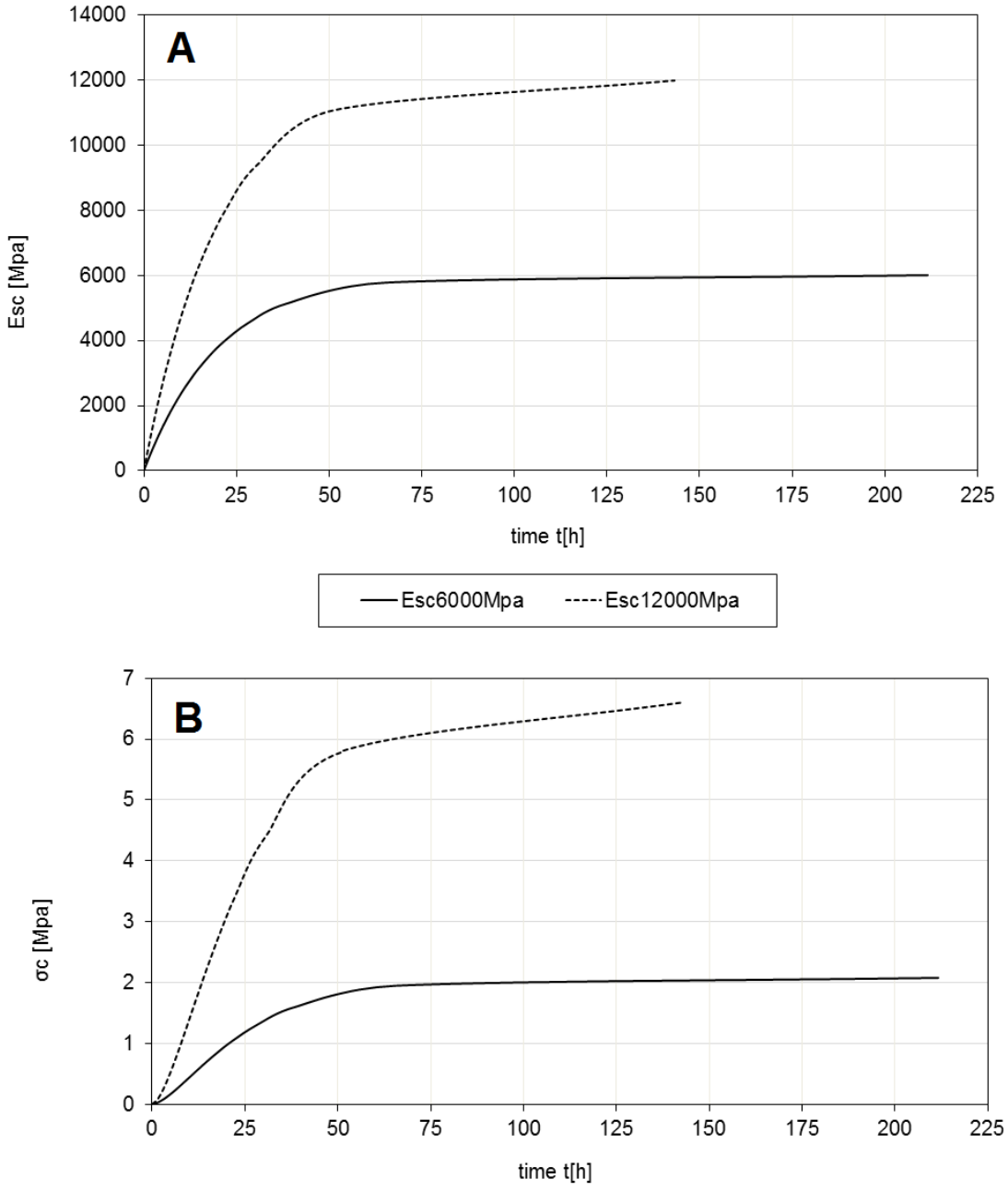

Figure 23. Progressive increase of the elastic modulus (A) and UCS (B) of the shotcrete over the time.

The reaction curves of the lining are shown in Figure 24 for the four cases analyzed.

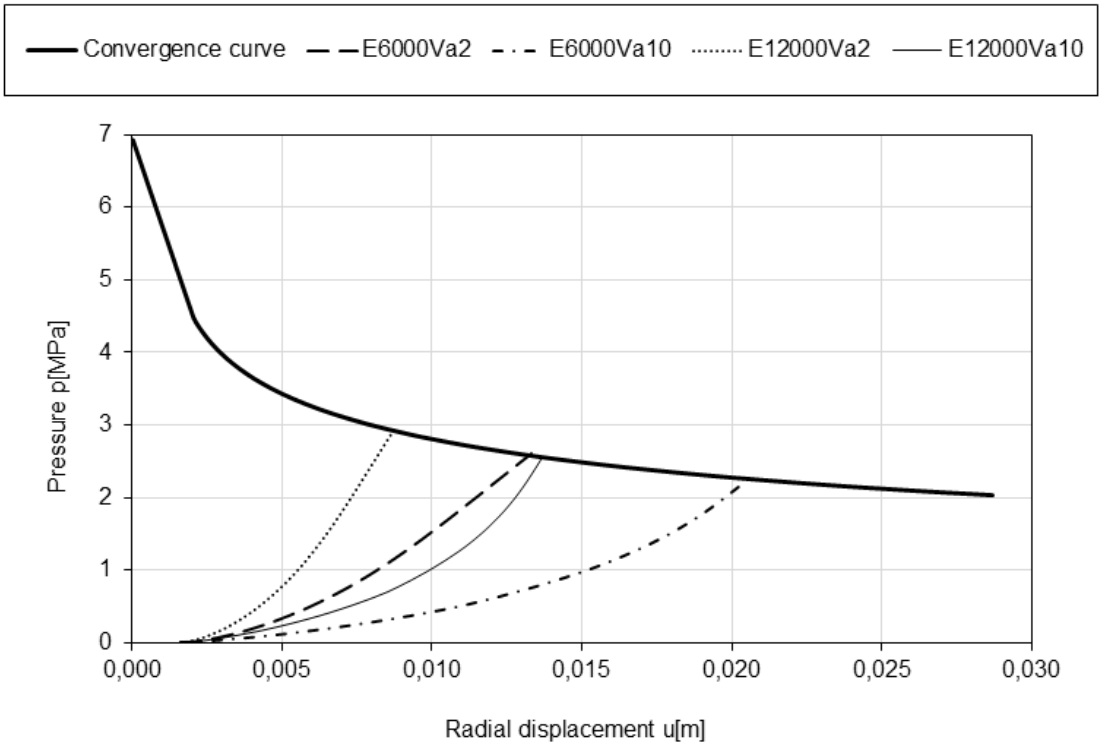

Figure 24. Reaction curve of the SC lining as a function of the face advancement rate and the apparent elastic modulus of the shotcrete for the example 1.

It is possible to see in Figure 24 the change of the equilibrium point (intersection between the CCC and the reaction line) for each of the cases. In addition, it can be observed that the reaction line is not straight but curved. This is because the calculation model considers the maturation time of the SC, i.e. the progressive increase of the modulus of elasticity and UCS from the installation of the support to the point at which the maximum resistance and stiffness of the SC has been obtained.

The influence of the concrete type and advance velocity appears to be very important in the final evaluation of the equilibrium point and, hence, of the final loading on the SC lining and the final displacement of the tunnel wall.

The final load on the lining, as well as the final displacement of the tunnel wall, may vary significantly depending on the type of concrete used and the tunnel face advancing speed. The highest final stress values are found for the most rigid type of concrete during the setting phase of the concrete and the lowest advance rate.

Also the stress and displacement characteristics of the individual contour points of the lining can vary significantly. In the following the values referring to the final condition (at the equilibrium point) for example 1 are shown (Figure 25).

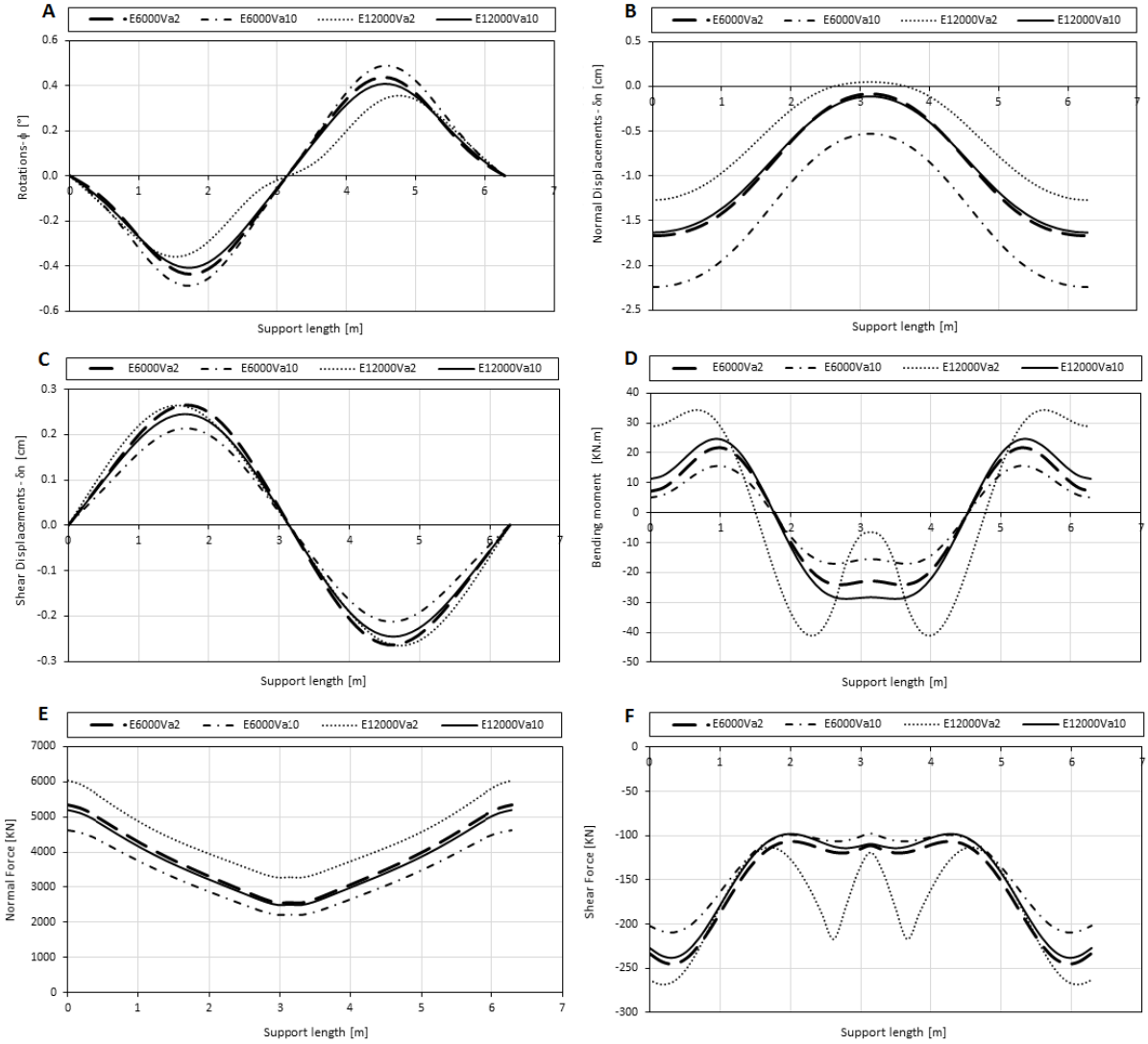

Figure 25. Variation of the rotation (A), normal displacement (B), shear displacement (C), bending moment (D), normal force (E) and shear force (F) for the two considered type of SC and the two assumed advance rates of the tunnel face, with reference to the final equilibrium point (example 1).

Of particular interest is the trend of normal displacements, bending moments, normal forces and shear forces along the lining.

Lower stiffness during the setting period and faster advance speed provide larger normal displacements. Conversely, higher stiffness and lower advance speed produce lower

normal displacements. The highest peak moments are detected in the lining when using high stiffness concrete and low advance speed. The opposite is for lower stiffness and higher advance speed. Same considerations can be made for normal and shear forces.

In the example 2 analyzes a tunnel of radius R equal to 2.5 m, excavated in a rock mass of poor mechanical properties (RMR = 40, Table 8). The lithostatic pressure p_0 is 5MPa. Also in this example the lining thickness is 20 cm and K_0 is 0.5.

Table 8. Geomechanical parameters for the rock mass for example 2.

Rock Mass Parameters	
Elastic modulus [Mpa]	21170
RMR	40
Poisson ratio	0,30
Peak Cohesion [Mpa]	1.5
Residual Cohesion [Mpa]	1.5
Peak Angle of Friction [°]	33
Residual Angle of Friction [°]	33
Dilatancy [°]	16

Four different cases were analyzed in which higher elastic modulus values of the support were taken as 12000 and 28000MPa. The alpha time constant α has a value of 0,05 h^{-1} and the Poisson ratio ν, of 0.15.

The tunnel advance daily rates were assumed to be 4m/day and 12m/day, with support installation time t_0 and the advancement step δ of 1h and 1.2m respectively. The diagrams of the face advancement for the two rates considered in this example are shown as follows below:

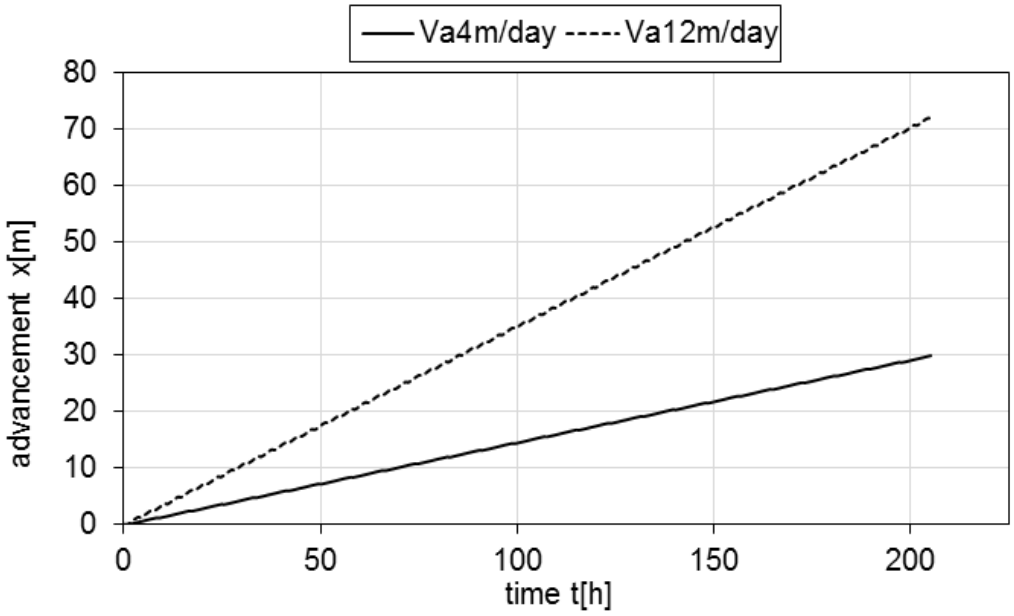

Figure 26. Graph of the tunnel excavation with face advancements rate equal to 4 and 12m/day.

The different reaction lines of the shotcrete lining in conjunction with the CCC are presented in the Figure 27, where it is possible to identify the equilibrium point corresponding to each analyzed case.

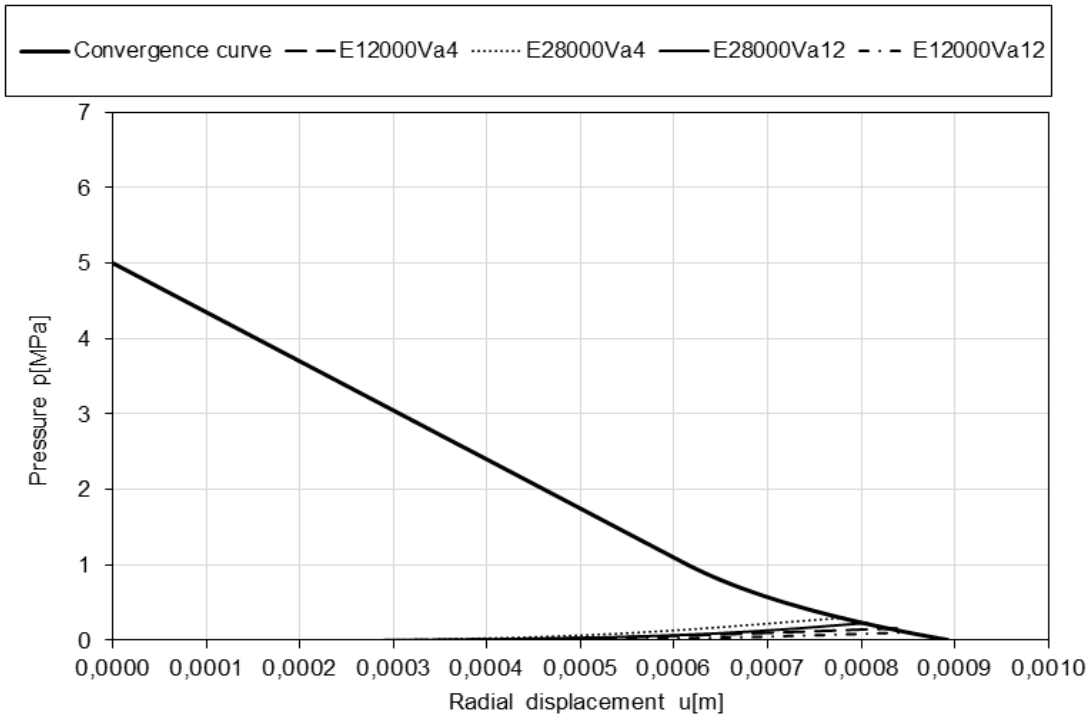

Figure 27. Reaction curve of the shotcrete lining as a function of the face advancement rate and the apparent elastic modulus of the shotcrete for the example 2.

In this second example, lower end loads are detected on the lining, but the differences between the 4 cases considered are in very high percentages. Even now, the higher end loads have a higher final elastic modulus and a lower face advancements rate.

The diagrams relating the time with the modulus of elasticity and UCS of SC are shown below. It is possible to observe the time in which the support reaches its maximum capacity of resistance.

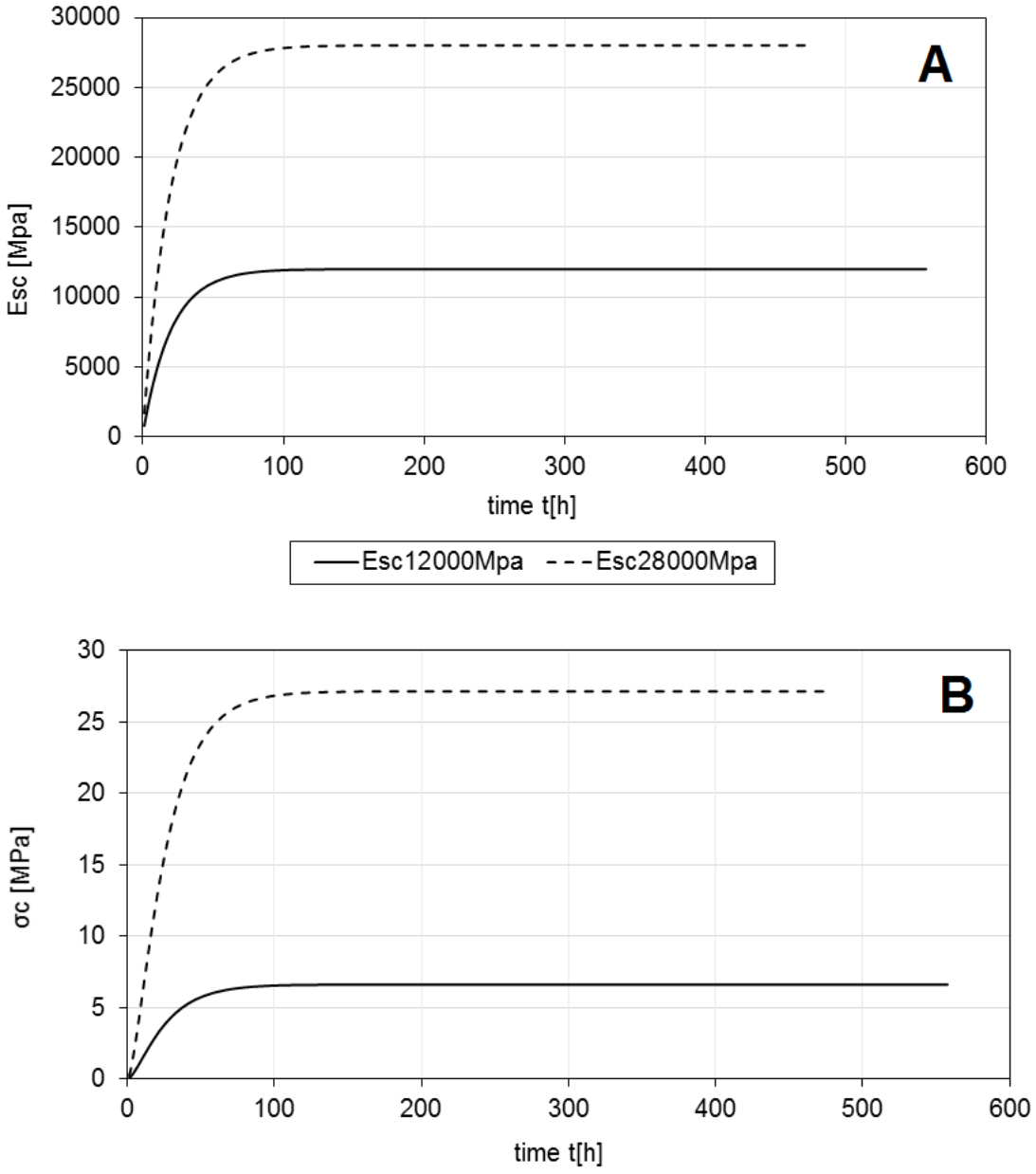

Figure 28. Progressive increase of the elastic modulus (A) and UCS (B) of the shotcrete over time.

The results in terms of displacements and stress characteristics along the lining circumference for the four cases presented in this example, when the final condition is reached, are shown in Figure 29.

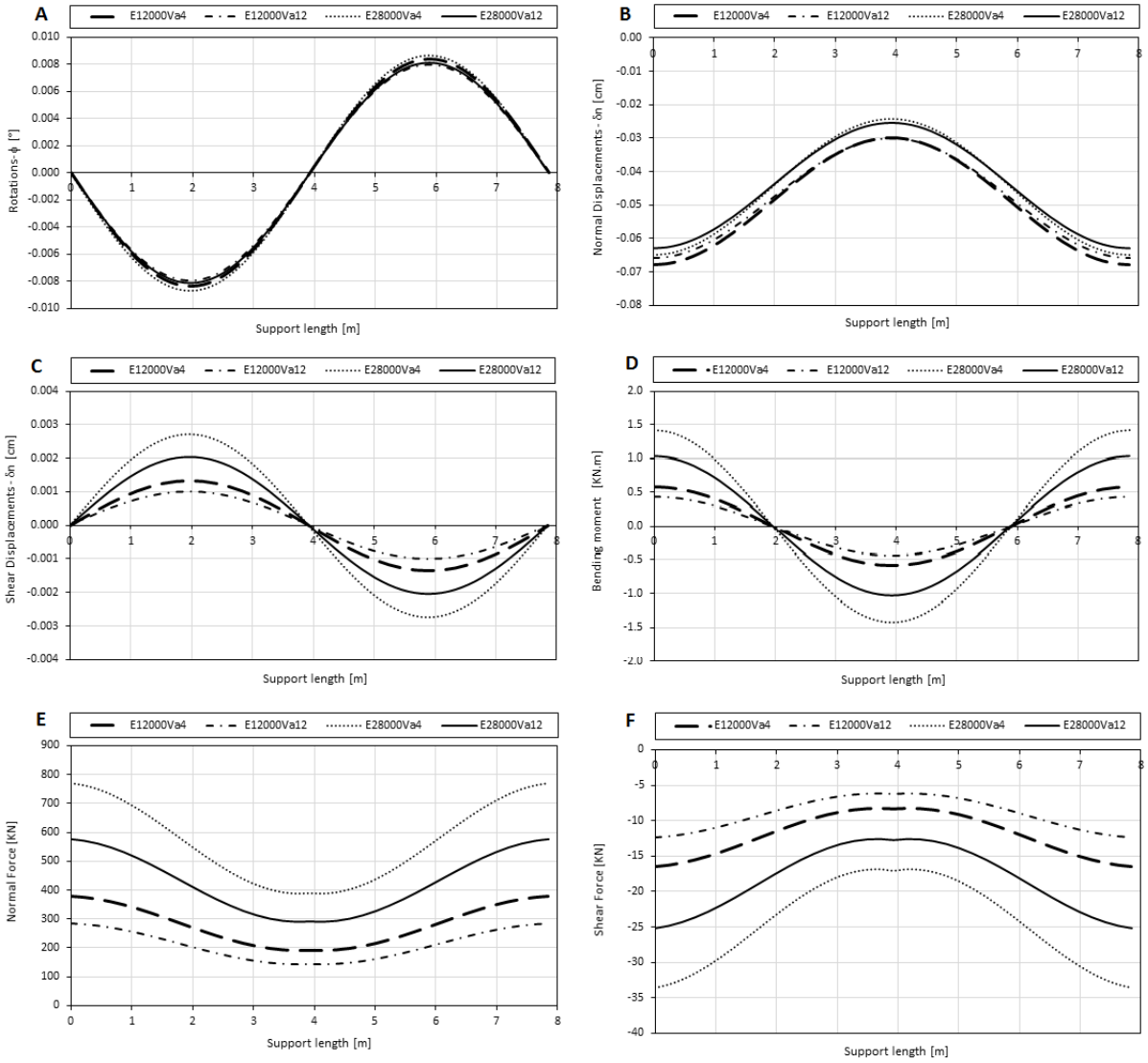

Figure 29. Variation of the rotation (A), normal displacement (B), shear displacement (C), bending moment (D), normal force (E) and shear force (F) for the two considered typology of shotcrete and the two assumed advance speeds of the tunnel face, with reference to the final equilibrium point (example 2).

Examples 3 and 4 refer to two tunnels built on rock mas with the same characteristics, differing from one another only in size. Examples three and four were analyzed in four different cases, in which the elastic modulus values of SC linings were obtained by Melbye (1994). The first proposed SC installation was implemented in the tunnel of Blisadona (Austria) which has a value of elastic modulus of 30000MPa. The second is a SC installed in a tunnel located at Quarry Bay Station (Hong Kong) which has an elastic modulus with a value of 42000MPa. The time constant α and Poisson ratio were assumed to be 0.05 h^{-1} and 0.15 respectively. However, the mechanical properties of the rock assumed for these examples (Table 9) does not refer to the real in situ geomechanical properties.

For the first (example 3) a radius of 2m has been assumed, while for the second (example 4) a larger dimension with a radius of 7m has been hypothesized. The in situ hydrostatic stress p_0 was assumed as 7MPa, with a concrete lining thickness of 20cm and K_0 value of 0.5.

In these two examples a rock mass of medium mechanical characteristics corresponding to an RMR of 40 is assumed. The geomechanical parameters are shown in Table 9.

Table 9. Geomechanical parameters for the rock mass for example 3 and example 4.

Rock Mass Parameters	
RMR	40
Elastic modulus [Mpa]	21170
Poisson ratio	0.30
Peak Cohesion [Mpa]	1.5
Residual Cohesion [Mpa]	1.5
Peak Angle of Friction [°]	33
Residual Angle of Friction [°]	33
Dilatancy [°]	16

The daily advance rates were assumed for both examples 2m/day and 6m/day, with installation time of the support t_0 equal to 6 h and the advancement step δ of 3.5m.

In the following tunnel face advancement diagrams for the two rates considered for these examples are shown.

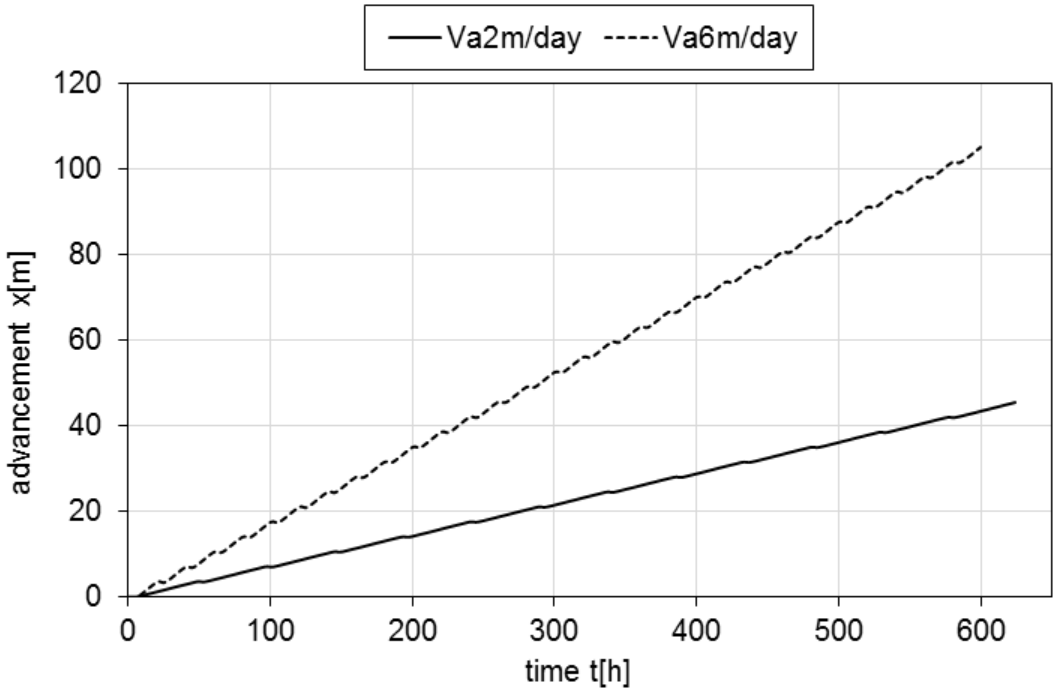

Figure 30. Graph of the tunnel excavation with face advancements rate equal to 2 and 6 m/day.

Figure 31 shows the reaction lines of the sprayed concrete lining for the 4 cases considered. Note that as for the example of the smallest tunnel (example 3), the same for all the other parameters involved in the calculation, the differences in final loading load and the displacement on the wall tunnel are more pronounced. In the case of a large gallery (example 4), the differences between the 4 cases examined are smaller. However, even in these two calculation examples it is noted that the major end loads are for the case of lining with a higher stiffness during the setting time and a lower face advancements rate.

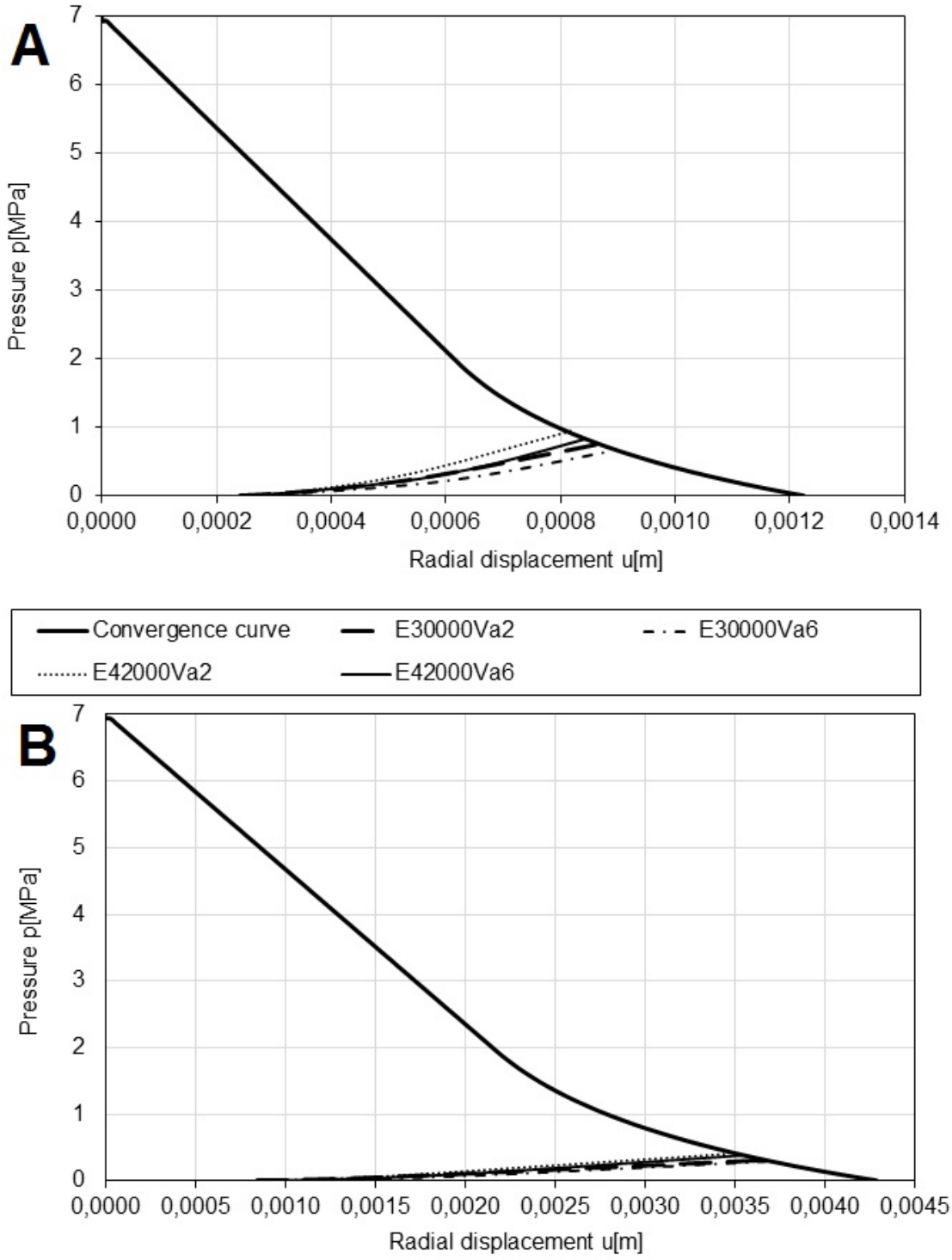

Figure 31. CCC and reaction curve of the shotcrete lining as a function of the face advancement rate and the apparent elastic modulus of the shotcrete for the example 3 (A) and example 4 (B).

Examples 3 and 4 use the same types of concrete, therefore the same diagrams relating the time with the elastic modulus and UCS of the SC are shown below.

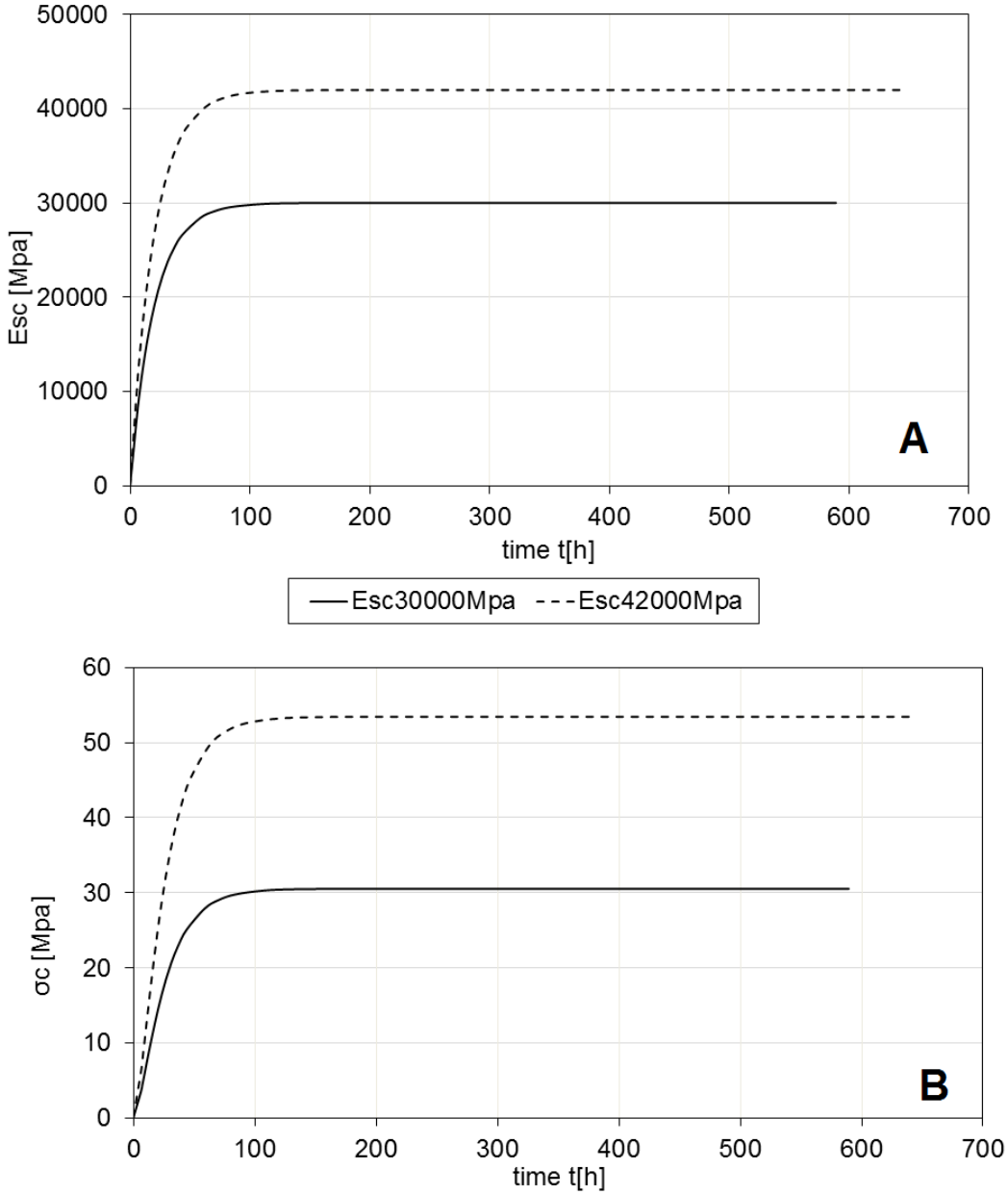

Figure 32. Progressive increase of the elastic modulus (A) and UCS (B) of the shotcrete over the time.

The displacements and stress characteristics developed along the lining are shown in Figures 33 and 34.

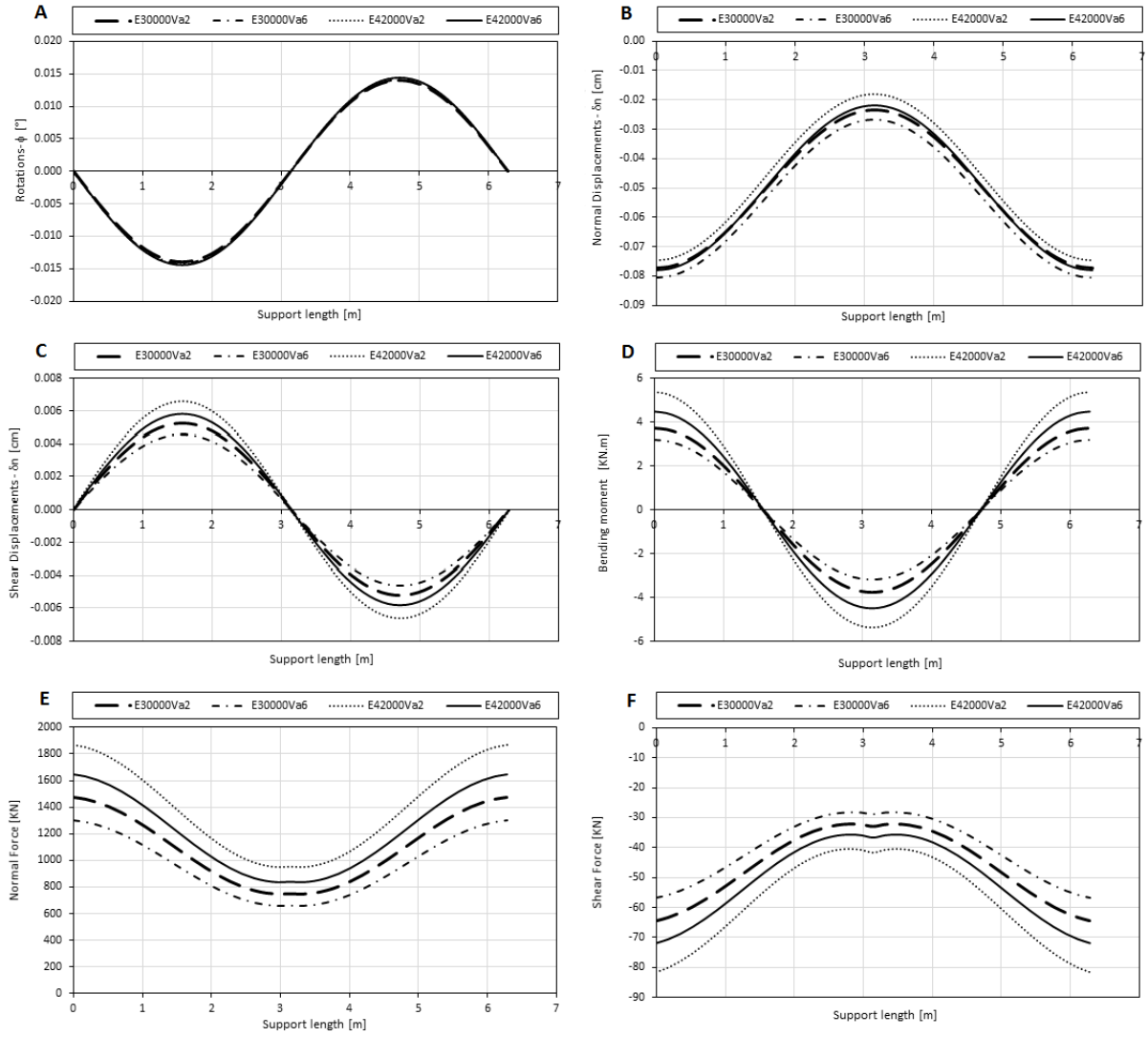

Figure 33. Variation of the rotation (A), normal displacement (B), shear displacement (C), bending moment (D), normal force (E) and shear force (F) for the two considered typology of shotcrete and the two assumed advance speeds of the tunnel face, with reference to the final equilibrium point (example 3).

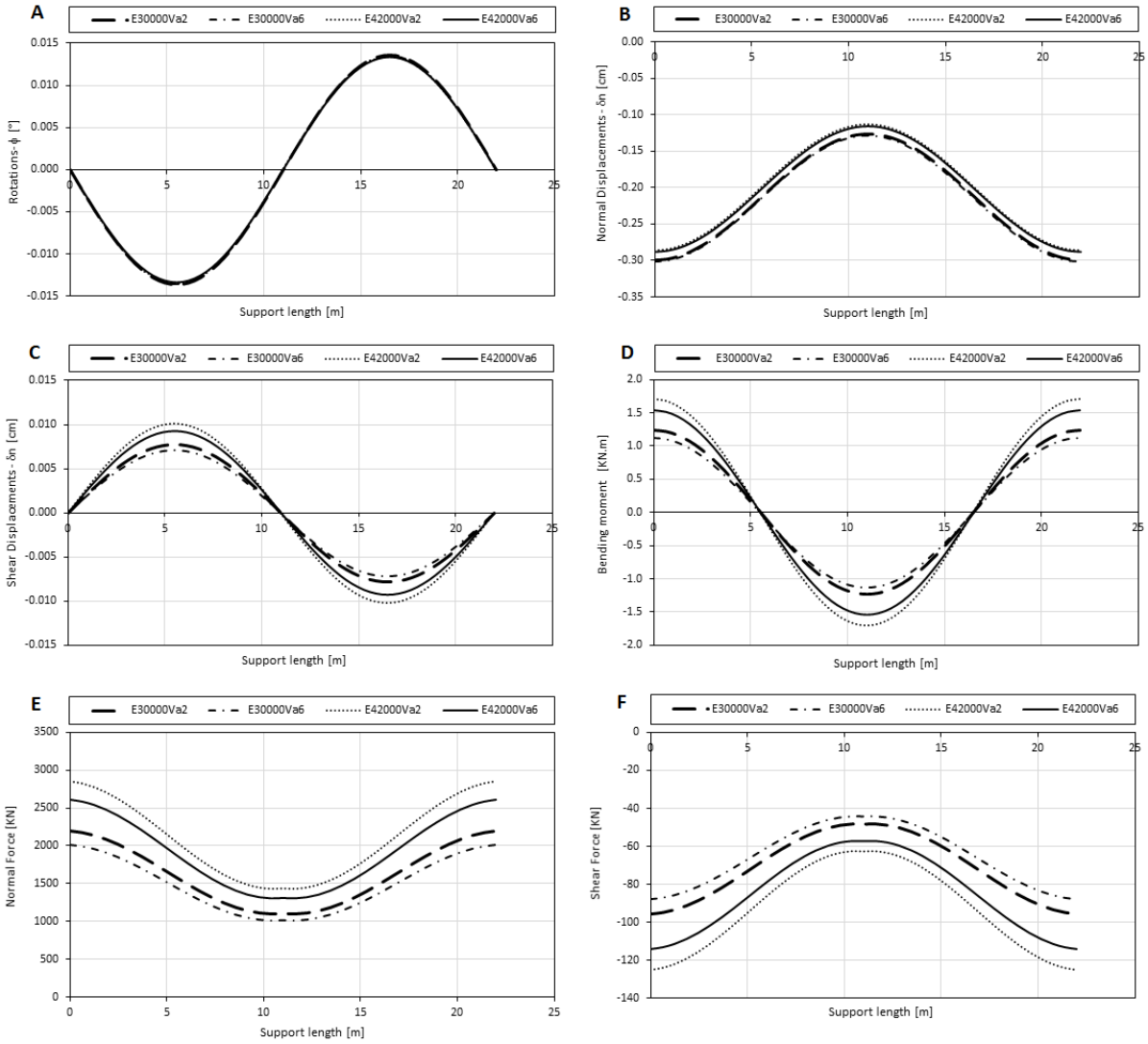

Figure 34. Variation of the rotation (A), normal displacement (B), shear displacement (C), bending moment (D), normal force (E) and shear force (F) for the two considered typology of shotcrete and the two assumed advance speeds of the tunnel face, with reference to the final equilibrium point (example 4).

Also for these two examples there are higher stress characteristics for sprayed concretes with greater stiffness during the setting time and a lower face advancements rate. Major percentage changes occur among the four cases analyzed for the smaller tunnel, compared to the larger gallery example.

Examples five and six refer to two tunnels of size 7m and 2m, respectively, excavated in a rock mass with the same characteristics. The rock in these two examples, unlike the previous two, is a rock mass of good mechanical properties corresponding to RMR=80. The geomechanical parameters are listed in Table 10.

Table 10. Geomechanical parameters for the rock mass for example 5 and example 6.

Rock Mass Parameters	
Elastic modulus [MPa]	57500
RMR	80
Poisson ratio	0.30
Peak Cohesion [MPa]	3.75
Residual Cohesion [MPa]	3.75
Peak Angle of Friction [°]	42
Residual Angle of Friction [°]	42
Dilatancy [°]	16

The hydrostatic pressure p_0 is assumed to be 7MPa, the concrete lining has a thickness of 20cm and K_0 is equal to 0.5 for both examples. The daily advance rates and the concrete types implemented in the support of these two examples are assumed to be the same types as in examples 3 and 4. The reaction lines of the shotcrete lining in conjunction with the CCC are shown in Figure 35.

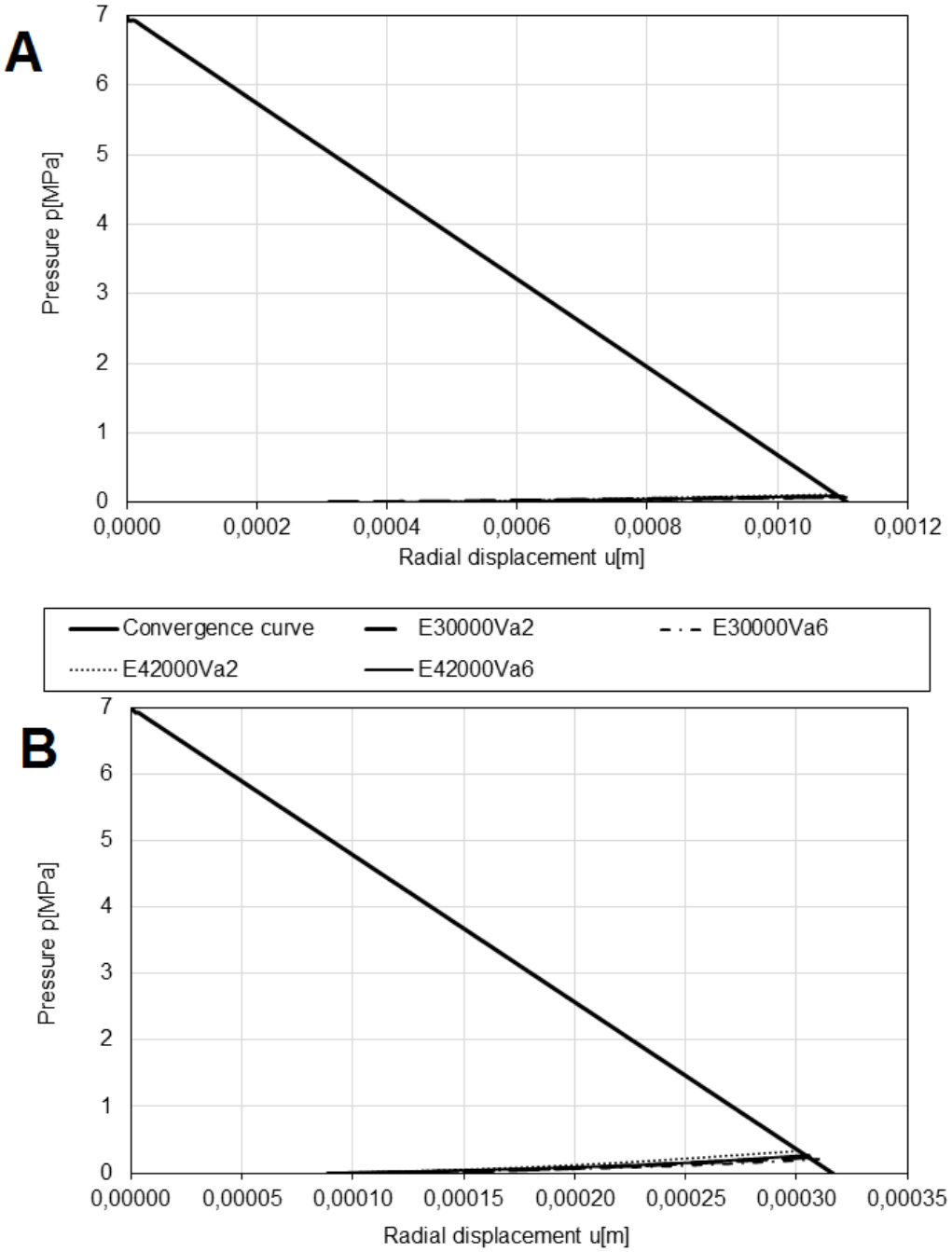

Figure 35. Reaction curve of the shotcrete lining as a function of the face advancement rate and the apparent elastic modulus of the shotcrete for the example 5 (A) and example 6 (B).

The stress characteristics (M, N and F) to determine the stress state in the lining and the more important displacements of the shotcrete lining are shown in Figure 36 and Figure 37.

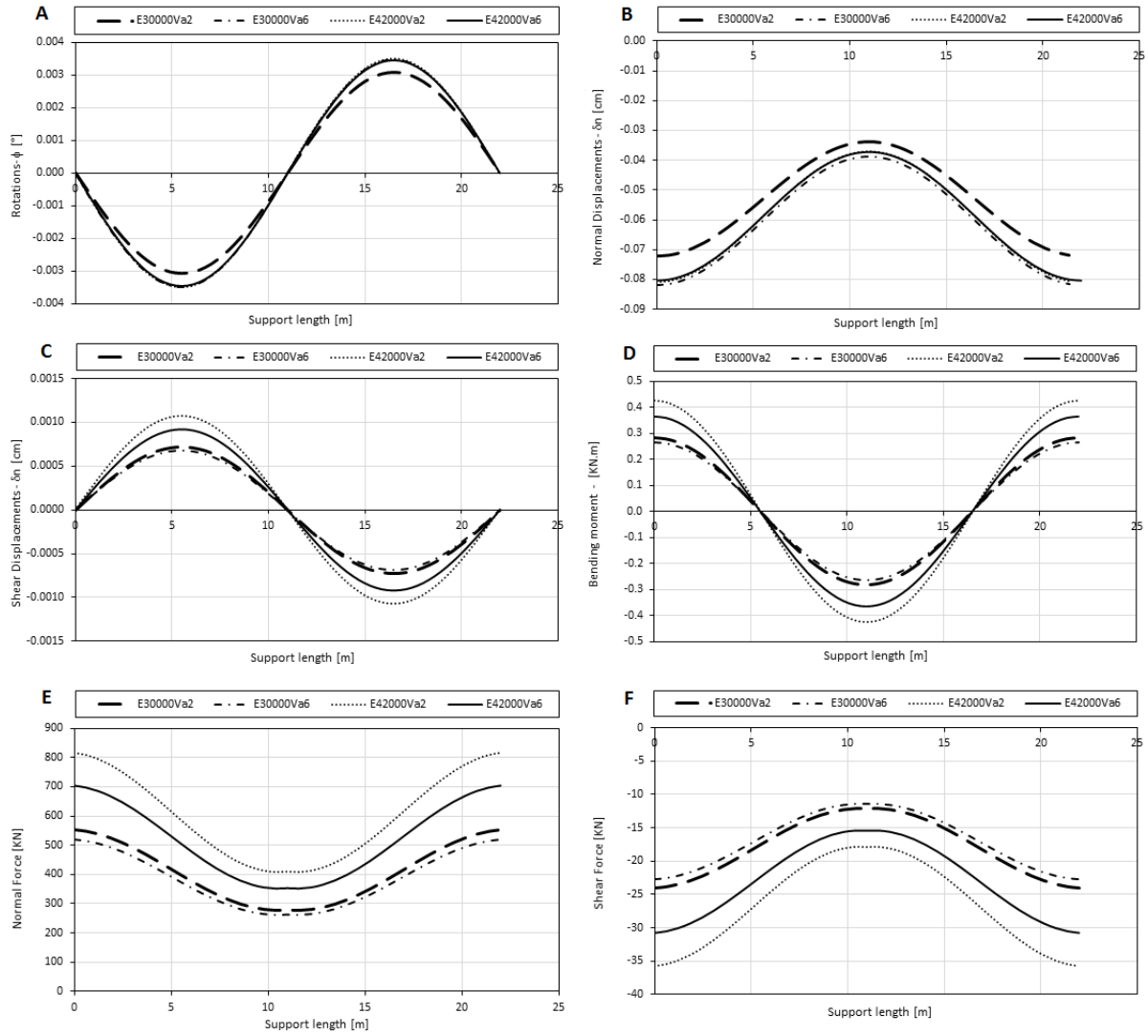

Figure 36. Variation of the rotation (A), normal displacement (B), shear displacement (C), bending moment (D), normal force (E) and shear force (F) for the two considered typology of shotcrete and the two assumed advance speeds of the tunnel face (2 m/s and 6 m/s), with reference to the final equilibrium point (example 5).

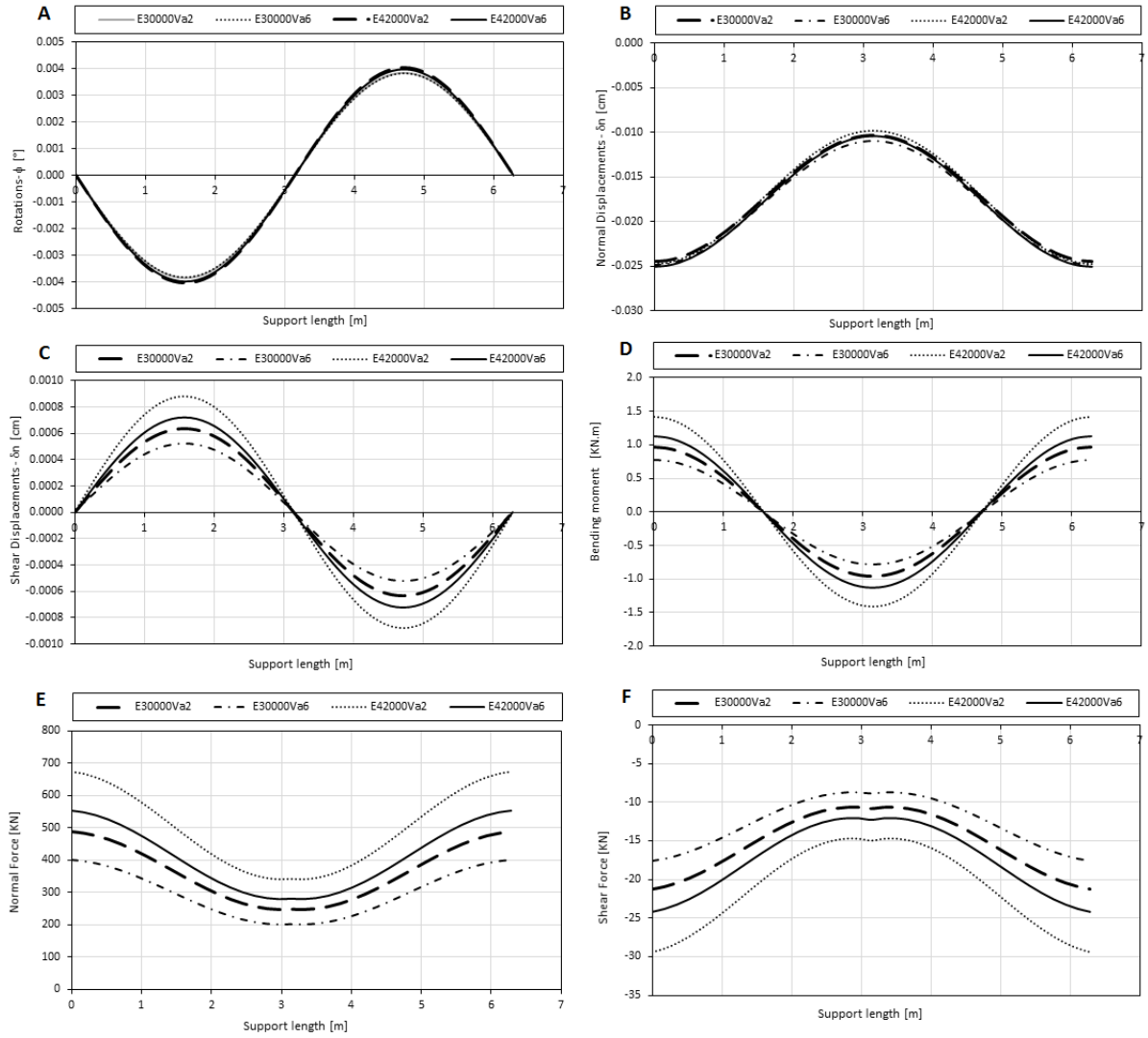

Figure 37. Fig. Variation of the rotation (A), normal displacement (B), shear displacement (C), bending moment (D), normal force (E) and shear force (F) for the two considered typology of shotcrete and the two assumed advance speeds of the tunnel face (2 m/s and 6 m/s), with reference to the final equilibrium point (example 6).

In high-quality rock masses, such as those for example 5 and 6, the final load on the lining is of low magnitude. In fact, the intersection between the CCC and the RLSL is for low pressure values. In the example 5 (R = 7m) there are no noticeable differences in the RLSL performance for the four cases examined, but there is some difference in example 6 (R = 2m).

On the other hand, the differences between the bending moments and the forces that develop inside the lining are more pronounced. The same considerations done previously are also here valid. In percentage terms, the variations found in the 4 cases

examined are higher for example 6 (R = 2m) than for example 5 (R = 7m). In addition, for R = 7m and final elastic modulus of SC of 30GPa (lower stiffness between the two types of concrete used), the advance rate appears to have a minor influence on the trend of bending moments, normal and shear forces developed in the lining.

CONCLUSIONS

The SC lining is very often employed in the tunneling sector. The design of this support type can be carried out with bi-dimensional or three-dimensional numerical models. The former requires complex simulation systems for the simulation of the load process of the lining, whereas the latter can be complex and slow during the definition phase of the numerical model and during the calculations.

A numerical model which is very effective during the SC lining design is the hyperstatic reaction methods (HRM). This finite element method considers the interaction between the lining and the rock through the Winkler spring types, both in the normal (perpendicular to the lining) and in the tangential direction (parallel to the lining). The lining is simulated by a series of straight beam elements, connected by nodes. HRM is very quick and allows performing numerous calculations in a short time. In order to analyze the SC lining behavior in different possible conditions, which can be encountered during the tunnel excavation in rock, an extensive parametric analysis has been performed, by varying the fundamental model parameters at defined intervals. From this analysis useful indications regarding the effect of the mechanical and geometrical characteristics of the SC lining on the forces acting (mainly bending moments and axial forces) on it have been obtained. The results of the extensive parametric analysis have been summarized in tables, which can result useful during the lining design.

From this study the importance of the stiffness Ks, describing the tangential interaction between the lining and tunnel rock wall, has been highlighted. This stiffness influences the results obtained, and the neglectance of this type of interaction leads to an overestimation of the bending moments, and therefore the overdesign of the lining.

The sprayed concrete linings represent one of the most popular tunnel supporting works. Its operating mechanism is quite complex due to the installation method, the particular load application phase and the concrete curing with the consequent modification of the mechanical properties of the concrete over time. Precisely because of the complexity of the operation of this support work, it is difficult to analyze the behavior and to evaluate its static conditions. The three-dimensional numerical analysis, able to consider all the

complex aspects of the operating mechanism, requires very long calculation times and difficulties in correctly assessing the stress state present in the lining.

In this research, after highlighting the fundamental characteristics of the shotcrete, a new calculation procedure based on the combined use of two widely used calculation methods for tunnel linings was introduced: the Convergence-Confinement Method (CCM) and the Hyperstatic Reaction Method (HRM).

The former, thanks to the evaluation of the sprayed concrete reaction line (RLSL) and the intersection of the Convergence Containment Curves (CCC), allows obtaining the final load on the support and the evolution of the load with the progress of the curing phase of the concrete. The latter, based on the results obtained with the former, allows determining the mechanical behavior of the lining and interaction with the tunnel wall with the progress of the applied load and the development of mechanical parameters of the concrete over time.

The interesting result is the trend of bending moments, normal and shear forces, and displacement along the lining circumference during the transient loading phase and in the final load conditions.

From the stress characteristics it is possible to assess the tension state in the concrete and the safety factors of the lining against compression or traction in the concrete. Note that the safety factors allow to correctly designing the lining, defining in particular the average of the tunnel lining thickness.

The calculation procedure was then applied to examples, differentiated by the tunnel geometry and the geomechanical quality of the surrounding rock. For each example, four different cases were considered, taking into account two different types of shotcrete and two different advance rates of the tunnel excavation front. From the results, it was possible to develop useful considerations on the parameters that are most influenced by the mechanical behavior of the lining. Thanks to the fact that the model is able to appropriately consider the evolution of mechanical properties of sprayed concrete over time and the advance rate of the excavation face, it is a useful tool for selecting the key parameters in a tunnel design, as the type of shotcrete and the thickness of the coating.

BIBLIOGRAPHY

American Shotcrete Association (ASA), 2014. Why shotcrete? https://www.shotcrete.org.

Aydan, O., Sezaki, M., Kawamoto, T. 1992. Mechanical and numerical modelling of shotcrete. Iin Pande, G., Pietruszczack, S. (Eds.) Numerical Models in Geomechanics, Taylor and Francis, London, pp. 707-716.

Barton, N., Lien, R., Lunde, J. 1974. Engineering classification of rock masses for the design of tunnel support. Rock Mechanics (6), pp. 183–236.

Barton, N. 2002. Some new Q-value correlations to assist in site characterisation and tunnel design. Int. J. Rock Mech. Min. Sci. 39, pp. 185–216.

Bernard, E. 2008. Early-age load resistance of fibre reinforced shotcrete linings. Tunnelling and Underground Space Technology, vol. 23, no. 4, pp. 451–460.

Berwanger, W. 1986. Dreidimensionale Berechnung von tiefliegenden Felstunneln unter Berücksichtigung des rheologischen Verhaltens von Spritzbeton und des Bauverfahrens. PhD thesis, University of Hannover, Germany.

Bieniawski, Z.T. 1989. Engineering Rock Mass Classification. John Wiley, New York.

Brykov, A.S., Vasil'ev, A.S., Mokeev, M.V. 2013. Hydration of Portland Cement in the Presence of Aluminum-Containing Setting Accelerators. Russian Journal of Applied Chemistry 86, pp. 793−801.

Chang, Y., Stille, H. 1993. Influence of early age properties of shotcrete on tunnel construction sequences. In Wood, D.F., Morgan, D.R. (Eds.), Shotcrete for Underground Support VI, American Society of Civil Engineers, Reston, pp. 110-117.

Chen, W.F. 1982. Plasticity in Reinforced Concrete. McGraw-Hill, New York.

Clements, M. 2004. Comparison of methods for early age strength testing of sprayed fibre reinforced concrete. In: Bernard, E.S. (Ed.), Proceedings of the 2nd International Conference on Engineering Developments in Sprayed Fibre Reinforced Concrete, Cairns, Queensland, Australia. Taylor and Francis Group, London, pp. 81–87.

Concrete Institute of Australia. 2010. Shotcrete in Australia. Concrete Institute of Australia, Rhodes, Australia.

Cosciotti, L., Lembo-Fazio, A., Boldini, D., Graziani, A. 2001. Simplified behavior models of tunnel faces supported by shotcrete and bolts. In Adachi, T., Tateyama, K., Kimura, M. (Eds.), Proceedings of the International Conference on Modern Tunneling Science and Technology, Kyoto, Japan, pp. 407-412.

DIN 18551 1992. Spritzbeton - Nationale Anwendungsregeln zur Reihe DIN EN 14487 und Regeln für die Bemessung von Spritzbetonkonstruktionen. Deutsches Institut fur Normung, e.V.

DIN EN 14487-1 2006. Spritzbeton - Teil 1: Begriffe, Festlegungen und Konformität. Deutsches Institut fur Normung, e.V.

DIN EN 14488-2 2006. Prüfung von Spritzbeton - Teil 2: Druckfestigkeit von jungem Spritzbeton. Deutsches Institut fur Normung, e.V.

DIN EN 12504-1 2009. Prüfung von Beton in Bauwerken - Teil 1: Bohrkernproben - Herstellung, Untersuchung und Prüfung der Druckfestigkeit. Deutsches Institut fur Normung, e.V.

Do, N.A., Dias, D., Oreste, P., Djeran-Maigre, I., 2014a. The behavior of the segmental tunnel lining studied by the hyperstatic reaction method. Eur. J. Environmental Civil Eng. 18(4), pp. 489–510.

Do, N.A., Dias, D., Oreste, P., Djeran-Maigre, I., 2014b. A new numerical approach to the hyperstatic reaction method for segmental tunnel linings. Int. J. Numer. Anal. Meth. Geomech (38), pp. 1617–1632.

Duddeck, H., Erdmann, J. 1985. On structural design models for tunnels in soft soil. Underground Space (9), pp. 246–259.

EFNARC. 1996. European Specification for Sprayed Concrete. United Kingdom

Feenstra, P.H., de Borst, B. 1993. Aspects of robust computational models for plain and reinforced concrete. Heron 48(4), pp. 5-73.

Franzen, T., Garshol, K.F., Tomisawa, N. 2001. Sprayed concrete for final lining: ITA working group report. Tunn. Undergr. Space Technol (16), pp. 295–309.

Goel, R.K., Jethwa, J.L., Paithankar, A.G. 1995. Indian experience with Q and RMR system. Tunnelling and Underground Space Technology, 10. Pergamon, pp. 97–109.

Gugliota, A. 2002. Elementi finiti, Parte I. Otto editore. Torino

Hassani, R., Basirat, R. 2016. Application of Hyperstatic Reaction Method for Designing of Tunnel Permanent Lining, Part I: 2D Numerical Modelling. Civil Engineering Journal 2(6), pp. 244-253.

Hemphill, G.B. 2013. Practical tunnel construction. John Wiley & Sons, Hoboken.

Höfler, J., Schlumpf, J. 2004. Shotcrete in Tunnel Construction, Introduction to the basic technology of sprayed concre. Putzmeister AG.

Huebner, K.H., Dewhirst, D.L., Smith, D.E., Byrom, T.G. 2001. The Finite Element Method for Engineers. John Wiley and Sons, inc., New York.

Iwaki, K., Hirama, A., Mitani, K., Kaise, S., Nakagawa, K. 2001. A quality control method for shotcrete strength by pneumatic pin penetration test. NDT and E International, 34(6), pp. 395-402.

Jolin, M., Beaupré, D. 2003. Understanding Wet-Mix Shotcrete: Mix Design, Specifications, and Placement. American Shotcrete Association.

Kotsovos, M.D., Newman, J.B. 1978. Generalized stress-strain relation for concrete. J. Eng. Mech.-ASCE,104, pp. 845-856.

Leca, E., Clough, W. 1992. Preliminary design for NATM tunnel support in soil. Journal of Geotechnical Engineering 118 (4), pp. 558–575.

Li, S., Wang, B. 2008. Elastic analysis of stress–displacement field for a lined circular tunnel at great depth due to ground loads and internal pressure. Tunn. Undergr. Sp. Tech., 23, pp. 609–617.

Mason, D.P., Stacey, T.R. 2008. Support to rock excavations provided by sprayed liners. International Journal of Rock Mechanics & Mining Sciences 45, pp. 773–788.

Melbye, T. 1994. Sprayed Concrete for Rock Support. MBT International Underground Construction Group, Zürich.

Meschke, G. 1996. Consideration of aging of shotcrete in the context of a 3-D viscoplastic material model. Int. J. Numer. Methods. Eng., 39(18), pp. 3123–3143.

Mohajerani, A., Rodrigues, D, Ricciuti, C., Wilson, C. 2015. Early-Age Strength Measurement of Shotcrete. Journal of Materials, 2015 (ID 470160), http://dx.doi.org/10.1155/2015/470160.

Moussa, A.M. 1993. Finite element modelling of shotcrete in tunnelling. PhD thesis, University of Innsbruck, Austria.

Neville, A.M., Dilger, W.H., Brooks, J.J. 1983. Creep of Plain and Structural Concrete. Construction Press, Harlow.

ÖVBB. 2006. Guideline Sprayed Concrete. Österreichische Bautechnik Vereinigung.

Oreste, P. 2003. Analysis of Structural Interaction in Tunnels using the Convergence-Confinement Approach. Tunn. Undergr. Sp. Tech., 18(4):347-363, DOI: 10.1016/S0886-7798(03)00004-X.

Oreste, P. 2003. Procedure for Determining the Reaction Curve of Shotcrete Lining Considering Transient Conditions. Rock Mech. Rock Eng. 36 (3), 209–236, DOI 10.1007/s00603-002-0043-z.

Oreste, P. 2007. A numerical approach to the hyperstatic reaction method for the dimensioning of tunnel supports. Tunn. Undergr. Sp. Tech (22), pp. 185–205.

Oreste, P. 2009. The Convergence-Confinement Method: Roles and limits in modern geomechanical tunnel design. American Journal of Applied Sciences 6(4), pp. 757-771.

Oreste, P. 2009. The Determination of the Tunnel Structure Loads Through the Analysis of the Interaction between the Void and the Support Using the Convergence-Confinement Method. Am. J. Appl. Sci (11), pp. 1945-1954.

Oreste, P. 2015. Analysis of the Interaction between the Lining of a TBM Tunnel and the Ground Using the Convergence-Confinement Method. Am. J. Appl. Sci., 12(4) pp. 276-283. DOI: 10.3844/ajassp.2015.276.283.

Prudencio, L.R. 1998. Accelerating admixtures for shotcrete. Cement and Concrete Composites (20), pp. 213-219.

Panet, M., Guenot, A. 1982, Analysis of convergence behind the face of a tunnel. Proc. Tunnelling 82, Brighton, pp. 197–204.

Pottler, R. 1990. Time-dependent rock-shotcrete interaction. A numerical shortcut. Comput. Geotechn. 9, pp. 149–169.

Rispin, M., Howard, D., Kleven, O. B., Garshol, K., Gelson, J. 2009. Safer, Deeper, Faster: Sprayed Concrete—An Integral Component of Development Mining, Australian Centre for Geomechanics.

Rokhar, R.B., Zachow, R. 1997. Ein neues Verfahren zur taglichen Kontrolle der Auslastung einer Spritzbetonschale. Felsbau 15(6), pp. 430-434.

Sánchez, J., Cobo, A., Díaz, B., Mateos, I. 2015. Experimental study of performance self-compacting concrete reinforced with steel fibers. Anales de Edificación (1), pp. 17-26.

Saurer, E., Marcher, T., Schädlich, B., Schweiger, H.F. 2014. Validation of a novel constitutive model for shotcrete using data from an executed tunnel. Geomech. Tunnelling 7(4), pp. 353-361.

Schädlich, B., Schweiger, H.F. 2014. A new constitutive model for shotcrete. In: Hicks, M.A., Brinkgreve, R.B.J., Rohe, A. (Eds.), Numerical Methods in Geotechnical Engineering. Taylor & Francis, Oxam, pp. 103-108.

Schütz, R., Potts, D.M., Zdravkovic, L. 2011. Advanced constitutive modelling of shotcrete: Model formulation and calibration. Comput. Geotech. 38(6), pp. 834–845.

Singh, B., Jethwa, J.L., Dube, A.K., Singh, B. 1992. Correlation between observed support pressure and rock mass quality. Tunn. Undergr. Sp. Tech., 7, pp. 59–75.

Son, M., Cording, E.J. 2007. Ground–liner interaction in rock tunneling. Tunn. Undergr. Sp. Tech., pp. 22: 1-9.

Spagnoli, G., Oreste, P., Lo Bianco, L. 2017. Estimation of Shaft Radial Displacement beyond the Excavation Bottom before Installation of Permanent Lining in Nondilatant Weak Rocks with a Novel Formulation. Int. J. Geomechanics, 17, 04017051 https://doi.org/10.1061/(ASCE)GM.1943-5622.0000949.

Su, J., MacDonald, M. 2013. Design of SCL Tunnel Using Sprayed Waterproofing Membrane in Soft Ground. Harding Prize.

Sun, Y., McRae, M., Van Greunenk, J. 2013. Load Sharing in Two-pass Lining System for NATM Tunnels. Rapid Excavation and Tunneling Conference (RETC) Proceeding, San Francisco, CA.

Thomas, A. 2009. Sprayed Concrete Lined Tunnels. Taylor & Francis, Oxon.

Unal, E. 1983. Design guidelines and roof control standards for coal mine roofs, Ph.D. Thesis, Pennsylvania State University.

US Army Corps of Engineers. 1993. Engineering Manual: Engineering and Design - Standard Practice for Shotcrete, Washington, DC.

Wang, J., Niu, D., Zhang, Y. 2015. Mechanical properties, permeability and durability of accelerated shotcrete. Constr. Build. Mater (95), pp. 312–328.